

SECTION II. TASK 2. SUBMODEL DEVELOPMENT AND EVALUATION

Objectives

The objectives of this task are to develop or adapt advanced physics and chemistry submodels for the reactions of coal in an entrained-bed and a fixed-bed reactor and to validate the submodels by comparison with laboratory scale experiments.

Task Outline

The development of advanced submodels for the entrained-bed and fixed-bed reactor models will be organized into the following categories: a) Coal Chemistry (including coal pyrolysis chemistry, char formation, particle mass transfer, particle thermal properties, and particle physical behavior); b) Char Reaction Chemistry at high pressure; c) Secondary Reactions of Pyrolysis Products (including gas-phase cracking, soot formation, ignition, char burnout, sulfur capture, and tar/gas reactions); d) Ash Physics and Chemistry (including mineral characterization, evolution of volatile, molten and dry particle components, and ash fusion behavior); e) Large Coal Particle Effects (including temperature, composition, and pressure gradients and secondary reactions within the particle, and the physical affects of melting, agglomeration, bubble formation and bubble transport; f) Large Char Particle Effects (including oxidation); g) SO_x - NO_x Submodel Development (including the evolution and oxidation of sulfur and nitrogen species); and h) SO_x and NO_x Model Evaluation.

II.A. SUBTASK 2.a. - COAL TO CHAR CHEMISTRY SUBMODEL DEVELOPMENT AND EVALUATION

Senior Investigators - David G. Hamblen and Michael A. Serio
Advanced Fuel Research, Inc.
87 Church Street, East Hartford, CT 06108
(203) 528-9806

Objective

The objective of this subtask is to develop and evaluate, by comparison with laboratory experiments, an integrated and compatible submodel to describe the organic chemistry and physical changes occurring during the transformation from coal to char in coal conversion processes. Many of the data and some computer codes for this submodel are available, so it is expected that a complete integrated code will be developed during Phase I. Improvements in accuracy and efficiency will be pursued during Phase II.

Accomplishments

Additional characterization of the coal samples for this program was performed by pyrolysis experiments in a TG-FTIR and in Field Ionization Mass Spectrometry (FIMS) apparatus. The FG-DVC model was used to predict baseline pyrolysis data for the eight Argonne coals from these two reactors as well as from an Entrained Flow Reactor (EFR). In general, the model did a good job in predicting the data for gas, tar and char yields and for the tar molecular weight distributions.

Additional improvements were made in the FG-DVC model. A second version of the model was developed for reactors in which the tar is quenched after being evolved. The model run procedure was modified so that successive cases could be run in a batch mode and the results could be averaged, stored and/or plotted. The creation and loss of methyl groups in the DVC model due to bridge breaking and in the FG model due to methane formation was made consistent. Some refinements were also made to the treatment of internal and external transport in the model. In addition, work was done on comparing the FG-DVC model to the statistical model of Pugmire and Grant at the University of Utah which is based on percolation theory.

A review of internal pore transport models was prepared by Professor Eric Suuberg of Brown University. It was determined that differences in the pressure drops calculated by the Simons and Gavaias approaches to internal transport were primarily due to different assumptions regarding the pyrolysis rate. The geometry of the Simons approach makes it the easiest model to use in predicting swelling based on knowledge of the pressure inside pores and so it will be used in the future swelling model. However, the model will be modified to reflect the fact that transport in the finest pores needs to be described by an activated diffusion process. The review is presented in Appendix A of the Fifth Quarterly Report.

In order to refine the combined kinetic/mass transport submodel used in the FG-DVC model, a search was made of literature pyrolysis data for the Pittsburgh Seam coal, starting with heated grid experiments. When a comparison was made of data produced by heating at 1000 K/s to various peak temperatures, it was found that the results of different investigators did not agree, even when obtained from the same laboratory. We begin an experimental and theoretical study into possible reasons for these variations, which we are doing in conjunction with Professor Eric Suuberg of Brown University.

To examine the effect of product evolution, char viscosity, and transport on the swelling of char, drop tube experiments have been done with a Pittsburgh coal at temperatures varying from 475-600°C in 25°C intervals. The chars collected from

these experiments have been characterized for volatile content and reactivity in a TGA. Selected chars were potted and polished for analysis of their morphology by SEM.

Preliminary measurements were made of the spectral emissivity for coals of varying particle size and rank. The average emittance increased with increasing rank and particle size. The total extinction efficiency for scattering out of the aperture of our instrument needs to be measured before more accurate values of the spectral emissivity can be determined.

Coal Characterization

Additional characterization of the coal samples for this program was performed by doing pyrolysis experiments in a TG-FTIR, a Field Ionization Mass Spectrometry (FIMS) apparatus, and an entrained flow reactor (EFR).

TG-FTIR Experiments

This analysis consists of thermogravimetric analysis (TGA) with analysis of the evolved products by Fourier Transform Infrared (FT-IR) spectroscopy. The TG-FTIR consists of a sample suspended from a balance in a programmable furnace. The evolved products are swept into a gas cell for analysis by FT-IR. The FT-IR allows on-line measurements of the gas and tar concentration and composition. The apparatus has been described by Carangelo et al. (1987) and Whelan et al. (1988).

The results of monitoring the tar evolution for eight of the coal samples is presented in Fig. II.A-1. The temperature at which the peak evolution rate is reached varies from 465°C for the Zap lignite to 525°C for the Pocahontas. This corresponds to about a factor of 10 variation in the kinetic rate. The temperatures for the peak tar evolution rate are plotted versus oxygen content for the parent coal in Fig. II.A-2, which show that the rank variation is rather consistent.

The results are shown for CH₄ and CO evolution in Figs. II.A-3 and II.A-4, respectively. The data for SO₂, CO₂, and H₂O were shown in the Sixth Quarterly Report and in Serio et al. (1988a). The coals are arranged on each plot according to the rank order given in Table II.A-1, where the analysis for the coals are also given. The actual temperature-time profiles are given on the first plot in each figure.

The results show how the structure of the product gas evolution curves varies from simple in the case of hydrocarbons to complex in the case of oxygenated species. One reason is that the latter are likely to be influenced by mineral decomposition peaks. Of course this can be assessed to a large extent by running demineralized samples, which we plan to do.

In order to determine how well pyrolysis of the Argonne coals agreed with the assumption of rank-insensitive kinetics, a compilation was made of the temperatures for maximum evolution rate for the evolution of the most consistently prominent peaks for each gaseous product. This was difficult in some cases because of the fact that numerous "subpeaks", shoulders and minor peaks were often present. However, it was the usual case that an identifiable peak appeared in the same temperature vicinity for each coal. The results of this analysis are tabulated in Table II.A-4 of the Sixth Quarterly Report and in Serio et al. (1988a). The mean temperatures for the major peaks are shown as solid lines in Figs. II.A-1, II.A-3 and II.A-4.

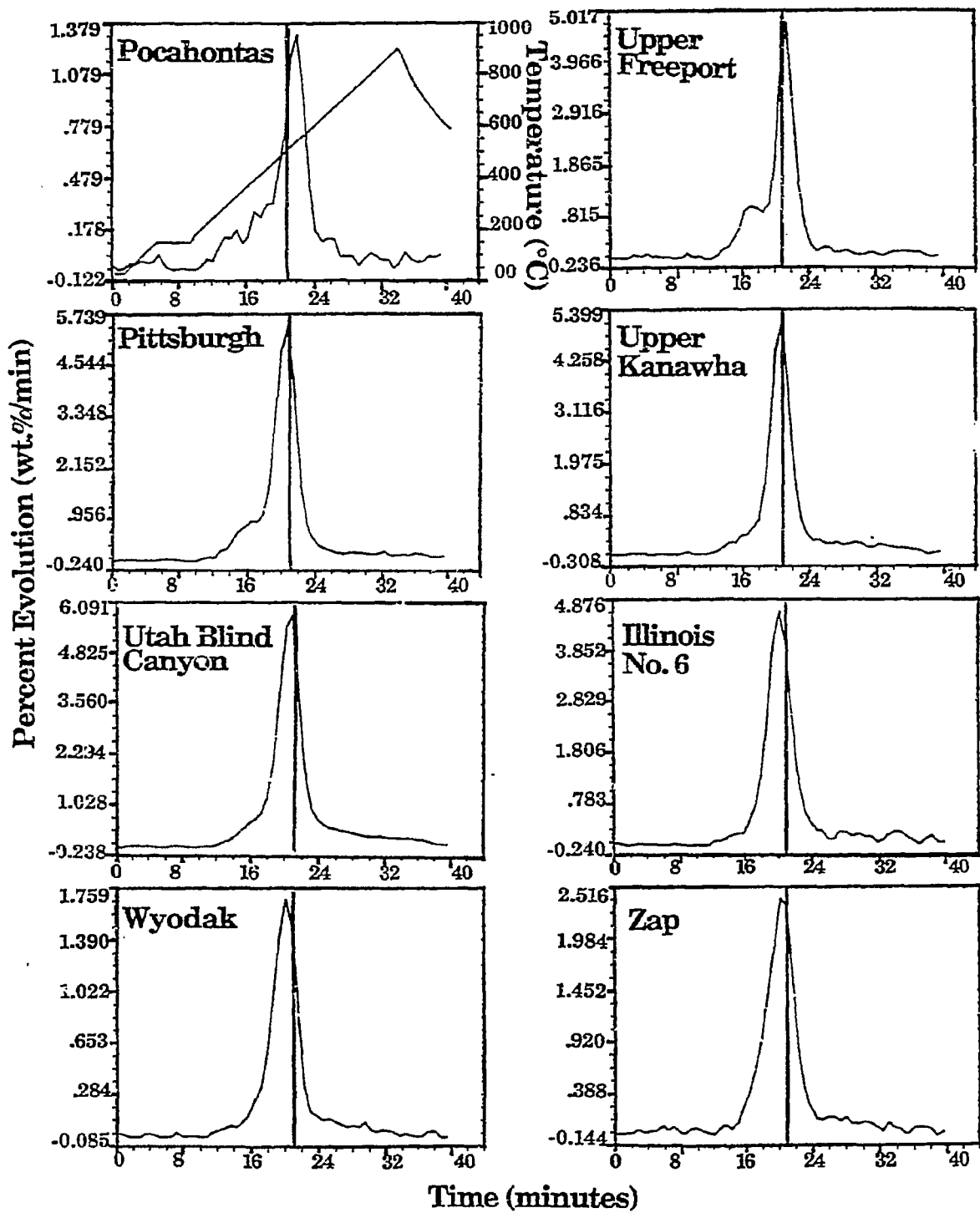


Figure II.A-1 Evolution Rate for Tars/Aliphatic from the Eight Argonne Coals in a TG-FTIR at 0.5°C/s.

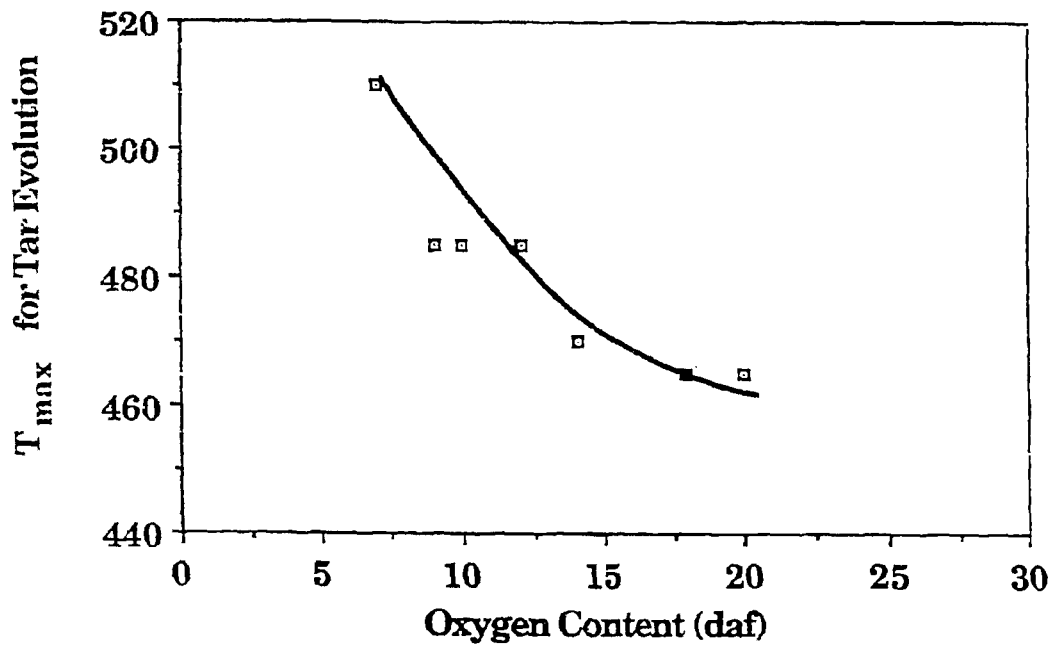


Figure II.A-2. Effect of Coal Rank on Tar Evolution Kinetics.

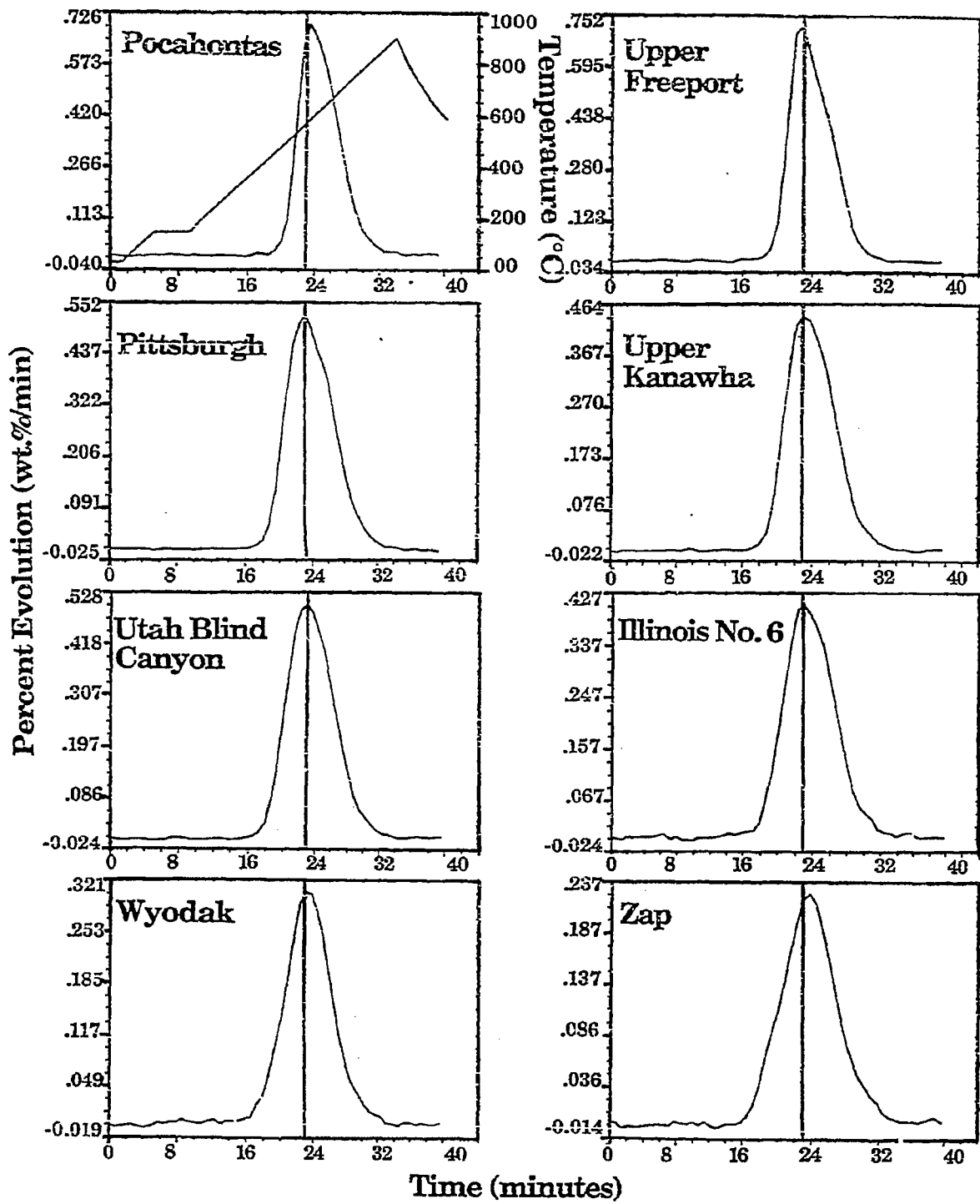


Figure IIA- 3. Evolution Rate for CH₄ from the Eight Argonne Coals in a TG-FTIR at 0.5°C/s.

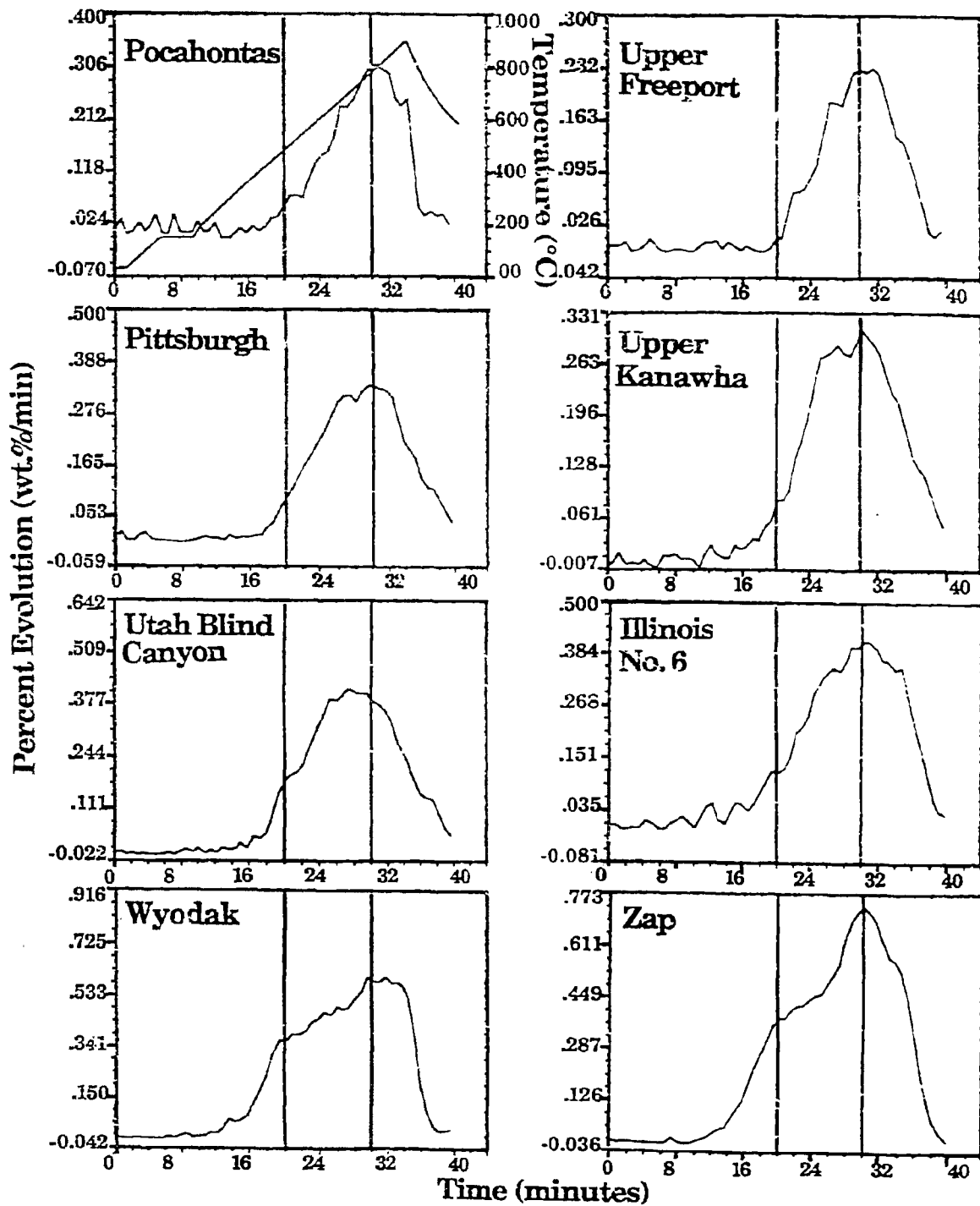


Figure IIA- 4. Evolution Rate for CO from the Eight Argonne Coals in a TG-FTIR at 0.5°C/s.

Table II.A-1
Elemental Analysis of Argonne Premium Coal Samples.

	% daf Basis				% Dry Basis	As-Received Basis	
	C	H	O	N	S	Ash	Moisture
1. Pocahontas	91	4.4	3	1.3	0.7	5	0.6
2. Upper Freeport	86	4.7	7	1.5	0.8	13	1.1
3. Pittsburgh #8	83	5.3	9	1.6	1.0	9	1.6
4. Lewiston-Stockton	83	5.3	10	1.6	0.5	20	2.4
5. Utah Blind Canyon	81	5.8	12	1.6	0.3	5	4.6
6. Illinois #6	73	5.0	14	1.4	2.2	16	8.0
7. Wyodak	75	5.4	18	1.1	0.4	8	28.1
8. Beulah-Zap	73	4.8	20	1.1	0.7	6	32.2

In general, the standard deviations are greatest for oxygenated gases (CO₂, CO, SO₂, H₂O) compared to hydrocarbon gases (CH₄, tar/aliphatics). This phenomena was also observed previously (Solomon and Hamblen, 1983). If one assumes a 50 Kcal/mole activation energy, a range in the peak temperature of 40°C corresponds to roughly a factor of 5 in the rate while a range in the peak temperature of 65°C corresponds to roughly a factor of 10 (Solomon and Hamblen, 1983). It appears that about one-half of the volatile products show a variation of x5 or less, while one-half show a variation of x10 or less.

The conclusion was that, for most species, there is a trend of increasing evolution temperature with increasing rank. However, the variations are small enough that the assumption of rank-insensitive kinetics is a good first approximation for all of the major volatile products.

If the TG-FTIR curves are replotted on the same scale, one can see the variations in the amounts of each species with rank. This has been done for CH₄ in Fig. II.A-5. The amount of CH₄ evolved increased consistently with rank. The oxygenated gases show the opposite trend with rank while the tar yield maximizes for the medium rank coals.

EFR Experiments

During the past year, two additional coals, 200 x 325 fractions of Montana Rosebud subbituminous and Indian Head Zap lignite, were pyrolyzed in the entrained flow reactor. Due to its high water content, the lignite was vacuum dried at 105°C for two days prior to use, while the subbituminous coal was vacuum dried for 1 hour prior to use, as previously practiced with the Argonne coals. Additional EFR experiments will be done at 1400°C with these two coals. In addition, runs will be done at 700, 1100, and 1400°C with Illinois No.6 coal (which was recently received) and selected demineralized coals.

FIMS Analysis

Molecular weight distributions of coals were obtained at SRI International using the Field Ionization Mass Spectrometry (FIMS) apparatus described by St. John et al. (1978). The coal samples were pyrolyzed directly in the FIMS apparatus. The FIMS technique produces little fragmentation of the evolved tars and so provides a good determination of the tar molecular weight distribution. The results for the eight Argonne coals are shown in Figs. II.A-6 and II.A-7.

The spectra show a distinct progression from low to high rank. The highest rank coals, Pocahontas (Fig. II.A-6a) and Upper Freeport (Fig. II.A-6b) both show low intensities at low molecular weights (100 - 200 amu). This suggests few one and two ring clusters. The intensity in the 200 - 600 amu range, however, suggests the presence of three, four and higher ring cluster sizes and dimers and trimers of these. The low yield for the Pocahontas is due to its higher bond energies (525°C tar peak in Fig. II.A-1) and lower number of small ring clusters capable of being volatilized.

The intermediate rank coals, Pittsburgh (Fig. II.A-6c), Utah (Fig. II.A-7a), Illinois (Fig. II.A-7b) and Upper Kanawha (Fig. II.A-6d) all have similar molecular weight distributions showing substantial intensities in the 100 to 200 amu region indicative of one and two ring clusters as well as in the 200 to 600 amu range.

The low rank coals, Wyodak (Fig. II.A-7c) and Zap (Fig. II.A-7d), show high intensity between 100 and 200 amu, but substantially lower intensity above 200 amu. This has been explained by extensive cross linking related carboxyl groups in low rank coals (Solomon et al., 1988).

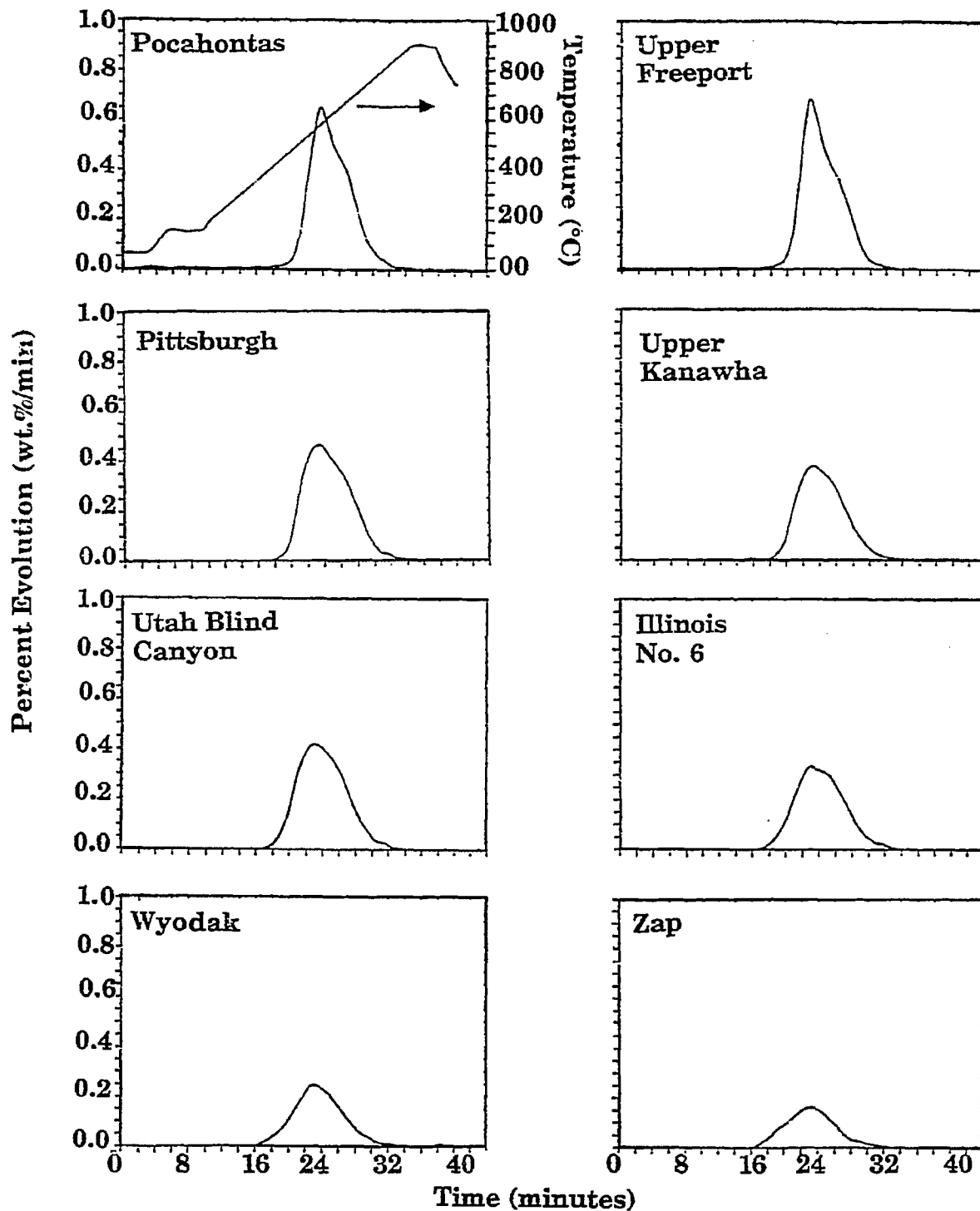


Figure IIA- 5. Evolution Rate for CH₄ from the Eight Argonne Coals in a TG-FTIR at 0.5°C/s.

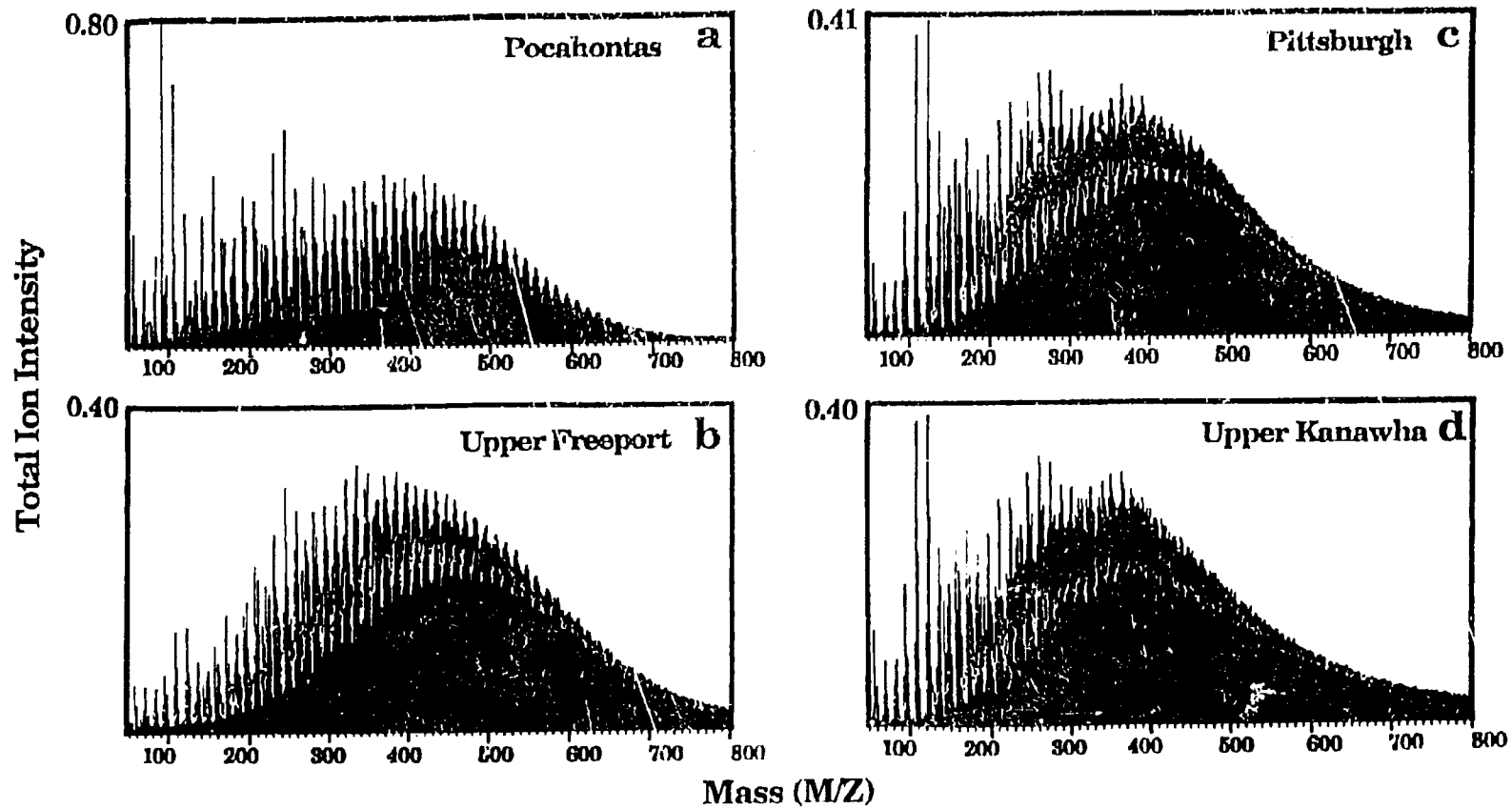


Figure II.A- 6. Tar Molecular Weight Distributions for Four Argonne Coals.

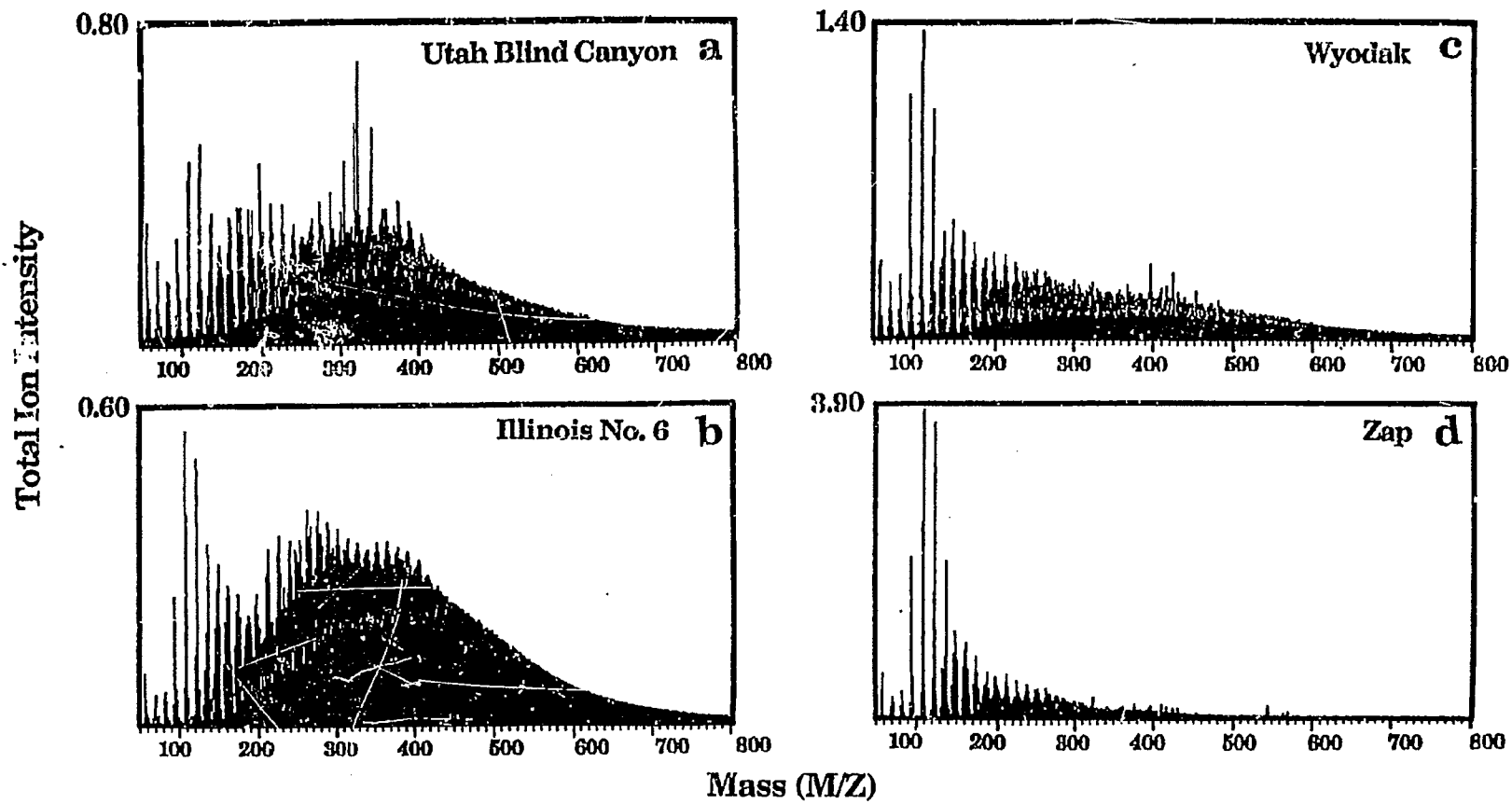


Figure II.A-7. Tar Molecular Weight Distributions for Four Argonne Coals.

FIMS analysis experiments were done on the Zap Lignite and Illinois No. 6 coals. In addition, FIMS analysis of the Pocahontas coal was repeated at a higher temperature (500°C maximum instead of 450°C). A method was developed for reading the raw FIMS data obtained from SRI International directly into the SUN 3/260 computer on which the FG-DVC model simulations are done. This allows an easier comparison between experiment and theory.

Modeling

The modeling effort was very active during the past year. Improvements were made to the FG-DVC model and it was used to model pyrolysis data from the various reactors. Work was also done on comparing the FG-DVC model to the statistical model of Pugmire and Grant. Finally, work resumed on the viscosity model.

FG-DVC Model Improvements

A lot of work was done on studying the treatment of internal and external transport in the FG-DVC model during the past year. In addition, a sensitivity analysis was done on the various model parameters. Finally, the ability of the model to predict yield variations with heating rate for a bituminous coal was demonstrated. These efforts were undertaken partly to respond to reviewers comments made on the paper "A General Model of Coal Devolatilization" submitted to **Energy and Fuel**. A revised version of the paper was published (Solomon et al., 1988) and was included as Appendix A in the Sixth Quarterly Report.

In the case of the mass transport effects, it was decided that if the resistances were in series, the internal transport term was dominant in all of the cases that were studied and the external transport term was not needed. We also considered treating the resistances in parallel. However, in this case the surface concentration of tar needed for the external transport equation cannot be readily calculated. For this reason, and because the assumed (convective) mode of internal transport provides for transport out of the particle, it was decided to drop the external transport term for the time being. However, it is recognized that this may be needed for small particles.

The results of the sensitivity analysis can be summarized as follows. The model has eight coal structure parameters which must be determined for each coal from selected laboratory experiments. Once determined, these remain fixed for all experiments. The model also contains one adjustable parameter, ΔP , the internal pressure difference which drives the volatiles out of the particle. A sensitivity analysis shows that the volatile yield is most sensitive to the fraction of labile bridges, W_B , the crosslinking efficiency parameters $m(\text{CO}_2)$ and $m(\text{CH}_4)$, and, in some cases (low rank coals, low pressure), to ΔP . The monomer molecular weight distribution parameters, M_{avg} and σ , have only a weak effect on yields and tar molecular weight distributions. The initial molecular weight between crosslinks, M_C , and the initial oligomer length, L , affect the coal's solvent swelling ratio and extract yield but have little effect on the subsequent pyrolysis behavior.

Work was done on comparing the FG-DVC model to the statistical model of Pugmire and Grant at the University of Utah, which is based on percolation theory. The Utah model does not contain the transport or chemistry which we believe are relevant. The percolation theory, however, has some advantages in terms of computational efficiency when compared to the Monte Carlo method used in the FG-DVC model. However, we concluded that this efficiency advantage is lost if the tar transport is included, so we are staying with the Monte Carlo method.

A second version of the FG-DVC model was developed for reactors in which the tar is quenched after being evolved, such as in a heated grid reactor. This

version is being used for the simulations of the TG/FTIR and FIMS experiments, while the previous version is used in the simulations for the entrained flow reactor (EFR), in which the tar continues to react to form light gases after being evolved. The models to describe gas phase cracking of hydrocarbon volatiles and equilibrium of CH_4 , H_2O , CO , H_2 and CO_2 , which were developed under previous DOE projects to work with the FG model (Serio, et al., 1987) were added to the FG-DVC model.

The creation and loss of methyl groups in the DVC model due to bridge breaking and in the FG model due to methane formation was made consistent so that both parts of the model are in agreement. In addition, further improvements were made in regard to the crosslinking coefficients for CO_2 and CH_4 . Previously, the crosslinking coefficients for CO_2 and CH_4 were chosen to be 1.0 and 0.75, respectively, based on the amount of each gas species evolved from both the char and tar. Since the CO_2 and CH_4 evolved from tar make no contribution to crosslinking, the modified code now takes the crosslinking coefficients of both CO_2 and CH_4 as unity and only counts the part of these gases formed from char as being responsible for crosslinking in the char.

Due to the statistical nature of the Monte Carlo method, the tar molecular weight distributions predicted by individual runs of the FG-DVC simulation often show a noticeable fluctuation. To eliminate the statistical fluctuations, the FG-DVC code has been modified so that the code can be run continuously for as many times as designated without interruption and the tar molecular weight distributions are automatically summed up and averaged over these runs.

FG-DVC Model Applications

The FG-DVC model was used to model baseline pyrolysis data for the eight Argonne coals from three reactors (entrained flow reactor (EFR), TG-FTIR, and Field Ionization Mass Spectrometry (FIMS)). Elemental and ultimate analysis data are given for the eight Argonne coals in Table II.A-1. The conditions for the three reactor systems are shown in Table II.A-2.

Determination of Parameters for the FG-DVC Model - The FG-DVC model contains several parameters, some of which depend on the coal and one which depends on the experiment type. The large number of parameters has been criticized by some. However, it should be pointed out that the model is able to predict a large number of pyrolysis phenomena such as the yields of individual gas species, the yields of tar and char, the tar molecular weight distribution, the crosslink density and the viscosity. The model also accounts for the variation of these quantities with temperature, heating rate, residence time, and pressure in a manner that agrees well with experiment. The details of the model inputs and a sensitivity analysis are included in a recent paper (Solomon et al., 1988).

The first step is to obtain elemental analysis data for C, H, N, O, and S. This is needed to construct a coal composition file. The next step is to determine the amounts of the individual functional group (FG) pools (CO_2 -extra loose, CO_2 -loose, CO_2 -tight, CH_4 -loose, etc). This requires data from at least two standard pyrolysis experiments. The first is a slow heating pyrolysis experiment, like the TG-FTIR experiment, which can provide good quantitative gas yields and differential evolution curves. This type of experiment is best able to resolve the individual loose, tight, etc. pools for a given gas, especially when both the integral and differential curves are compared with the model predictions. The values of the FG pools so determined are checked against a second pyrolysis experiment done at high heating rates, such as the EFR 1100°C data. The pools are adjusted to simultaneously fit the low and high heating rate experiments. This usually involves a series of iterations.

Table II.A-2. Conditions for Experiments with the Argonne Premium Coals in Three Reactors.

Reactor	Temperature (°C)	Heating Rate °C/s	Hold Time s	Pressure atm
TG-FTIR	900	0.5	0	1
EFR	700, 1100, 1400	5000	0.5	1
FIMS	500	0.05	0	0

This procedure has been followed for the eight Argonne coals and the results are shown in Fig. II.A-8 for the major FG pools, which are CH₄, CO₂, H₂O, and CO. These values have not yet been fully optimized and may change slightly in the future, but give good agreement with experiment, except in the case of H₂O where the data are scattered. The oxygenated species show a systematic increase with decreasing rank, while the opposite trend is observed for CH₄.

Once the functional group pools have been established to allow a good match between the integral and/or differential yield curves for two pyrolysis experiments, the input parameters for the DVC (tar formation) part of the model are determined. The first step is to adjust the average oligomer length to match the coal extract yield. The next step is to adjust the number of unbreakable bridges ("hard" bonds) between monomer clusters to fit the experimentally observed tar yields for the same low and high heating rate experiments used to calibrate the functional group pools. The relationships between these input quantities and the experimentally measured quantities are shown in Fig. II.A-9. The extract yield data (which were obtained from Professor Milton Lee at Brigham Young University) and the average oligomer length are inversely correlated. The same is true of the number of hard bonds and the tar yield. Again, these values have not been fully optimized and are subject to change.

Other parameters which go into the tar formation model are the average monomer molecular weight (M_{avg}) and the average molecular weight between crosslinks (M_c). The value of M_c is interpolated from the literature data of Nelson (1983). We eventually plan to use literature data for M_{avg} as well. However, the size of the average cluster varies significantly among different research groups and the reported rank variations are not systematic or clearly understood. Currently, we are using a value of 256 for all the coals except the Pocahontas where a value of 506 is used. The significantly higher average cluster size for the Pocahontas compared to the others is supported by the calculations of Gerstein et al. (1982) based on NMR, FT-IR and elemental analysis data obtained for a number of coals.

The last important parameter to be selected is the value of ΔP , which is the average pressure difference between the ambient and the particle's interior during pyrolysis. This parameter is used in the internal transport model. The choice of ΔP has a significant effect on tar yield and the tar molecular weight distribution for non-softening coals under most conditions except high pressure. For fluid coals, a value of $\Delta P = 0$ is a good approximation for pressures of one atm or higher. The sensitivity of the model to the choice of ΔP is discussed in a recent paper (Solomon et al., 1988). This is the only parameter in the model which is adjusted for each type of experiment. The original FG model also had a fitting parameter, X_0 , which was used to match the final tar yield to account for differences in particle size, heating rate, bed depth and reactor geometry (Solomon et al., 1988). While it can be said that we have traded one adjustable parameter, X_0 , in the FG model for another, ΔP , in the FG-DVC model, this is not exactly true as the latter model is much richer in its ability to predict a variety of pyrolysis events. The values of ΔP are more restricted than X_0 and have a more fundamental basis that it is related to the coal's viscosity.

The use of the FG-DVC model involves several constraints: 1) Where experimental data are available on the starting coal, such as for the molecular weight between crosslinks (M_c), the extract yield, or the elemental analysis, they are used as inputs. Additional information will be incorporated as it becomes available. 2) The kinetic parameters for the evolution of the FG group pools are assumed to be invariant with coal type. 3) The amounts of the FG pools are constrained to fit data from experiments at very low (0.5°C/s) and very high (5000°C/s) heating rates. This results in a model which is very robust in its ability to fit pyrolysis data over a wide range of conditions. It is also true

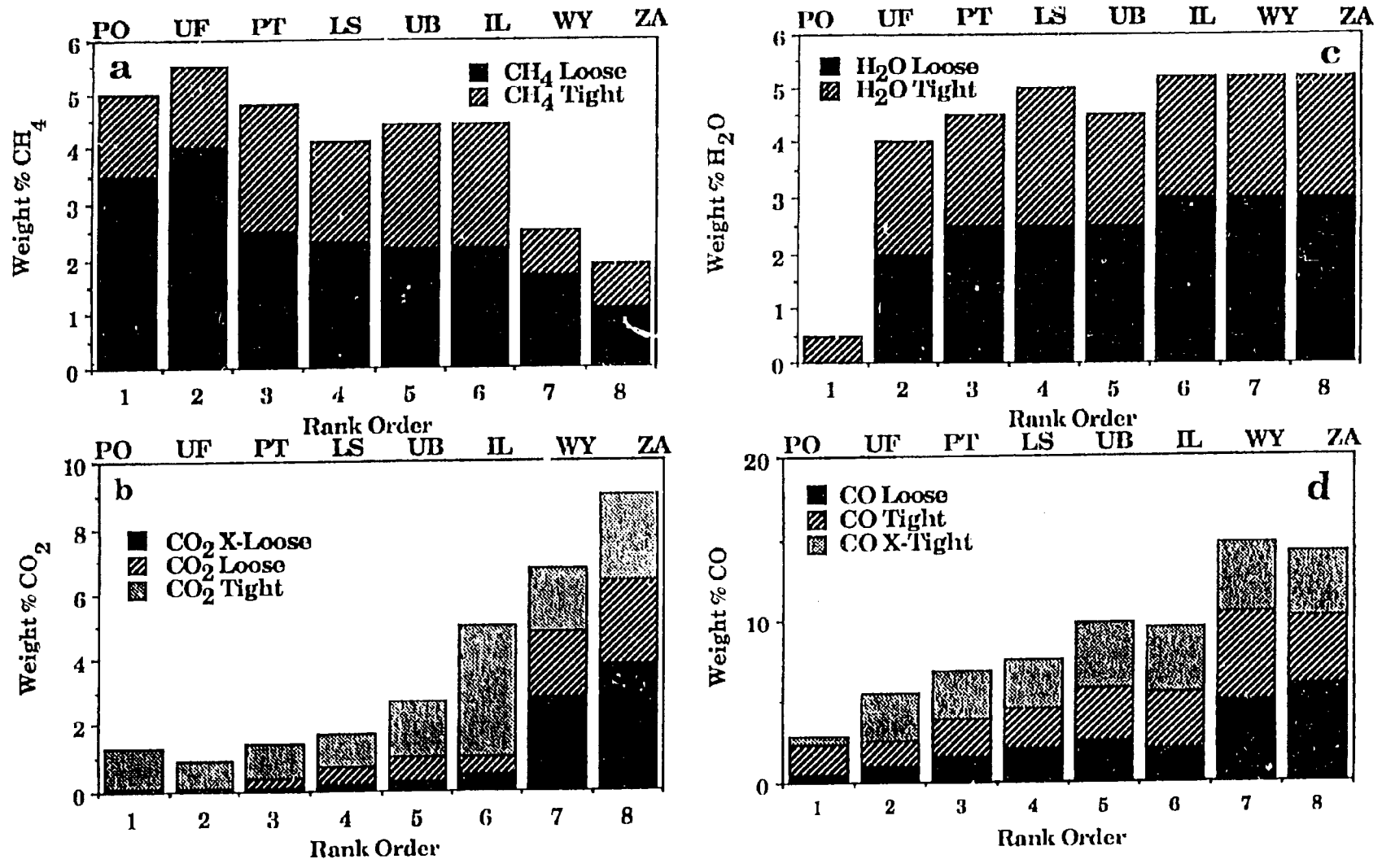


Figure II.A- 8. Variation of Functional Group Pools with Rank Order.

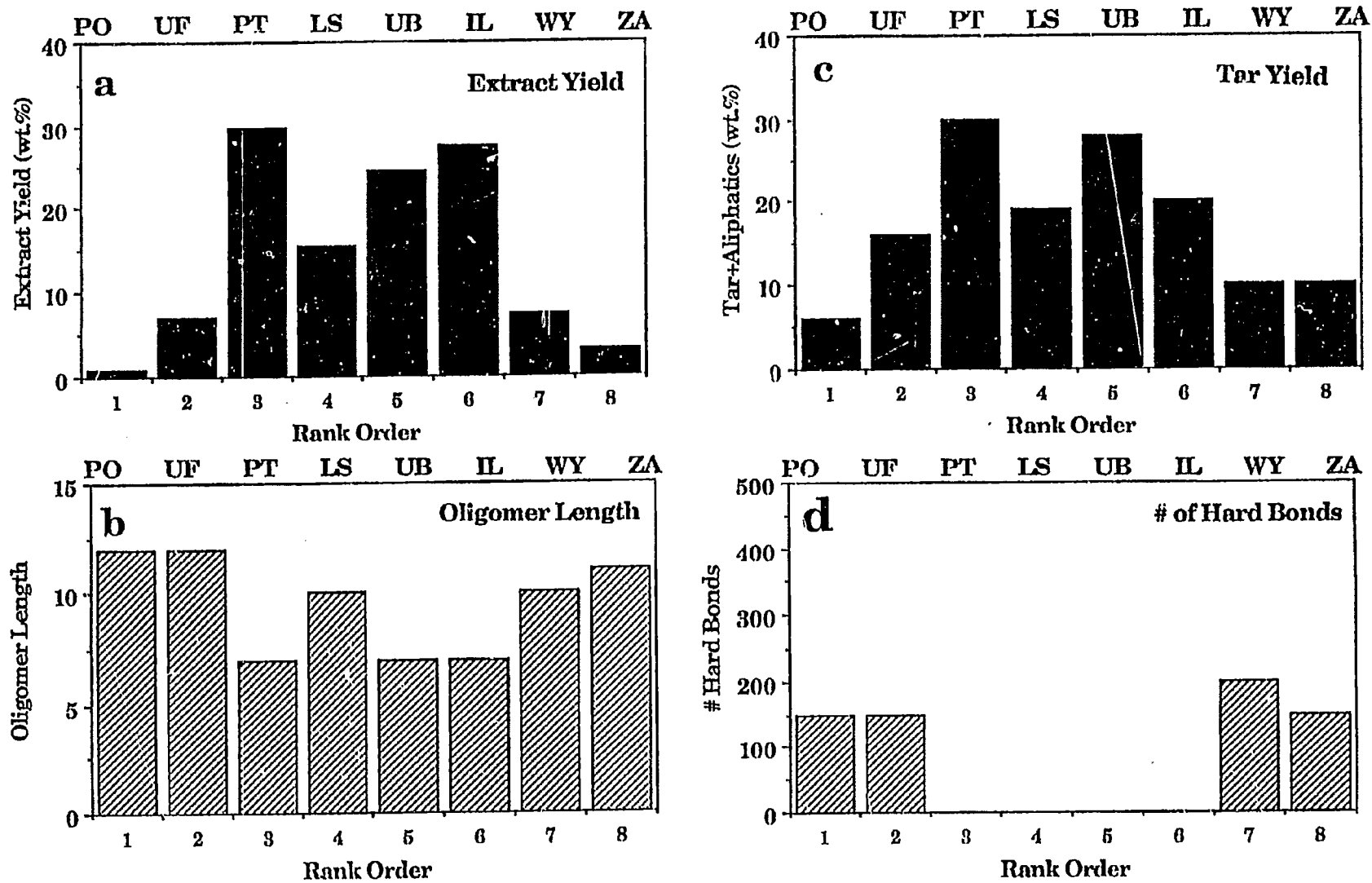


Figure II.A-9. Variation of DVC Parameters with Rank Order.

that when enough coals have been studied, a detailed calibration of the model may not be needed and perhaps the elemental analysis, the particle size and the reactor conditions will be sufficient.

Comparison of Model with Experimental Data - The FG-DVC model predictions are compared with experimental data in Figs. II.A-10 to II.A-17. Figures II.A-10 and II.A-11 compare the predictions with differential data from the TG-FTIR experiment for CH₄ and CO, respectively. In general, the agreement for CH₄ is very good. The kinetics for CH₄ loose appear to be somewhat too fast for the high rank coals. This could be fixed by making the kinetics rank dependent. In the case of CO evolution (Figs. II.A-11) the CO extra-tight rate needs to be increased slightly to match the high temperature CO evolution. In Fig. II.A-12, the integral weight loss curves are compared with the model predictions and are in fairly good agreement.

The model is compared with experimental yield data from all three reactors in Figs. II.A-13 and II.A-14. Except for H₂O, the agreement of the model is generally quite good over a wide range of extents of pyrolysis and for what is a wide range of coal types. In Fig. II.A-15, the model predictions and experimental data for C₂H₄, paraffins, and olefins are compared with and without the gas-phase hydrocarbon cracking model turned on for EFR experiments at 1100°C. It can be seen that this model significantly improves the prediction of C₂H₄ yields. In Fig. II.A-16 the model predictions and experimental data for CO, H₂, and the \sum CH₄ + CO₂ + H₂O for EFR experiments at 1400°C are compared with and without the equilibrium model turned on. It can be seen that at 1400°C, the volatile products are close to being in thermodynamic equilibrium. A comparison is made between the tar molecular weight distributions measured by FIMS and the predicted values in Fig. II.A-17. The model predicts rank dependent phenomena, such as the steep drop off in the distribution for the low rank coal due to crosslinking events (Solomon et al. 1988).

Literature Review of Pyrolysis Data

In order to refine the combined kinetic/mass transport model used for tar in the FG-DVC model, a search was made of literature pyrolysis data obtained for the Pittsburgh Seam bituminous coal. Data from several wire grid experiments with this coal were entered into a spreadsheet program so they could be converted to the same basis and plotted. When a comparison was made of data produced by heating at 1000 K/s to various peak temperatures at one atmosphere pressure, it was found that the results from different investigators did not agree, even when obtained from the same laboratory. These comparisons are shown for the tar yield in Fig. II.A-18.

The difference in kinetic rates implied by these results is more than three orders of magnitude. An even wider variation in results is found when the literature data for weight loss is examined, as shown in Fig. II.A-19. Some of this variation can be attributed to differences in the actual heating profile when compared to the nominal 1000 K/s profile or differences between the various samples of Pittsburgh Seam coal. However, these effects could not account for much more than a factor of 10 in the discrepancies. The major reason for these differences must be the lack of a direct measure of the coal particle temperature. The thermocouple (TC) only infers the actual coal temperature and it can be affected by the local coal loading and the installation, both of which determine how well the TC is coupled to the coal sample.

The results for the tar kinetic rates implied by these investigators can be summarized in an Arrhenius plot, shown in Fig. II.A-20. The capital letters are estimates for the tar evolution rate obtained by fitting a first order model to the data and evaluating the rate at the temperature where one-half of the tar has evolved. The other data points were obtained at AFR from experiments on a variety

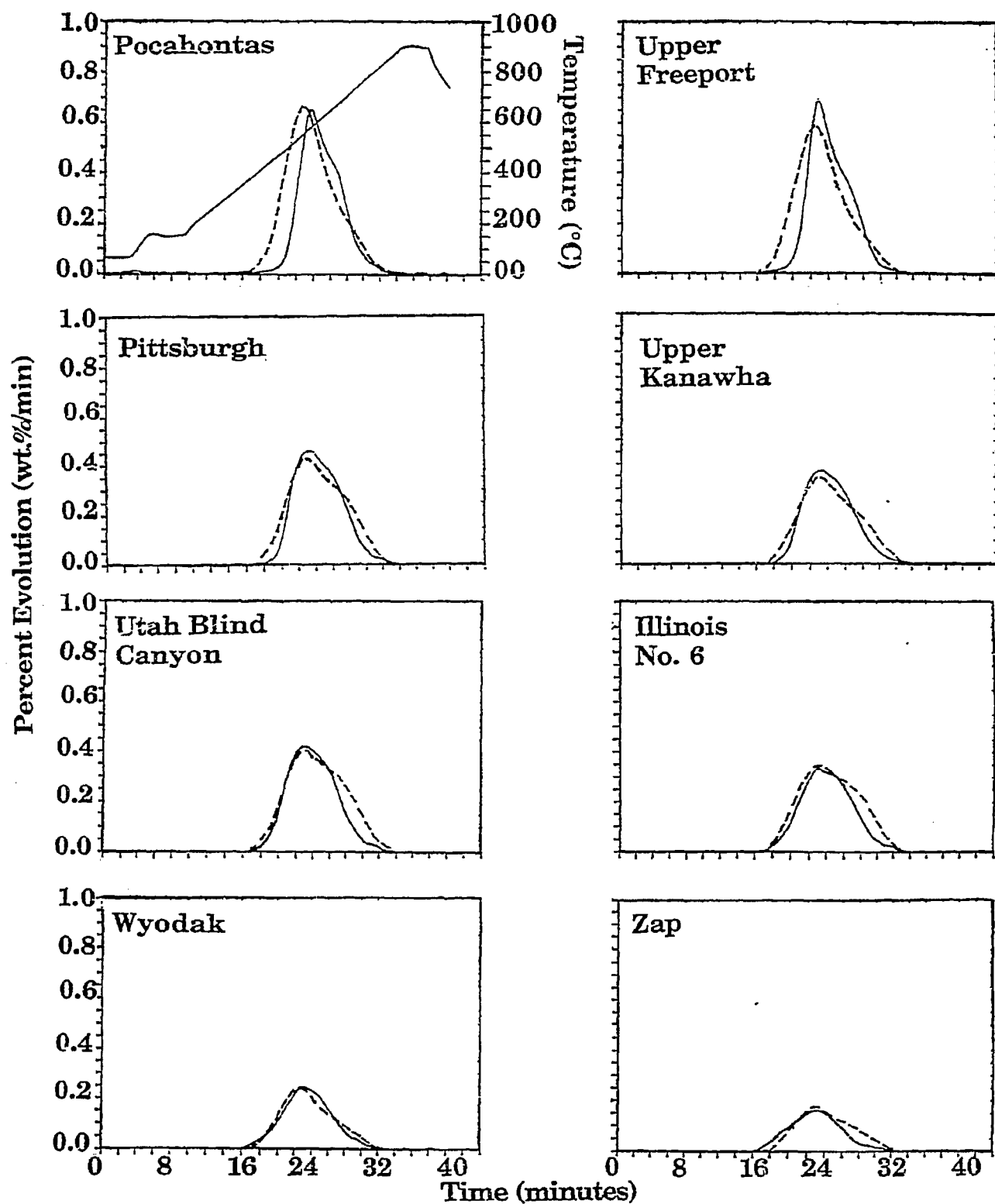


Figure II.A- 10. Comparison of FG-DVC Model Predictions (dashed lines) and Experiments (solid lines) for the Evolution Rate of CH₄ from the Eight Argonne Coals in a TG-FTIR at 0.5°C/s.

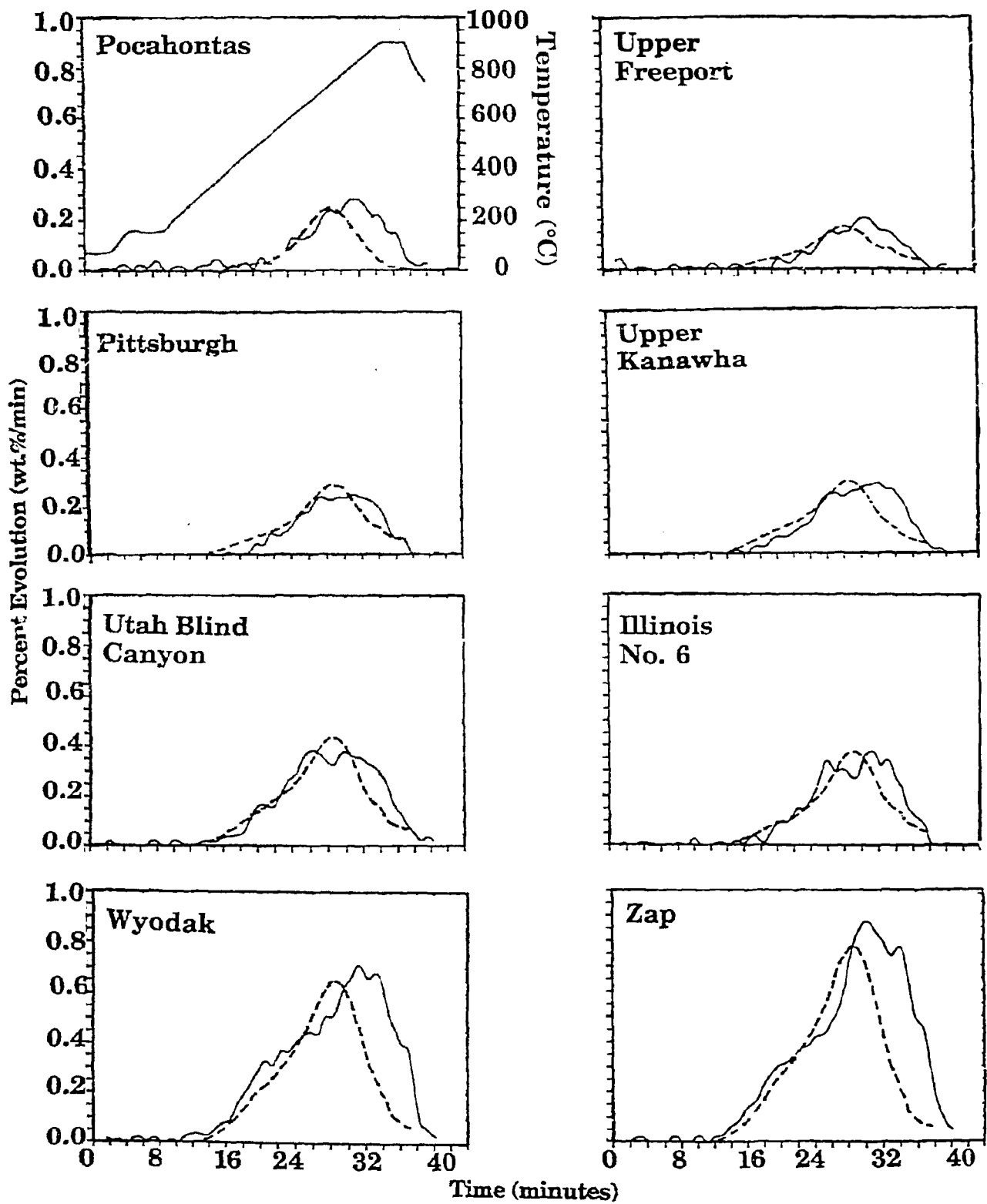


Figure IIA-11. Comparison of FG-DVC Model Predictions (dashed lines) and Experiments (solid lines) for the Evolution Rate of CO from the Eight Argonne Coals in a TG-FTIR at 0.5°C/s.

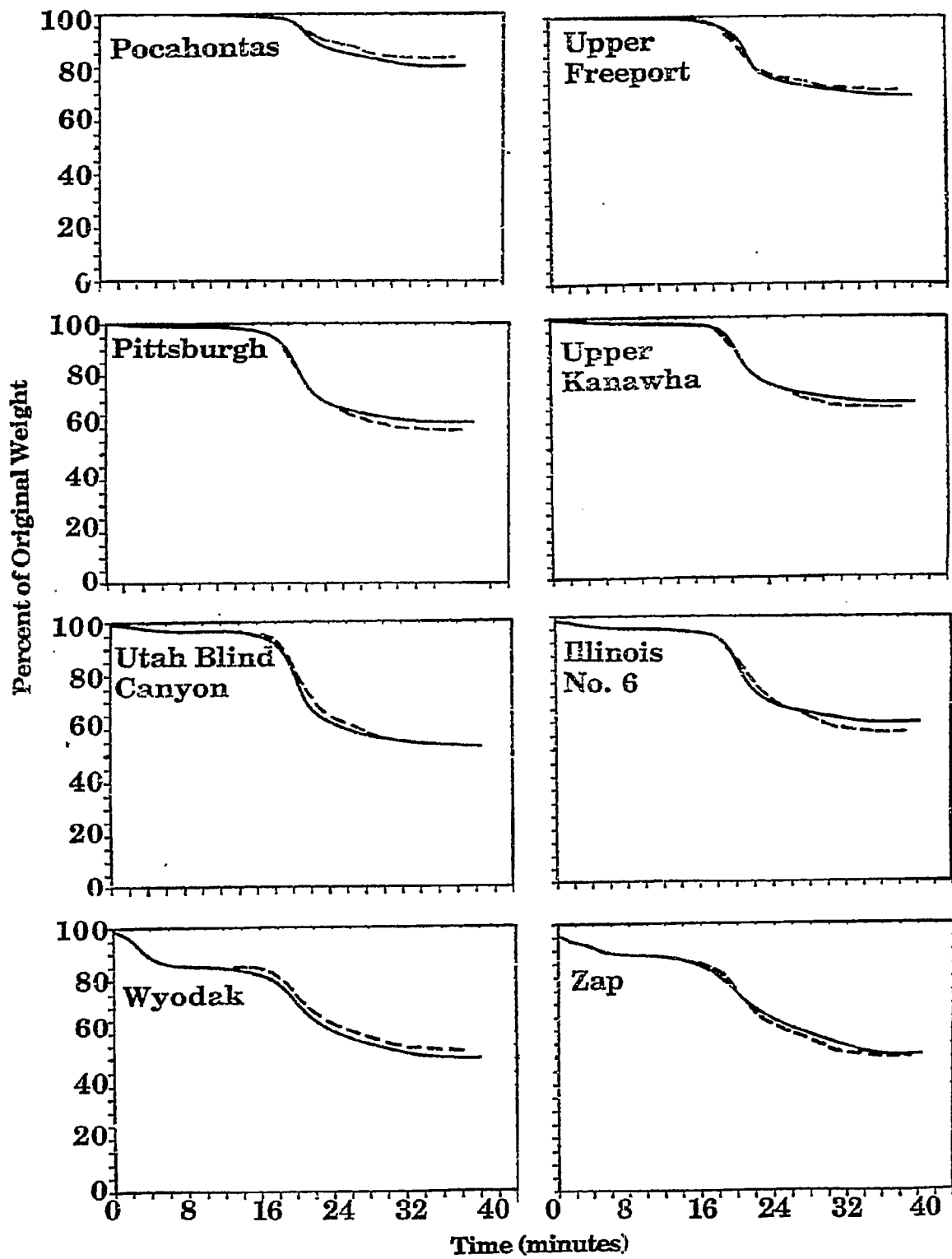


Figure II.A-12. Comparison of FG-DVC Model Predictions (dashed lines) and Experiments (solid lines) for Integral Weight Loss for the Eight Argonne Coals in a TG-FTIR at 0.5°C/s.

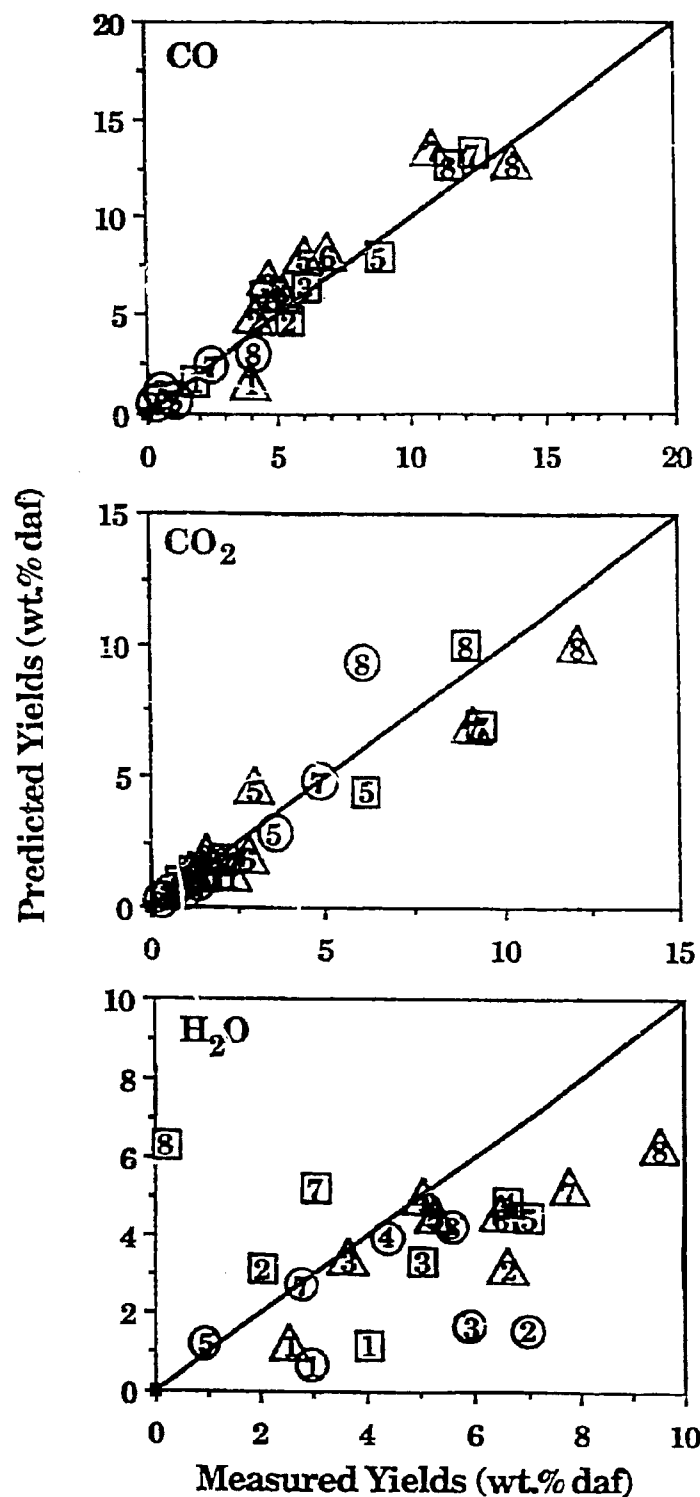


Figure IIA-13. Comparison of Model Predictions with the Data for the Yields of Oxygenated Species. The Numbers Refer to the Coal Type. The Symbols Around the Numbers Refer to the Reactor Type.
 ○ - EFR, 700°C; □ - EFR, 1100°C; △ - TG-FTIR; No Symbol - FIMS.

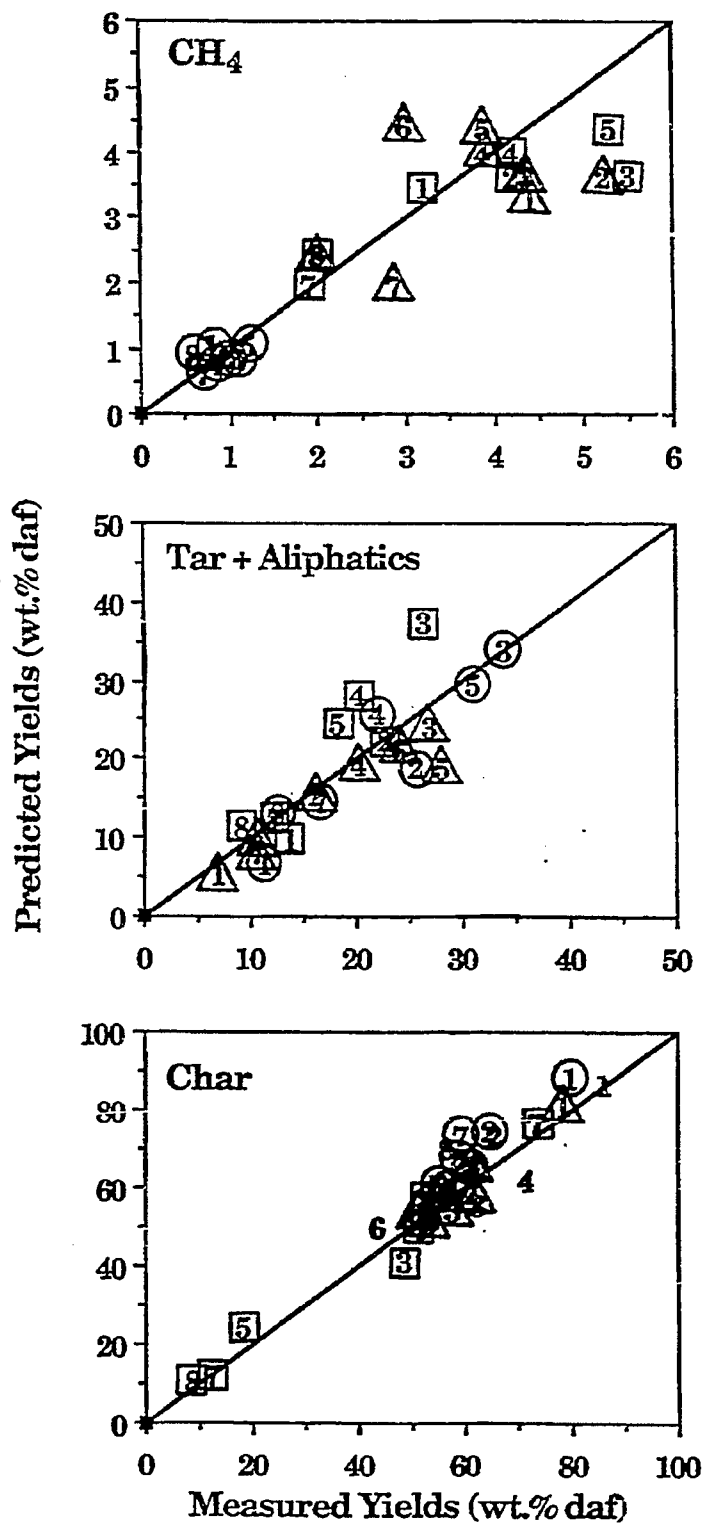


Figure II.A-14. Comparison of Model Predictions with the Data for CH₄, Tar Plus Aliphatics and Char. The Numbers Refer to the Coal Type. The Symbols Around the Numbers Refer to the Reactor Type. ○ - EFR, 700°C; □ - EFR, 1100°C; △ - TG-FTIR; No Symbol - FMS.

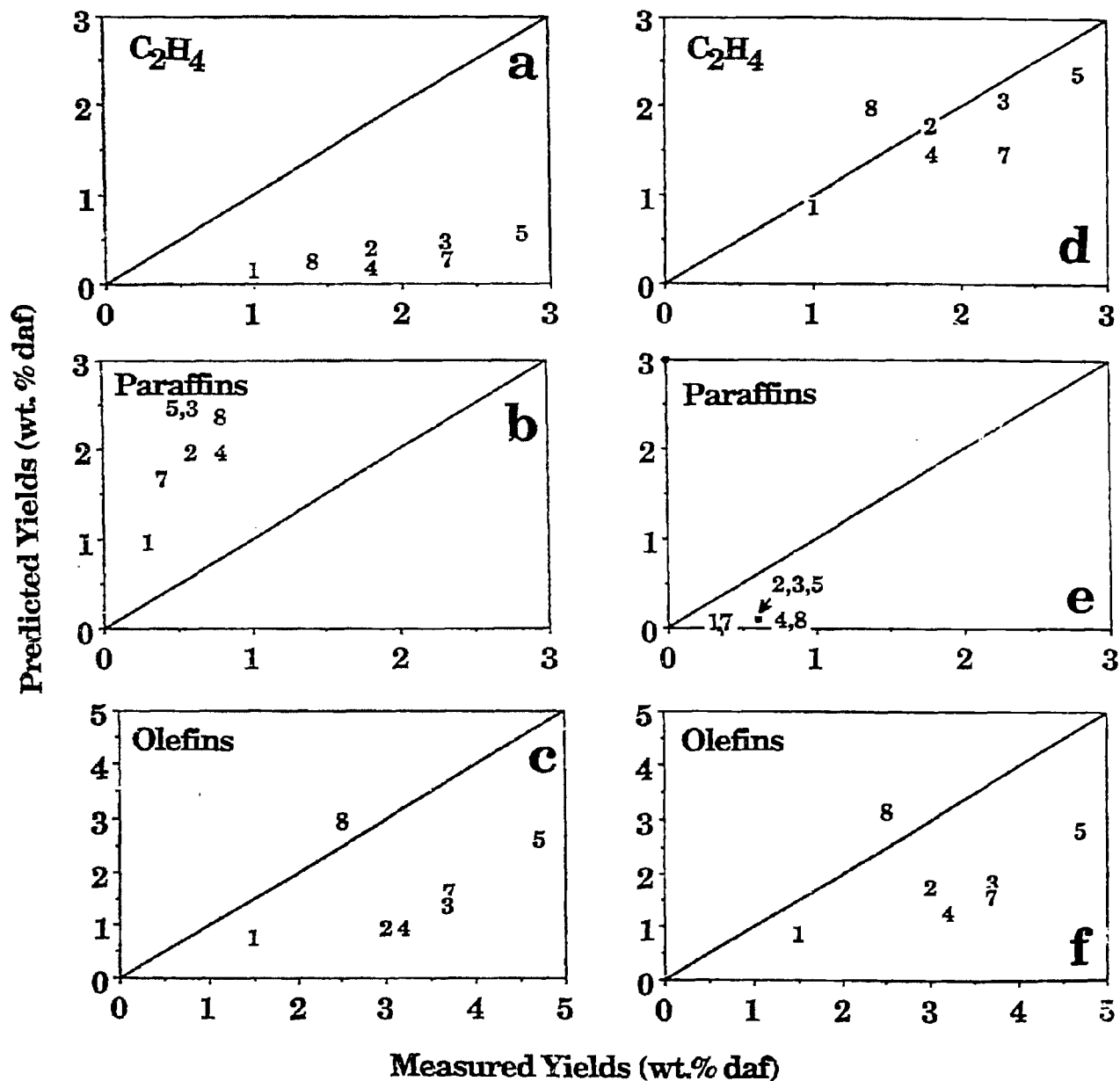


Figure IIA-15. Comparison of Model Predictions and Data for EFR Experiments at 1100°C. a-c) Without Hydrocarbon Cracking Model; d-f) With Hydrocarbon Cracking Model.

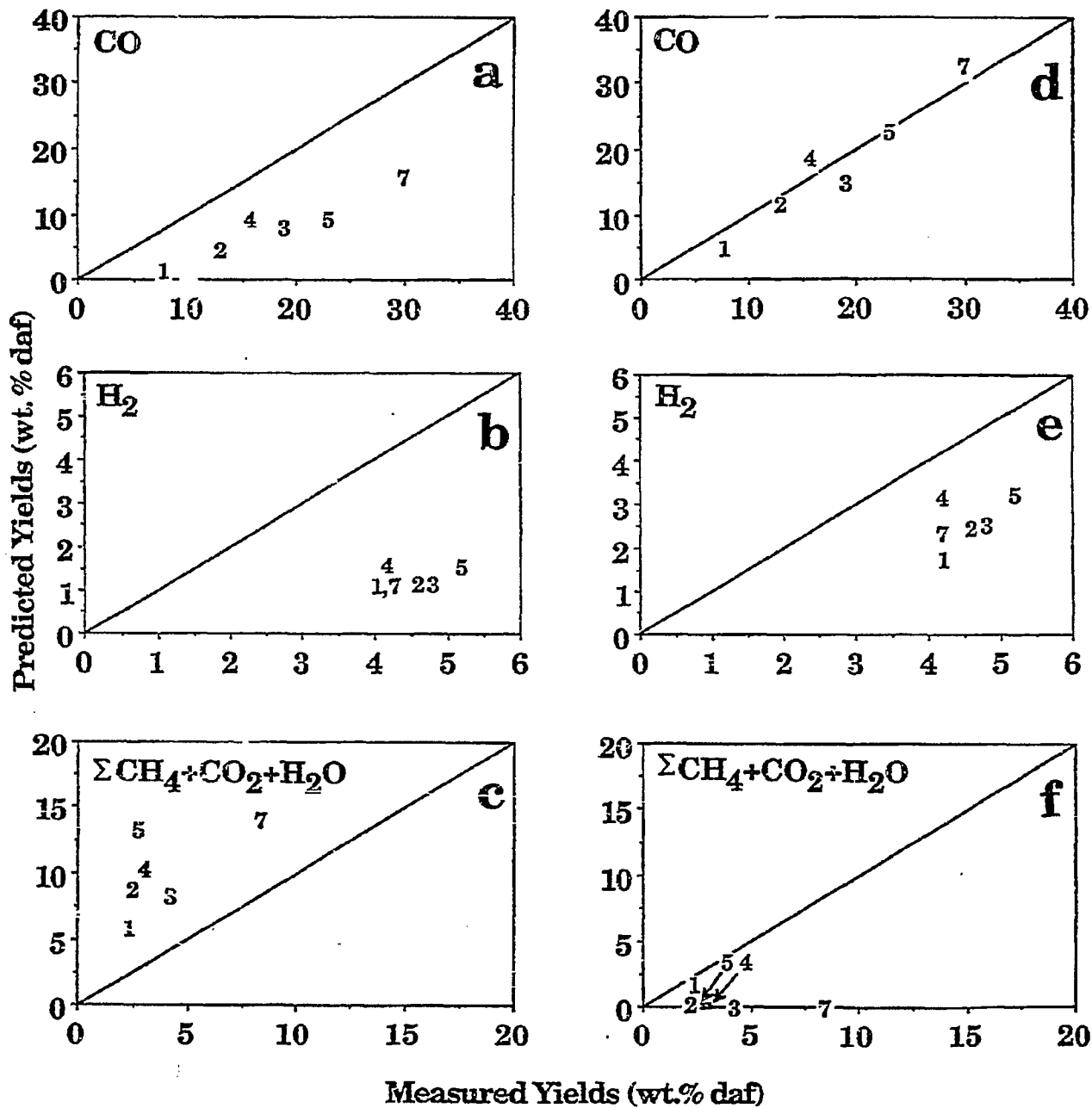


Figure IIA-16. Comparison of Model Predictions and Data for EFR Experiments at 1400°C. a-c) Without Equilibrium Model; d-f) With Equilibrium Model.

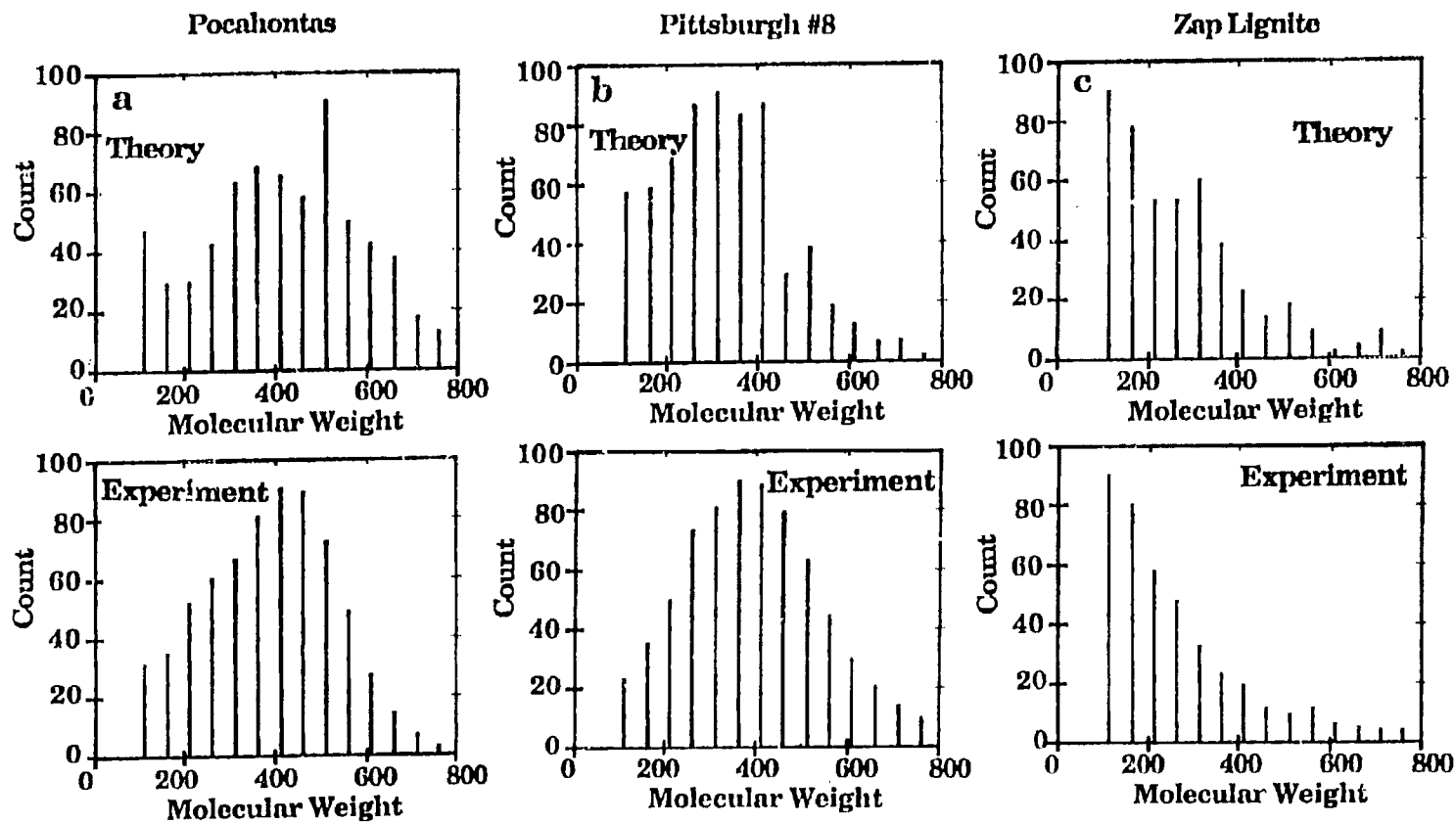


Figure II.A-17. Comparison of Measured and Predicted Tar Molecular Weight Distributions.

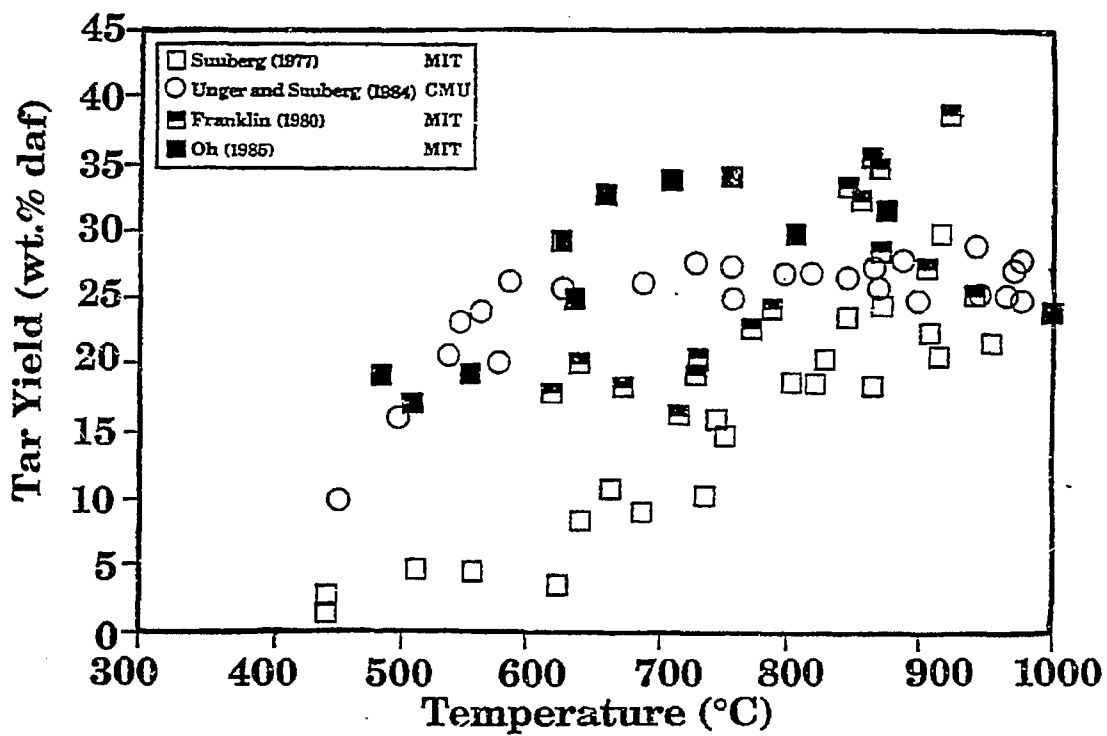


Figure IIA-18. Comparison of Experimental Tar Yield Data for Non-Isothermal Pyrolysis of Pittsburgh Seam Coal in a Heated Grid. Conditions: 1000 K/s, 1 atm, No Holding Time.

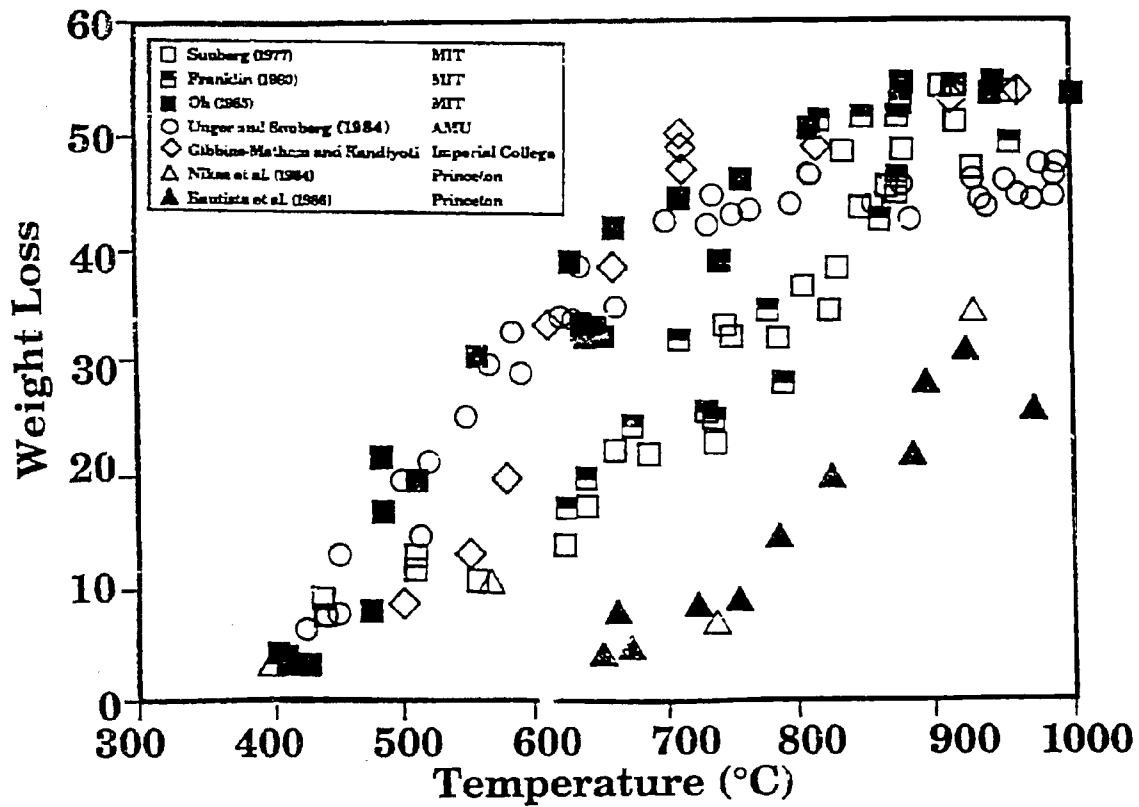


Figure IIA-19. Comparison of Experimental Weight Loss Data for Non-Isothermal Pyrolysis of Pittsburgh Seam Coal in a Heated Grid. Conditions: 1000 K/s, 1 atm, No Holding Time.

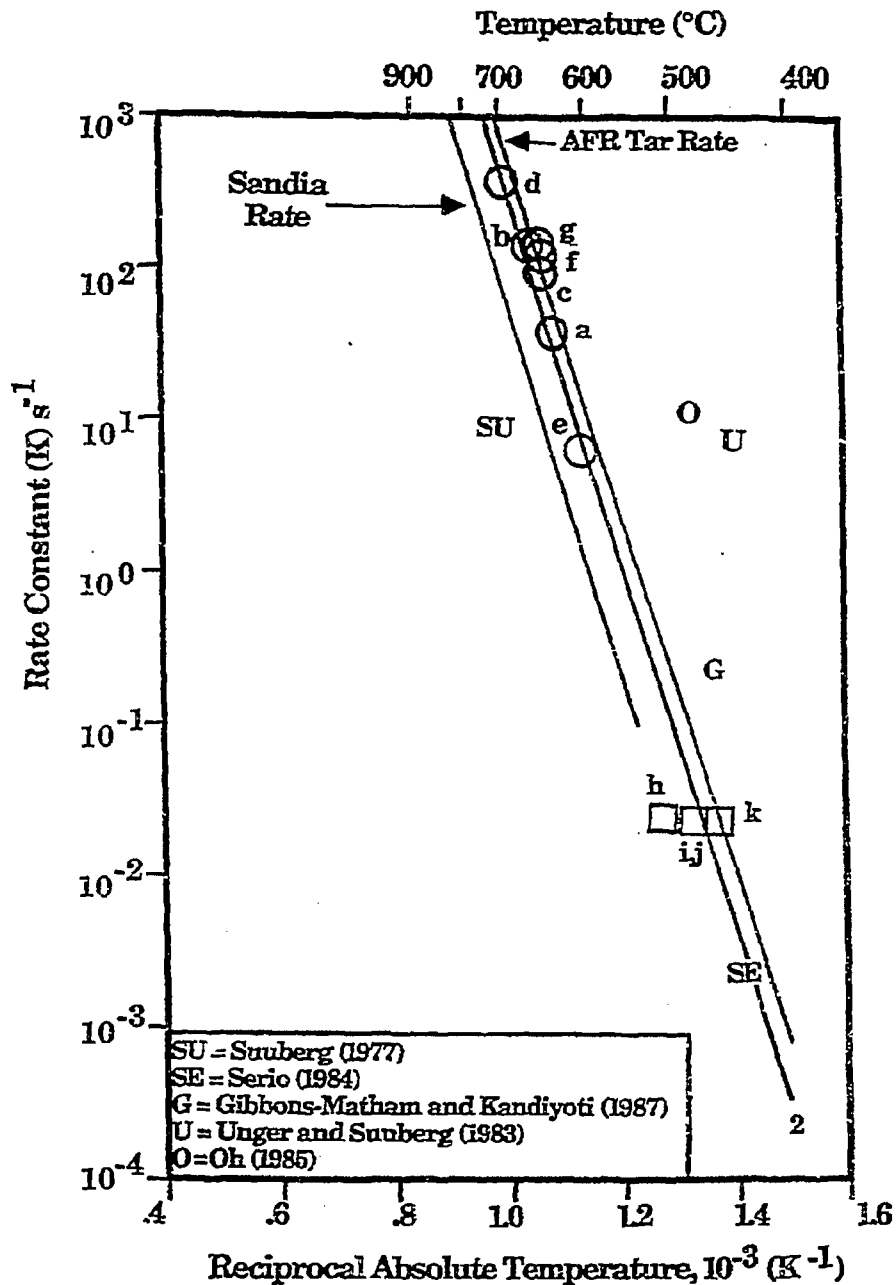


Figure IIA-20. Comparison of Kinetic Rates for Tar Evolution from Coal and Polymers. The Capital Letters are Estimates for the Apparent Kinetic Rate at the Reported Temperature for Reaching One-half the Total Tar Yield for Literature Experiments with Pittsburgh Seam Coal, as Discussed in the Text. The Number 2 Refers to the Tar Evolution Rate for Ethylene-Bridged (EB) Naphthalene Polymer. The Data Points are Rates for Tar Evolution from Experiments in the Heated Tube Reactor (HTR) (O) and TG-FTIR (\square). The Small Letters Next to Each Data Point Indicate the Coal Type and Experimental Conditions. The Experimental Conditions for the HTR Experiments are Given in Solomon et al. (1986). Coal Types were as Follows: North Dakota (Zap) Lignite (b,c,d,e,k); Montana Rosebud Subbituminous (a,f,i); Illinois No. 6 (g,j); Pittsburgh No. 8 Bituminous (h).

of coals at low and high heating rates. The solid lines represent kinetic expressions for tar evolution rates from experiments with model polymers and coal done at AFR or Sandia National Labs (Hardesty, 1988). The "AFR TAR RATE" appears to be in the middle of the spread in the literature data and is in good agreement with the data for ethylene-bridged naphthalene polymers. It is also in good agreement with recent results from Sandia National Lab. for pyrolysis experiments where particle temperatures were directly measured, as was the case in the AFR experiments.

We began an experimental and theoretical study into possible reasons for the variations in the literature data for the heated grid experiment indicated in Figs. II.A-18 to II.A-20, which we are doing in conjunction with Professor Eric Suuberg of Brown University. The focus of our investigation is currently the location, size and characteristics of the thermocouples used.

Coal Softening and Swelling

Swelling Experiments

During the past year, work was done on developing a drop tube furnace in which individual char particles could be studied at various stages of pyrolysis. The apparatus is designed to drop a dilute sample of particles without carrier gas into a preheated furnace. This geometry insures rapid heating of the individual particles to the furnace temperature. A schematic of the apparatus is shown in Fig. II.A-21.

The coal samples subjected to pyrolysis were of the 200 x 325 mesh sieved fraction of Pittsburgh #8 bituminous coal. The experiments were done over a range of furnace temperatures from 450 to 700°C. Samples were dropped into the 2" 16 x 22" long radiation cavity from a gas cooled vial having a 200 mesh screen as a cap. The 200 mesh screen limited the number of particles entering the cavity with each shake or injection and thus prevented agglomeration. Prior to particle injection, the system was purged with nitrogen through upper and lower inlets. Immediately before particle injection the lower gas flow was shut off to allow the particles to free-fall through the tube. The chars were accumulated in a stainless steel collection chamber which was submerged in an ice bath to prevent further pyrolysis.

The TGA was employed to determine the amount of volatiles remaining in each of the chars collected. Char samples were heated in N₂ at 30°C/min to 900°C. The percent volatiles released (DAF) in the TGA is plotted in Fig. II.A-22a as a function of drop tube temperature. The results for sets of drop tube chars produced in the Fifth and Sixth Quarters are consistent. If a plot is made using the volatiles released by heating to 550°C, as shown in Fig. II.A.2b, the rapid tar loss that occurs in this temperature range is more evident.

Typical SEM micrographs of the collected chars are shown in Figs. II.A-23 to II.A-28. At 454°C, most particles are still angular in shape although some early stages of surface flowing and swelling are present. At 502°C, only a few particles still possess their angularity and cenospheres as large as 62 microns have formed. In some particles, bubble cells are observed. At 538°C, particles have begun to collapse and in the 558°C char case, the majority of particles have collapsed. The char particles must still be quite fluid at this point and must remain fluid as the gas inside the cenosphere cools. Cenosphere size cannot be determined at this point.

The collapsing of the cenospheres has not previously been observed, to the best of our knowledge. In most previous studies, the furnace temperature has been

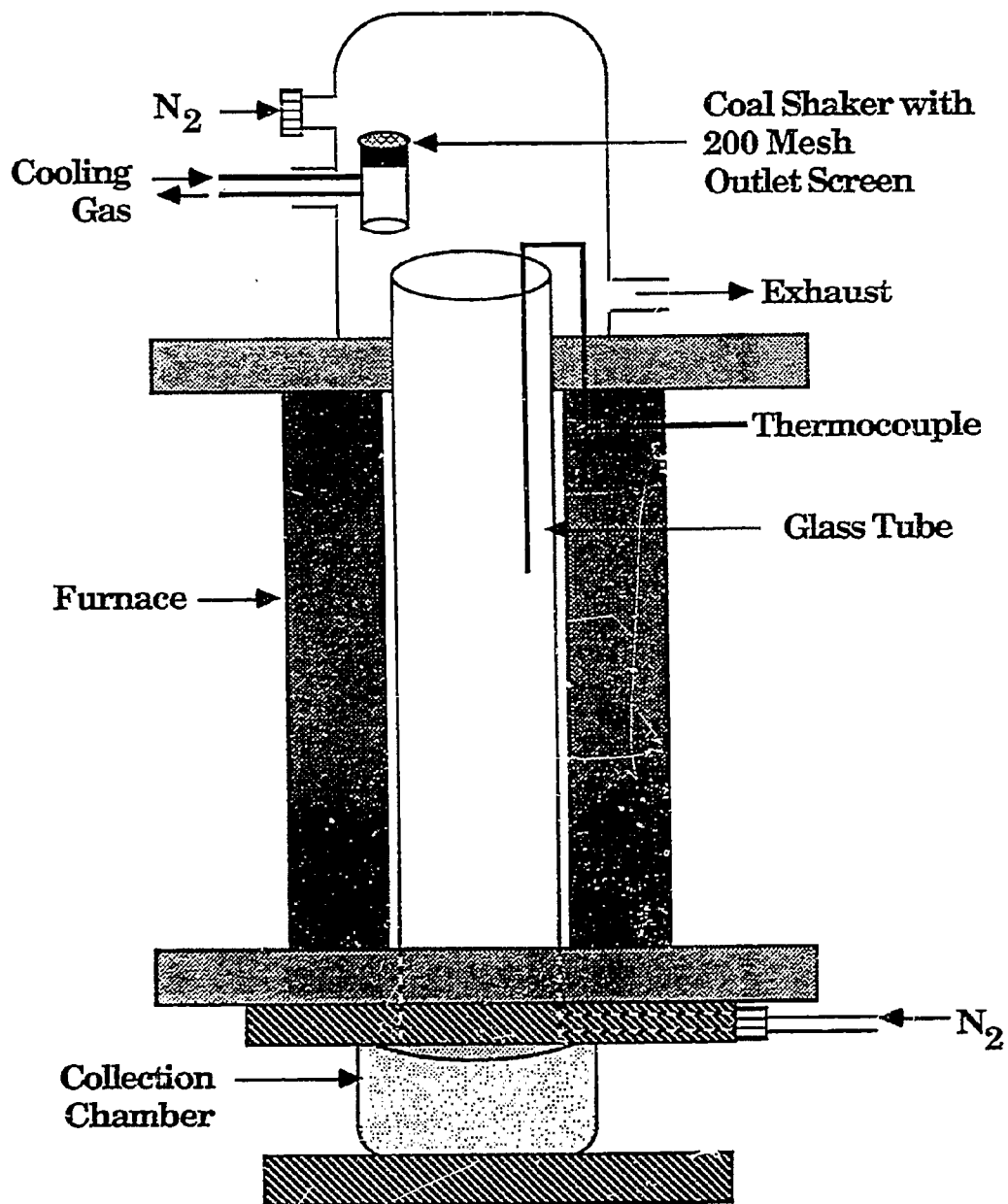


Figure IIA-21. Schematic Diagram of the Drop Tube Furnace.

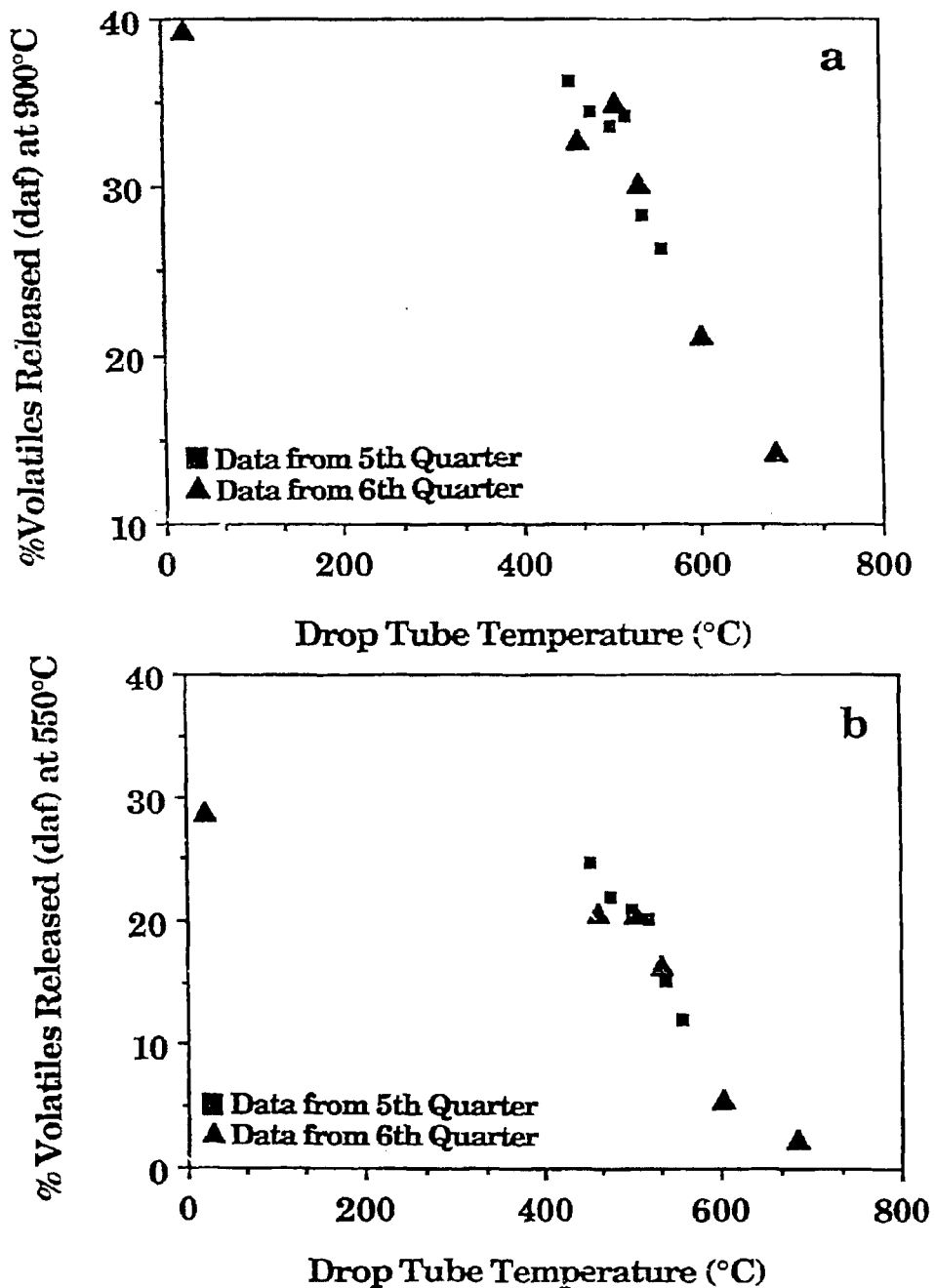


Figure II.A-22. Variation of Percent Volatiles Released (daf) for TGA Pyrolysis of the Chars Recovered from Drop Tube Experiments with Pittsburgh Seam Bituminous Coal. a) 30°C/min up to 900°C; b) 30°C/min up to 550°C.



Figure II.A-23. SEM Micrograph of a 454°C Drop Tube Char of Pittsburgh No. 8 bituminous Coal. Magnification: 300X.

Reproduced from
best available copy

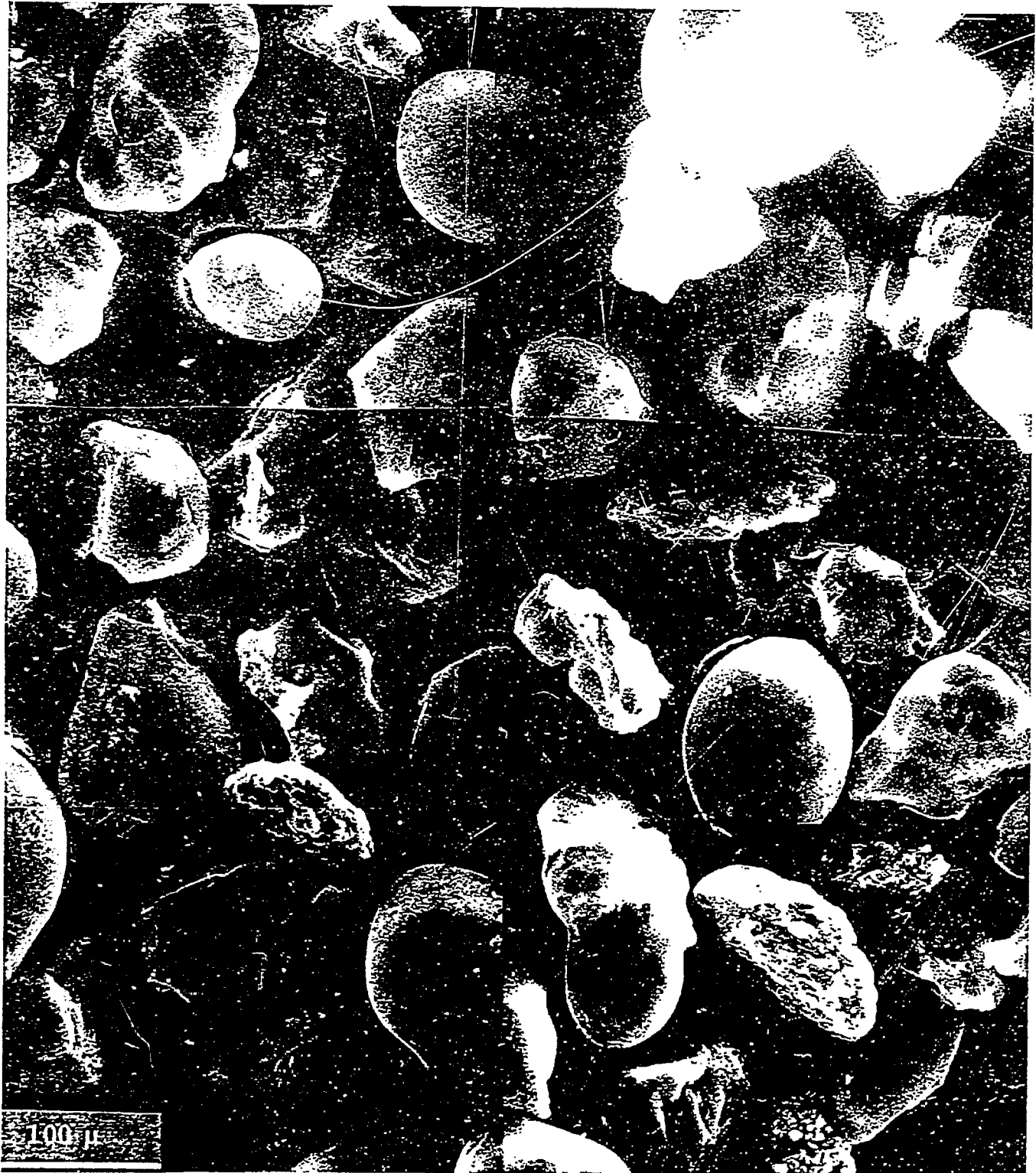


Figure IIA-25. SEM Micrograph of a 502°C Drop Tube Char of Pittsburgh No. 8 bituminous Coal. Magnification: 200X.

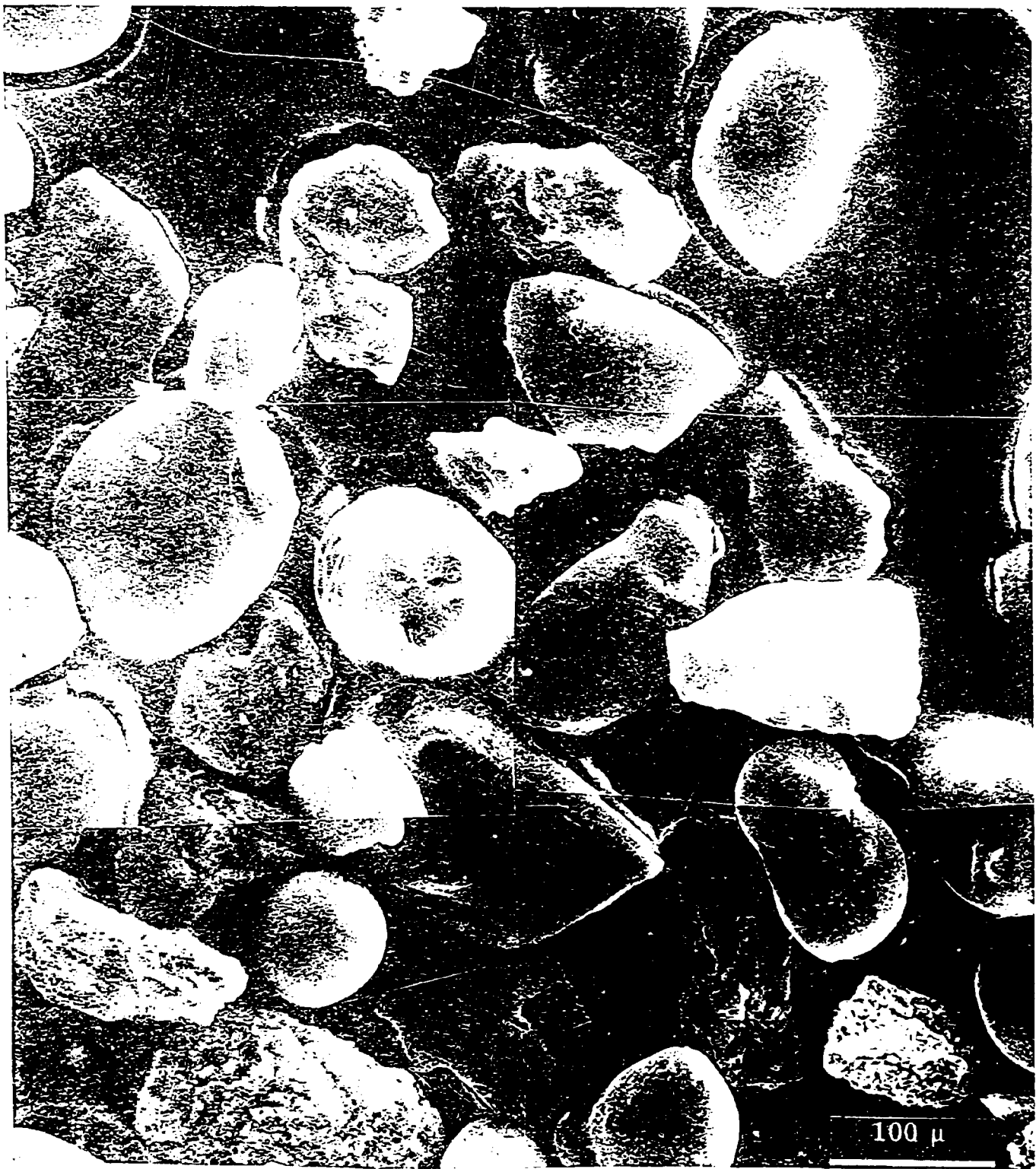


Figure 11. A-26. Section of plant tissue showing cellular structure. Scale bar = 100 μ.

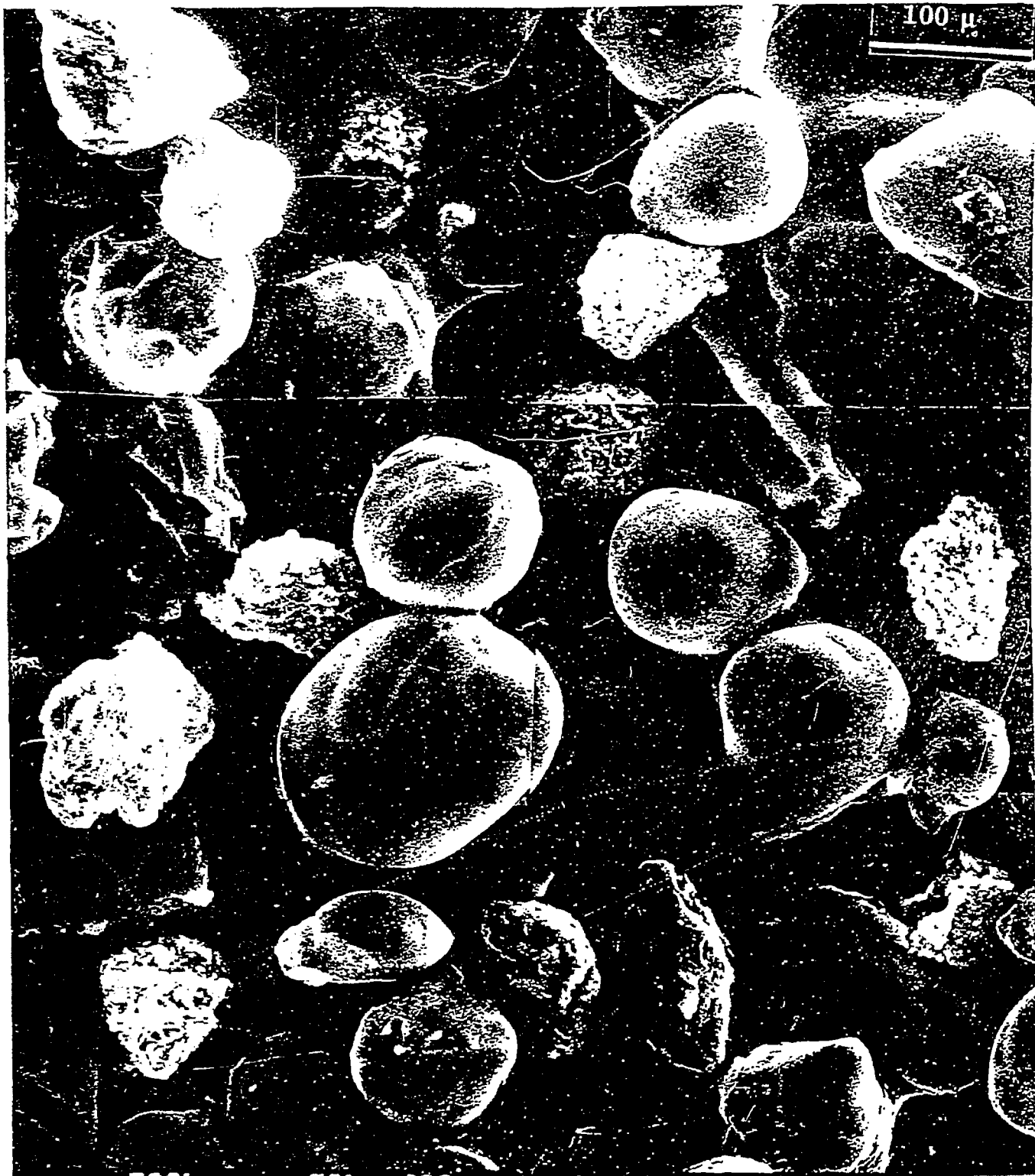


Figure II.A-27. SEM Micrograph of a 50% C Drop Tube Char of Pittsburgh No. 8 Bituminous Coal. Magnification: 300X

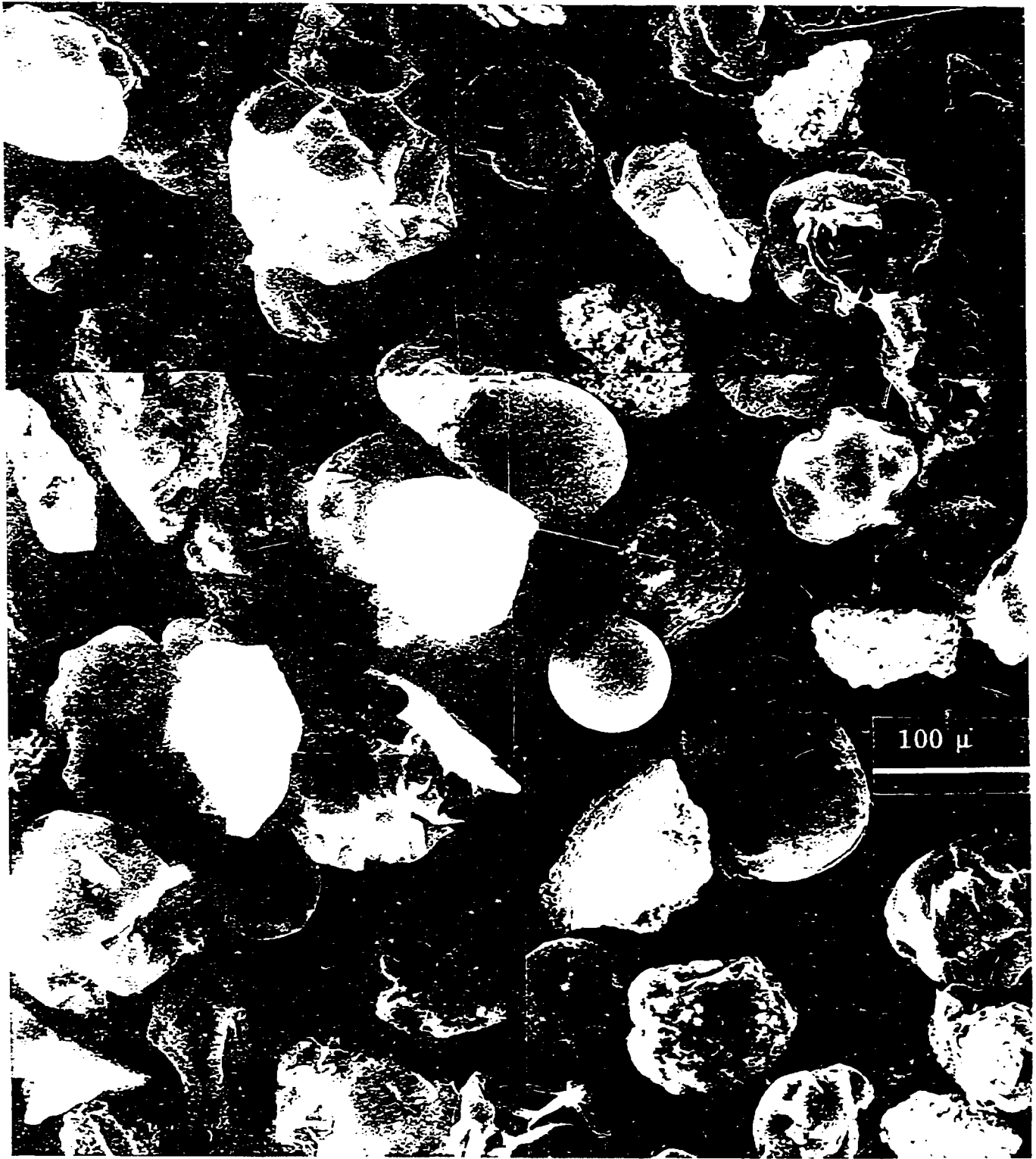


Figure II.A-28. SEM of *Staphylococcus aureus* cells. Magnification: 1000x. Scale bar: 100 μ.

700°C or higher. Under these conditions, the particle may go through its fluid phase and start to solidify prior to being cooled in the collector. The reason for the collapsing particles will be studied further.

The SEM was employed to obtain both external (Figs. II.A-23 to II.A-28) and internal (Figs. II.A-29) micrographs of the low temperature char particles. In order to micrograph the internal structure, the char particles were first subjected to potting and "cutting". This technique involved mixing approximately 20 mg of char sample and 1-2 ml of LR White hard grade acrylic resin in micron embedding mounts. With continued stirring, less than one drop of LR White accelerator was added to quicken polymerization. The potted samples were cured at 58°C for a twenty-four hour period and "cut" with a single edged razor blade.

Examination of the external micrographs suggests that three different pyrolysis pathways exist. Particles seem to undergo either 1) rapid swelling and cenosphere formation at lower temperatures or 2) gradual surface flowing, swelling and cenosphere formation or, 3) no obvious swelling and lack cenosphere formation even at higher temperatures.

A possible explanation for the differences in char morphology could be due to the differences in maceral content. According to data obtained from Karl Vorres at Argonne National Laboratories, Pittsburgh No. 8 bituminous coal contains 7% liptinite, 85% vitrinite and 8% inertinite (Vorres, 1988). In lower rank coals where the properties of macerals differ, Richard Neavel describes the inertinite as being carbon rich when compared to the vitrinite of the same coal, and the liptinite as being comparatively hydrogen rich (Neavel, 1981). Experiments were recently done with pure macerals which support this explanation.

Figure II.A-29 displays the internal structures which the majority of the particles possess at various stages of pyrolysis. In Fig. II.A-29a, the particle is quite angular and has micropores of approximately one micron in diameter. In Figs. II.A-29b and II.A-29c, the particles have begun to lose their angularity and the micropores have begun to increase in size, forming bubbles ranging from approximately 5-15 microns in diameter. In Figs. II.A-29d and II.A-29e, the bubbles have both decreased in quantity and increased in diameter to as large as 85 microns. Finally, in Fig. II.A-29f, a hollow cenosphere of approximately 110 micron diameter has formed.

Viscosity Model

In the First Annual Report, a semi-empirical predictive model for the viscosity of heated coal was described. The model was to be the same as that published by van Krevelen for linear polymers (van Krevelen, 1976), and included dependencies on functional group composition, average molecular weight, temperature, and chain length, amongst other features. The data used to compare with the model was that of Fong (1986). van Krevelen's model, without adjustable parameters, gave values of viscosity too low by about four orders of magnitude. The major part of this discrepancy is now attributed to the application of a model established for linear chain polymers, to a situation in which crosslinking undoubtedly plays a major part. Nevertheless, there are features of van Krevelen's model which appear to have application to a broader array of fluids than molten linear chain polymers, and these will be adapted for our purposes. Specifically, the average molecular weight and temperature dependence features will be included while introducing an additional parameter to account for the "coalness" of the fluid. A value of that parameter has been established from comparisons of the results of model calculations with the experimental results of Fong, and it will be determined whether the new model can describe results from our own measurements.

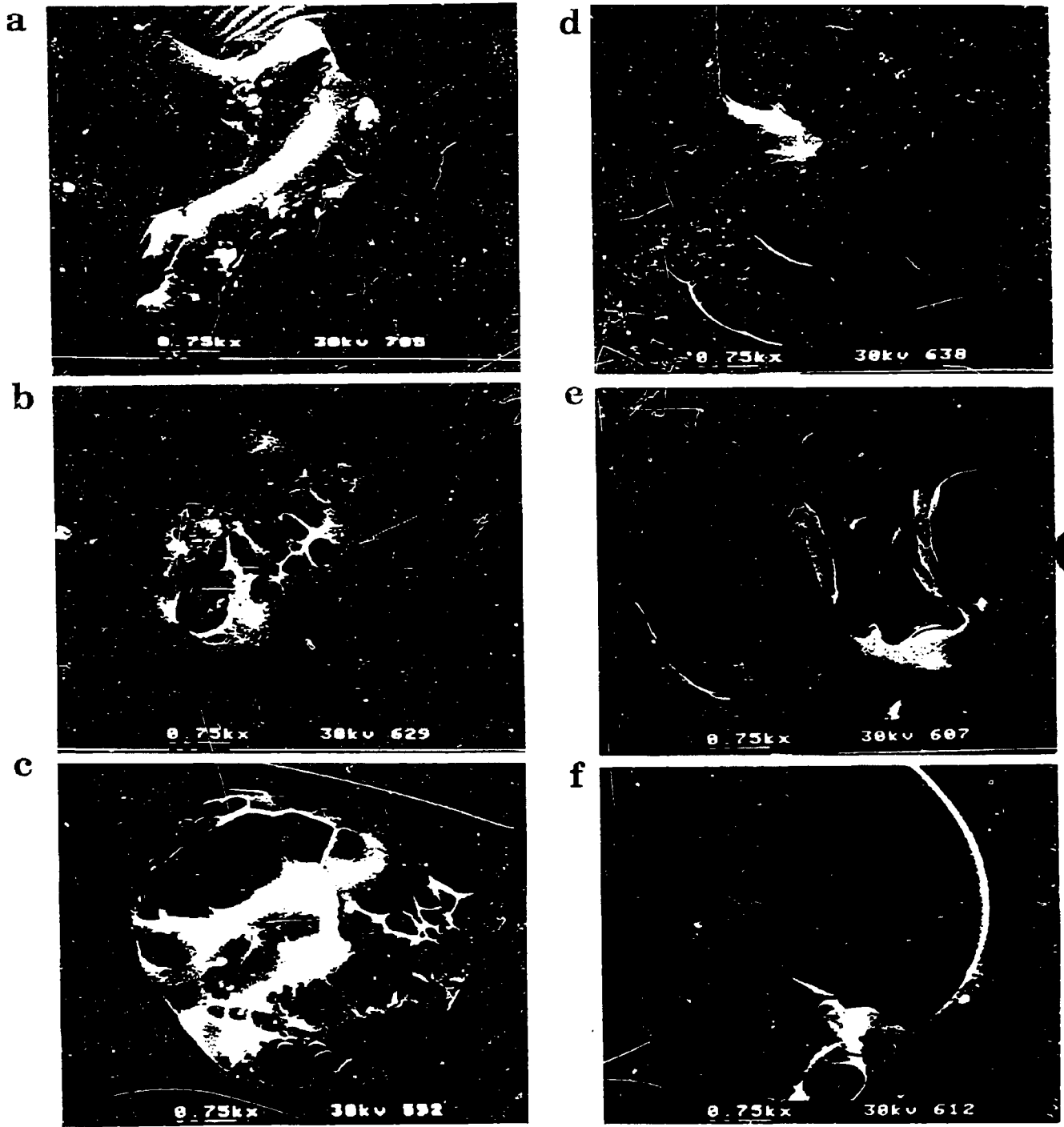


Figure IIA-29. Sem Micrographs of a) 454°C, b) 478°C, c) 454°C, d) 502°C, e) 538°C and f) 538°C, Drop Tube Chars of Pittsburgh No. 8 Bituminous Coal. Magnification: 75X.

Our initial measurements are not direct measurements of viscosity, but of char form and structure. An analysis which will provide relationships between these observations and viscosity is being performed.

The results of some earlier work on cenosphere swelling (Solomon, et al., 1983) are briefly reviewed here. In that research, a single bubble was considered, a cenosphere, under the influence of the contracting force of surface tension and the expanding force due to the pressure difference between the inside and outside of the cenosphere. The pressure difference arises from gas evolution from the pyrolyzing coal fluid, this gas being apportioned between inside and outside in the ratio of the corresponding surface areas. Gas diffusion from inside to outside of the cenosphere is also taken into account.

The above forces act against the resistance of viscosity, as described by Chiou and Levine (1978), giving rise to the following expression for the rate of change of the external radius of the cenosphere, r_2 .

$$dr_2/dt = \frac{r_1^3 r_2 (\Delta P_t)}{4\eta (r_2^3 - r_1^3)} \quad (\text{II.A-1})$$

where r_1 is the internal radius of the cenosphere, η is the viscosity, and ΔP_t is the effective outward pressure difference across the cenosphere wall, consisting of surface tension and real differential pressure as described above.

$$\Delta P_t = \frac{n_t RT}{(4\pi/3)r_1^3} - \sigma(1/r_1 + 1/r_2) \quad (\text{II.A-2})$$

where n_t is the total excess tar and gas within the cenosphere, R is the gas constant, T absolute temperature, and σ is the surface tension.

For moderate heating rates of coal, it is believed that there is a fairly well defined sequence of events during pyrolysis. Early in pyrolysis, hydrogen bonds are broken and melting occurs, before appreciable tar evolution. At this stage of development, surface tension is the dominant "active" (i.e., non-resistive) force, leading to the sealing off of larger pores, and tends to collapse these cavities. Surface tension is a classical force associated with a continuous medium, and so is not the appropriate concept to use to describe the behavior of the smallest cavities in coal. A pore radius of 3000 Å was tentatively adapted as a lower pore radius for which the concepts of Eqs. II.A-1 and II.A-2 are valid. Smaller pores will still tend to contract under the influence of intermolecular forces, but steric hindrances will begin to dominate the behavior of the system when only a few macromolecules fit around the "circumference" of a pore. Specifically, the behavior of the macropores (d_4) described by Suuberg (1987) should be described by Eqs. II.A-1 and II.A-2. In the model of Gavalas and Wilks (1980), there is a density of about one d_4 pore per square 10 μm by 10 μm area. This is of the order of the cavity density observed in our SEM measurements. An estimate of the minimum viscosity seen by the coal in this early stage can be obtained by the following analysis, which will be made more precise in computer simulations.

One assumes an early epoch in pyrolysis, when fluidity is established, but before appreciable gas and tar have been evolved. In Eq. II.A-2, let $n_t \rightarrow 0$, and take the internal wall radius, r_1 , to be much less than the outer radius, r_2 . One can rearrange Eq. II.A-1, and integrate to find that bubbles of initial radius r_1 will vanish as a rate

$$dr_1/dt = \sigma/4\eta \quad (\text{II.A-3})$$

where t is the period for which the coal has a viscosity η , and a surface tension

σ . One would count the frequency of occurrence of cavities of different radii in chars treated at different temperatures and time. From this data it should be possible to estimate η from Eq. II.A-3. Empirically predicted values of σ will be used in the computer simulations.

A second test of the viscosity calls for the incorporation of calculated values of the viscosity, η , in Eq. II.A-1, in model simulations of single cell cenosphere swelling, as we now describe. When particles have experienced more extensive pyrolysis at sufficiently high temperatures, evolved tars can cause expansion. The subsequent swelling of the single cell cenosphere is described by Eq. II.A-1. In practice, values of viscosity from the model will be inserted into Eq. 1, and predicted swelling compared with observed particle swelling. The case of multi-cell particles will be treated in future work.

Our experiments on particle heating were described above. Calculations have been performed of temperature histories for particles falling through the drop tube furnace, on the assumption of non-swelling (i.e., constant terminal velocity). The particle heats up to the ambient temperature in less than 0.1 sec, while the transit time through the furnace is about 2 sec.

To date, simulations at AFR have been based on average particle properties. As described above, when we take scanning electron microscope (SEM) photographs of a collection of pulverized coal particles it is primarily individual macerals that we see. These macerals have very different swelling histories, so it would be difficult, at best, to try to describe these by one "average" model. In the first simulations of the fluid properties of these particles, parameters derived from TG-FTIR experiments on differentiated macerals will be used.

It is with these results and comparisons that the model parameters established from Fong's viscosity data will be tested against our own results. It is believed that these comparisons will provide a good test for the earlier stages of pyrolysis, including swelling. However, as the experiments stand, they do not give information about the viscosity in the later stages of pyrolysis, when crosslinking is the dominating factor. This problem will be addressed during the next year.

Coal Optical Properties

Variations of Emittance with Coal Rank and Particle Size

Recent measurements (Solomon et al., 1987a, 1987b) show that pulverized coal particles of the size used in entrained gasification are non-gray with emissivities which depend on size and rank. Also coal undergoes a transition from highly non-gray moderately pyrolyzed coal to highly gray char. Here we present measurements on non-pyrolyzing, warm coal particles of different rank and particle sizes.

The coal particles were entrained in He through the HTR for a distance of 90 cm at a nominal tube temperature of 350°C. A radial temperature profile of the gas stream taken with a .005" thermocouple where it passes through the FT-IR beam focus is shown in Fig. II.A-30. The average of this profile across the distance of the stream diameter is 568 K.

To determine the spectral emittance for coal at a known temperature, measurements are made of the transmittance, τ_ν , and the radiance, R_ν , from which the normalized radiance, $R_\nu^n = R_\nu / (1 - \tau_\nu)$ is calculated.

For the geometry of the HTR, the sample consists of hot or warm particles surrounded by cold walls. The spectral emittance is then given by (Best et al., 1986)

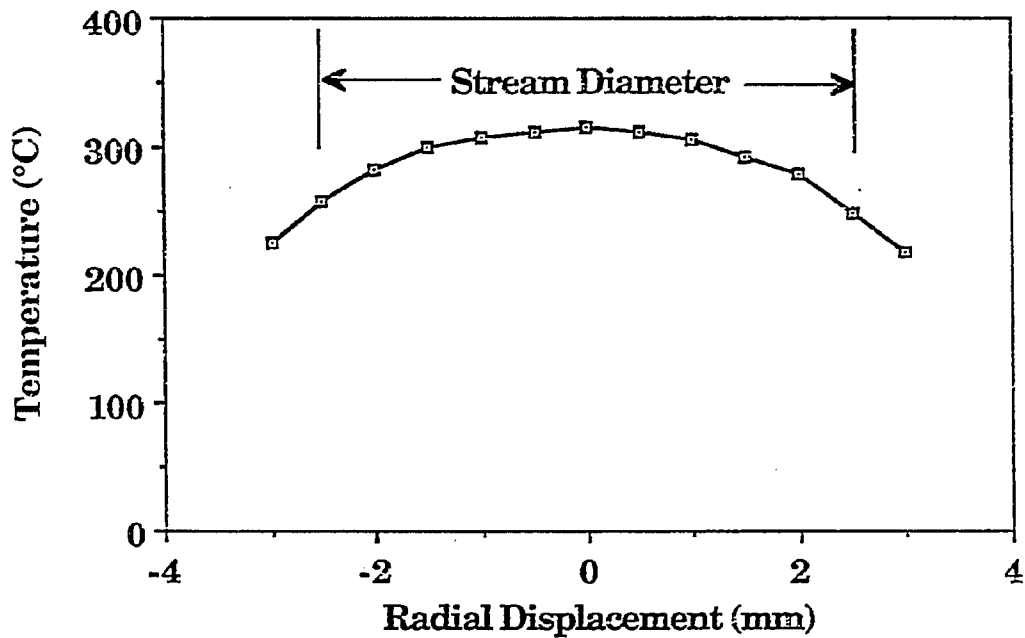


Figure IIA-30. Radial Thermocouple Temperature of Gas Stream Exiting the HTR at FT-IR Focus (.005" bead). Nominal HTR Temperature = 350°C. Radial Average = 295°C (568K).

$$\epsilon_{\nu} = F_{\nu}^T R_{\nu}^D / R_{\nu}^D(T_p) \quad (\text{II.A-4})$$

where $R_{\nu}^D(T_p)$ is the theoretical black-body radiance at the particle temperature, T_p , and F_{ν}^T is the total extinction efficiency for the particles to scatter radiation out of the angular acceptance aperture of our instrument plus absorption. If T_p and F_{ν}^T are known, then ϵ_{ν} can be determined. Conversely, if ϵ_{ν} and F_{ν}^T are known, T_p can be determined.

Prior to each coal particle experiment presented here, a gas temperature determination was performed on a trace amount of CO_2 added to the particle stream to track fluctuations in the HTR nominal temperatures. The accuracy of this measurement is illustrated in Fig. II.A-31 which presents R_{ν} , $1 - \tau_{\nu}$, and the normalized radiance for a mixture of carbon dioxide, butane and acetylene passed through the HTR. For this non-scattering, gaseous sample, excellent agreement is observed between the thermocouple average temperature (568 K) and the FT-IR line-of-sight determined average temperature (565 K). Figure II.A-32 indicates the sensitivity of this method to small shifts in temperature.

The coal samples used in this study (Table II.A-3) were obtained from the AFR/BYU sample bank (bulk samples) or from the Pittsburgh Energy Technology Center (PETC) of the Department of Energy. All samples having more than 3% moisture were dried before measurements were taken.

The transmittance spectra used to calculate the normalized radiance for the samples used in this study are presented in Figs. II.A-33 to II.A-36. The spectra are presented as $1 - \tau_{\nu}$ so that increased amplitude is proportional to increased attenuation.

The characteristics of large particles are that they scatter or absorb essentially all of the light incident on them. Any radiation hitting the particle which is not absorbed will be scattered. Consequently, the attenuation is proportional to the area of the particle and no absorption effects can be seen.

Figures II.A-33 to II.A-36 illustrate the effect of particle size on the shape of $1 - \tau_{\nu}$. As the particle size distribution is decreased, there is an increase in attenuation (sloping of the spectra) from short (6500 cm^{-1}) to long (500 cm^{-1}) wavelengths of incident radiation. This particle dependent change in the scattering (diffraction) component of F_{ν}^T indicates that the longer wavelengths of light have a higher efficiency of scattering out of the angular acceptance aperture of our instrument than the shorter wavelengths of light. As the particles get smaller, the higher efficiency to scatter extends further towards the short wavelength end of the spectrum.

Below a particle size of $20 \mu\text{m}$, a drop in attenuation is observed at the long wavelength end of the spectrum. This effect is caused by the particles being smaller than the wavelength of incident radiation ($1000 - 500 \text{ cm}^{-1} = 10 - 20 \mu\text{m}$) and will allow this radiation to pass through without any scattering or absorption effects.

To see trends in emissivity with varying particle size and composition, $(1 - \tau_{\nu})_{6500 \text{ cm}^{-1}}$ was used for the percent attenuation in the following analysis. Figures II.A-37 to II.A-39 are the normalized radiance, $R_{\nu}^D = R_{\nu} / (1 - \tau)_{6500 \text{ cm}^{-1}}$, for three coals with different size distributions. Overlaid on the experimental data is the theoretical black-body curve $R_{\nu}^D(T)$, corresponding to the temperature determined from the CO_2 tracer test, multiplied by a constant $(\epsilon_{\nu} / F_{\nu}^T)_{6500}$ to give the best fit to the coal spectrum in the strong absorption region ($\nu < 1700 \text{ cm}^{-1}$) for coal.

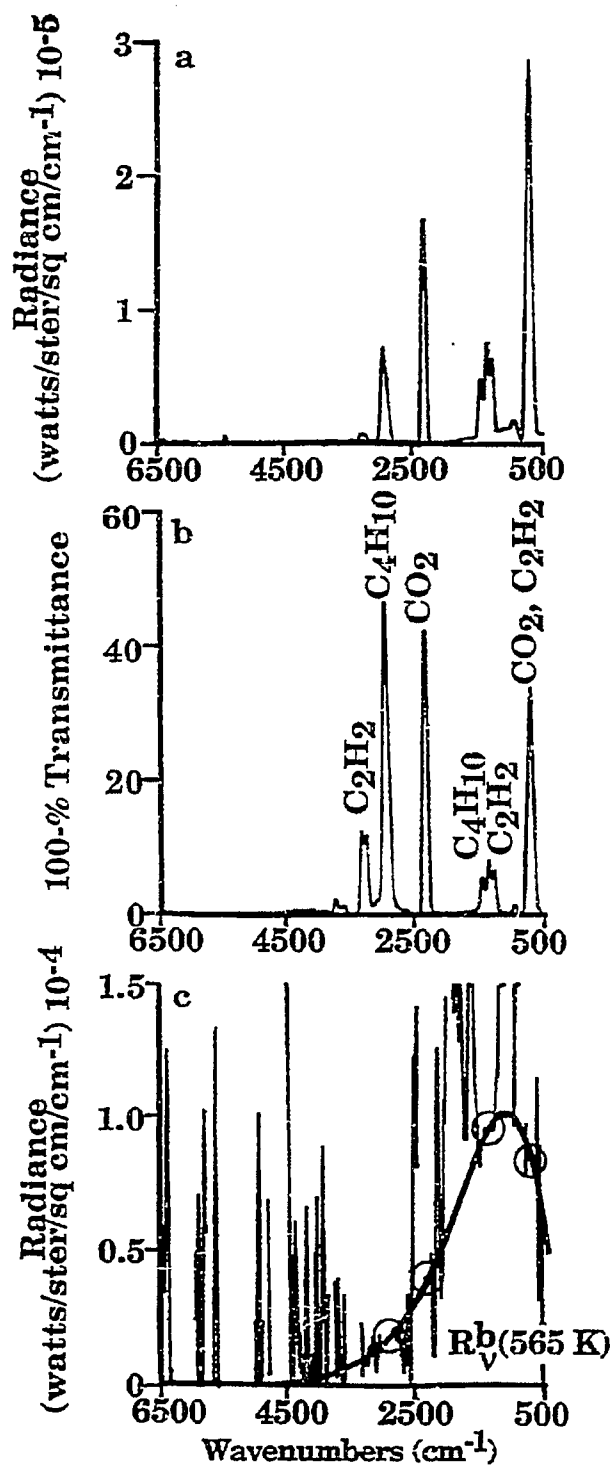


Figure IIA-31. FT-IR E/T Spectra for a Mixture of CO_2 , C_4H_{10} , and C_2H_2 Exiting the HTR. a) Raw Radiance (R_V), b) 100%-Transmittance ($1-\tau_V$), and c) Normalized Radiance, $R_V^n = R_V/(1-\tau_V)$. $R_V^b(565\text{K})$ Represents Theoretical Black Body Distribution Best Fit to Regions of Absorption/Emission for the Mixture (circled regions).

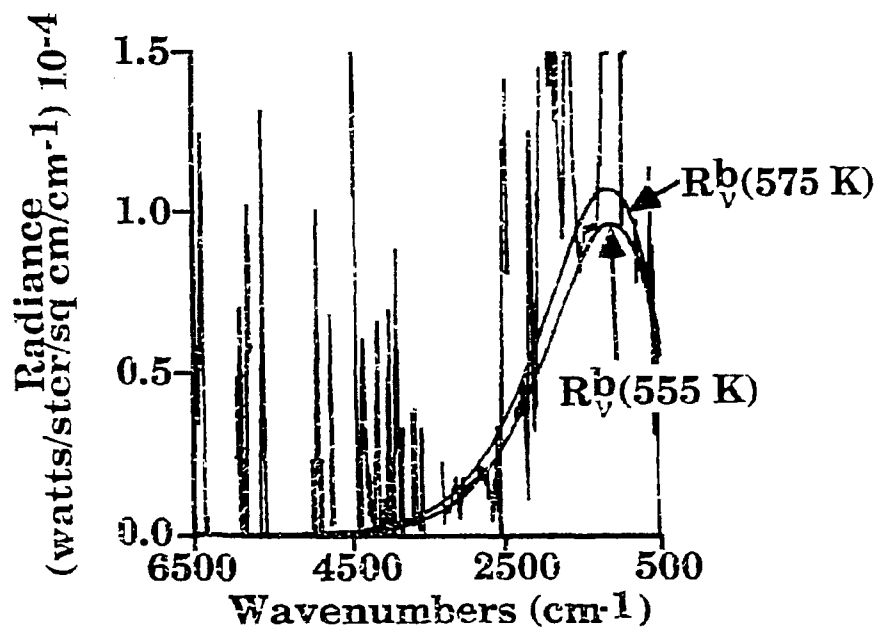


Figure IIA-32. Normalized Radiance Spectrum with $\pm 10\text{K}$ Shift from the Best Fit $R_b^p(T)$.

TABLE II.A-3
 SAMPLE DATA FOR OPTICAL PROPERTIES MEASUREMENTS

<u>Coal Name</u>	<u>Rank</u>	<u>Particle Size Distribution (μm)</u>	<u>%C (DAF)</u>	<u>%Ash (Dry Basis)</u>	<u>%Moisture</u>	<u>Source</u>
I Pocahontas #3	LVB	75-45	91	4.83	0.61	AFR/BYU
Upper Freeport	MVB	75-45	87	11.63	0.83	AFR/BYU
Pittsburgh #8	HVAB	75-45	83	9.02	1.80	AFR/BYU
Upper Kanawha	MVB	75-45	81	26.44	2.60	AFR/BYU
Utah Blind Canyon	HVCB	75-45	79	4.68	4.71	AFR/BYU
Illinois #6	HCVB	75-45	77	23.42	2.94	AFR/BYU
Smith Roland	SUBC	250-210	72.97	9.23	24.51	PETC
Smith Roland	SUBC	106-75	73.26	12.27	20.97	PETC
Smith Roland	SUBC	63-45	72.38	18.29	13.26	PETC
Smith Roland	SUBC	30-20	73.67	12.87	9.96	PETC
Smith Roland	SUBC	20-10	73.24	14.03	9.10	PETC
Smith Roland	SUBC	-10	73.17	15.64	8.23	PETC
Lower Kittaning	LVB	106-75	88.65	19.31	0.62	PETC
Lower Kittaning	LVB	36-45	87.73	17.43	0.64	PETC
Lower Kittaning	LVB	30-20	90.53	9.17	0.83	PETC
Lower Kittaning	LVB	20-10	90.55	8.03	0.91	PETC
Lower Kittaning	LVB	-10	89.82	7.68	0.93	PETC
Beulah N.D.	Lignite	250-210	69.48	8.86	28.49	PETC
Beulah N.D.	Lignite	106-750	69.82	15.23	22.63	PETC
Beulah N.D.	Lignite	63-45	71.25	32.81	13.41	PETC

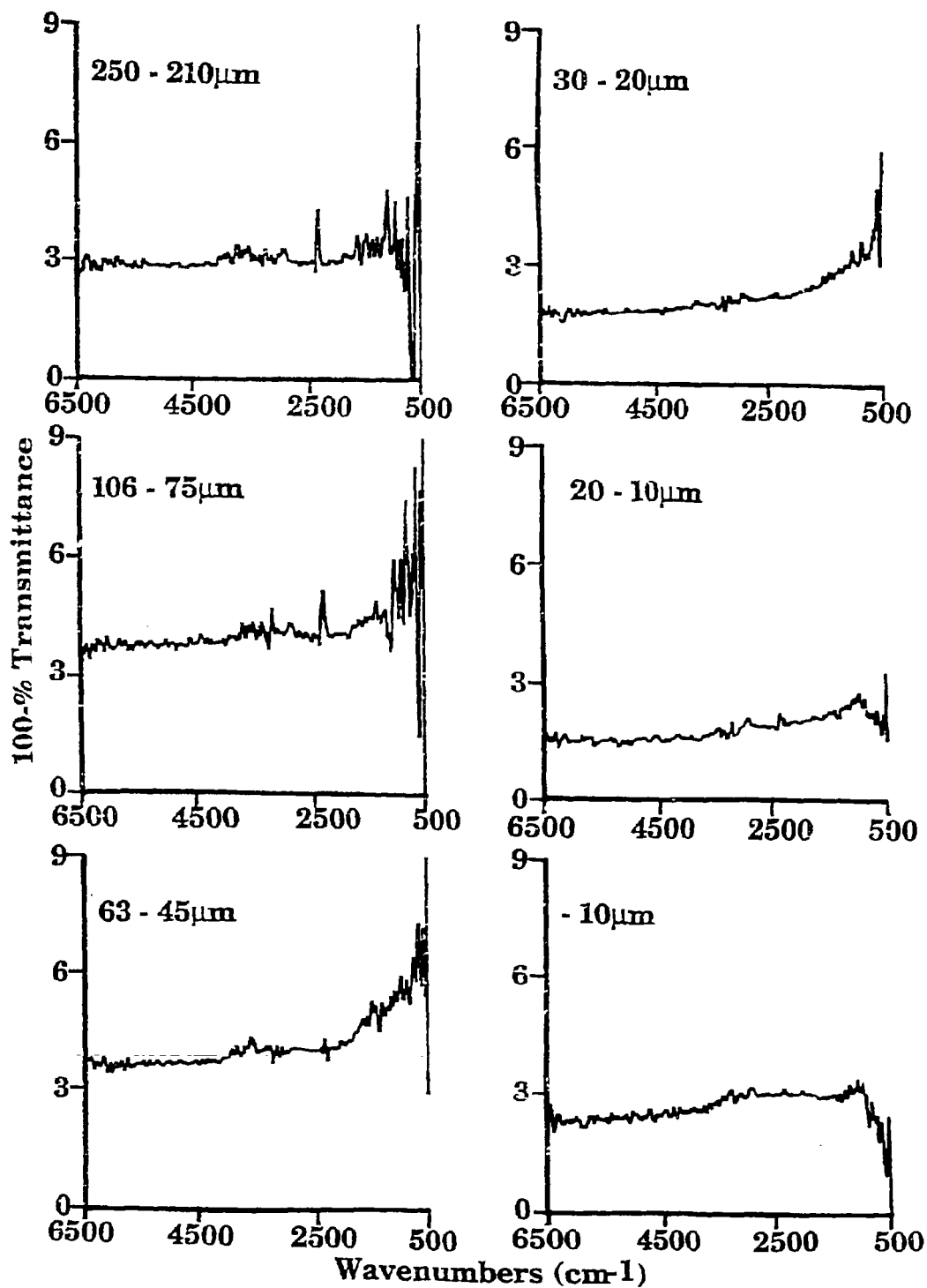


Figure IIA-33. 100-% Transmittance Spectra for Different Particle Size Distributions of Smith Roland Subbituminous Coal.

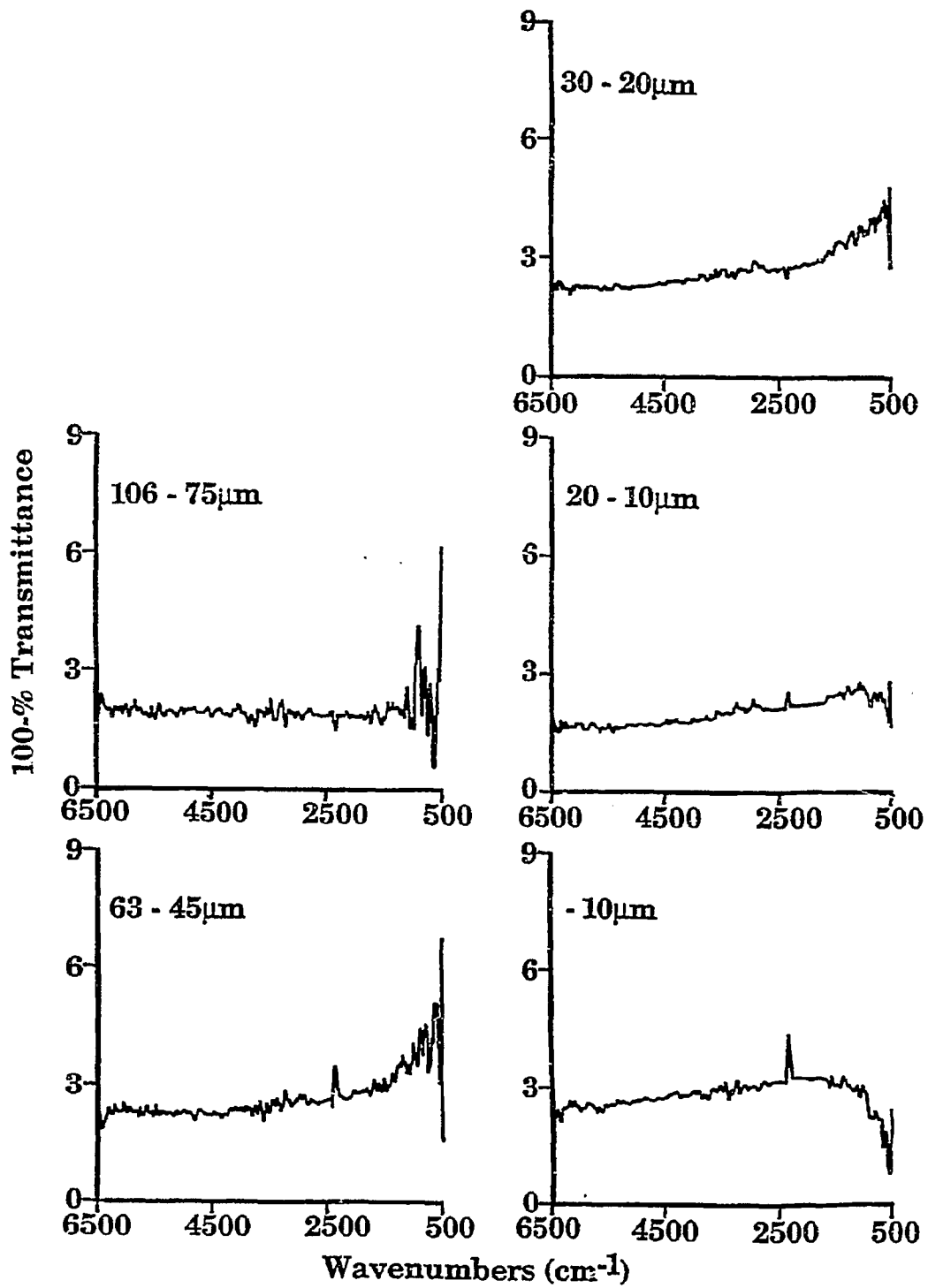


Figure IIA-34, 100-% Transmittance Spectra for Different Particle Size Distributions of Lower Kittanning Bituminous Coal.

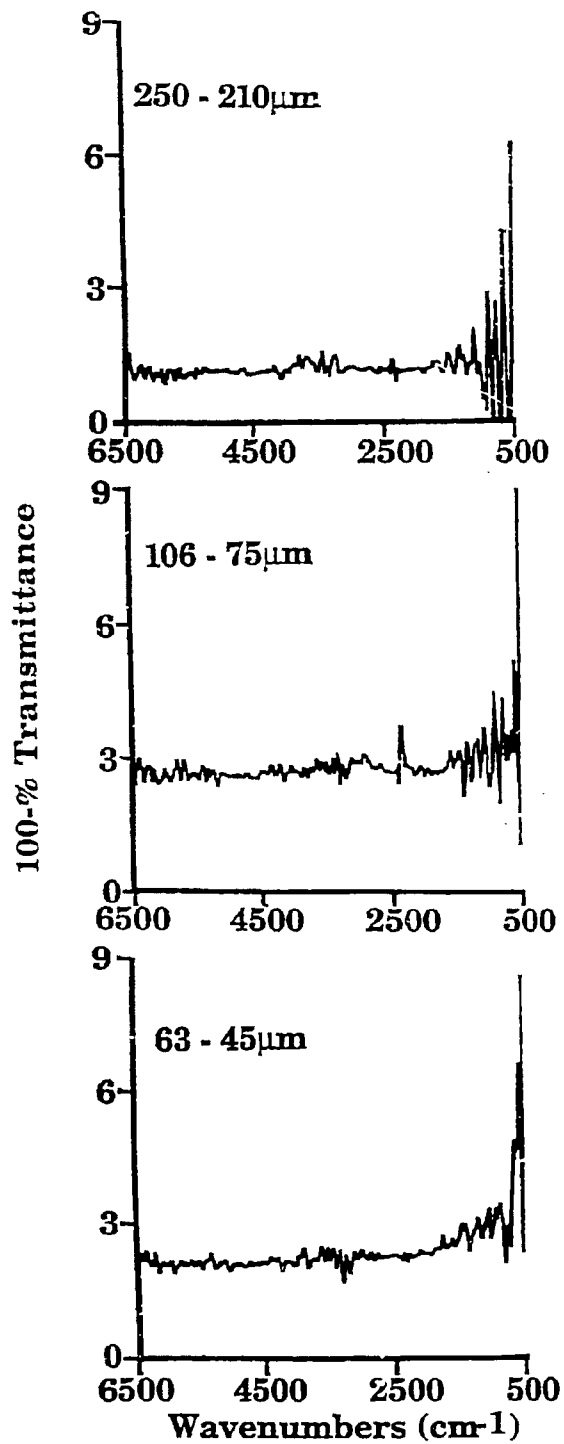


Figure IIA-35. 100-% Transmittance Spectra for Different Particle Size Distributions of Beulah North Dakota Lignite.

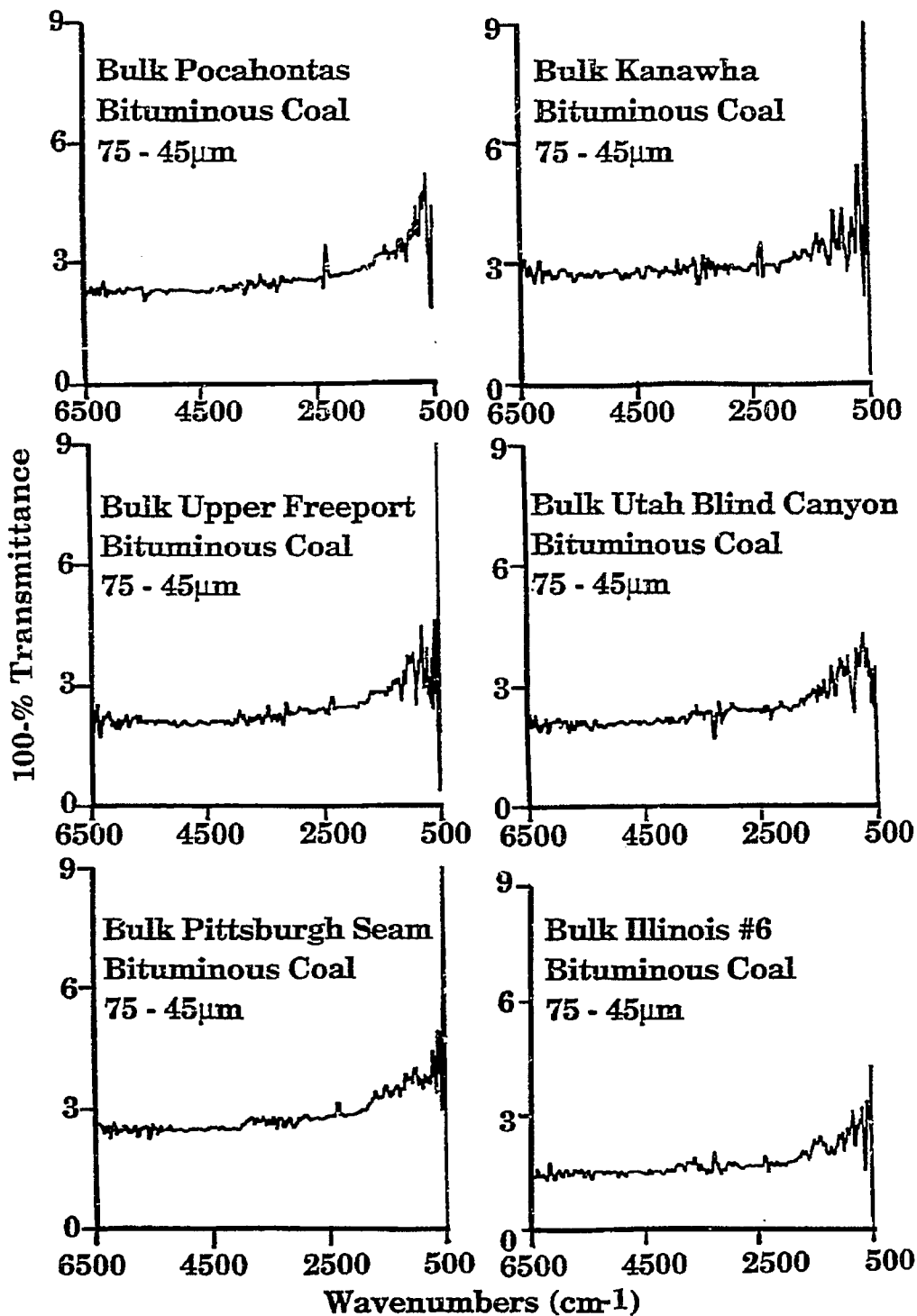


Figure II.A-36. 100-% Transmittance Spectra for Bituminous Coals from the AFR/BYU Sample Bank (bank bulk samples).

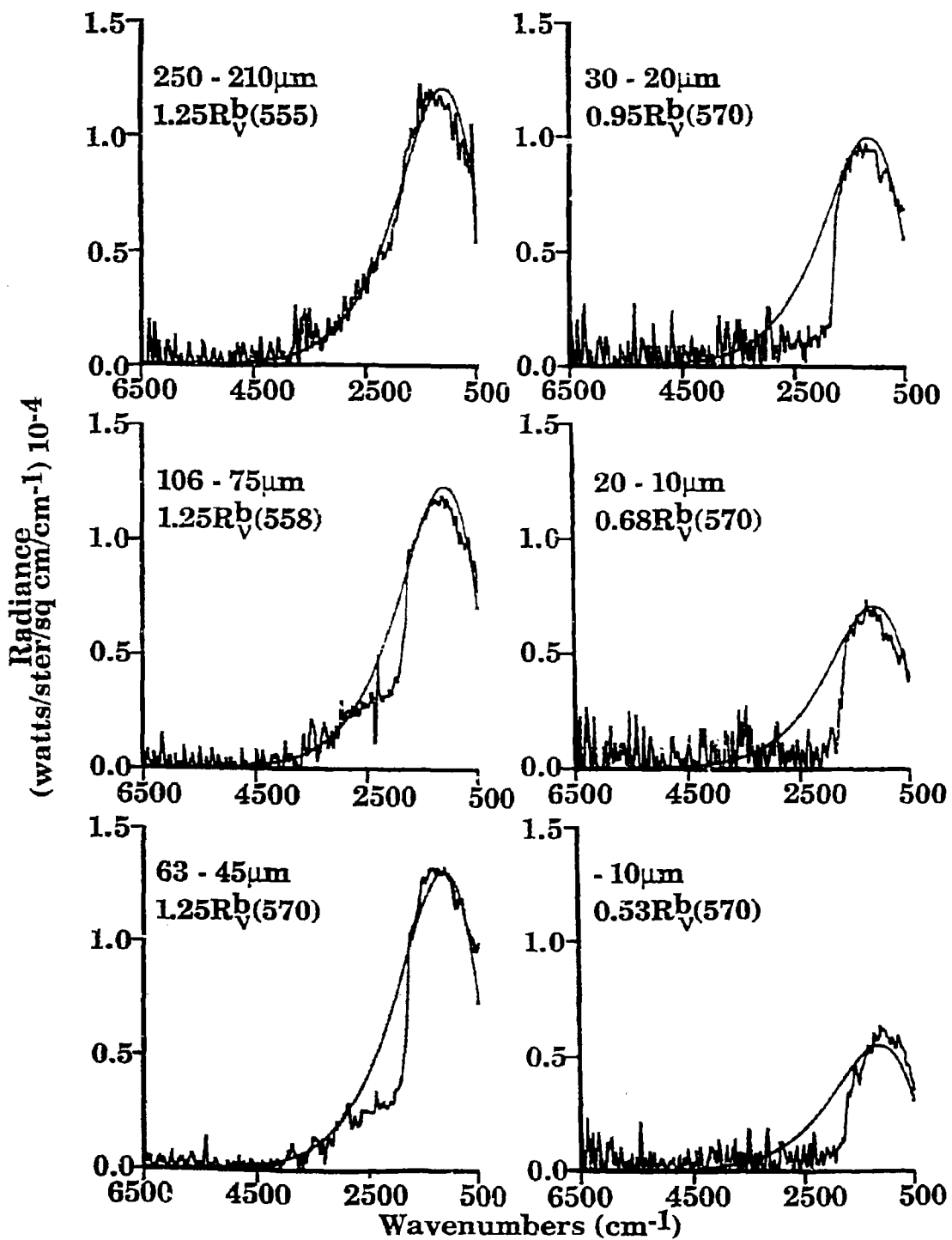


Figure 1LA-37. Normalized Radiance Spectra for Different Particle Size Distributions of Smith Roland Subbituminous Coal. $R_V^b(T)$ is in Degrees Kelvin.

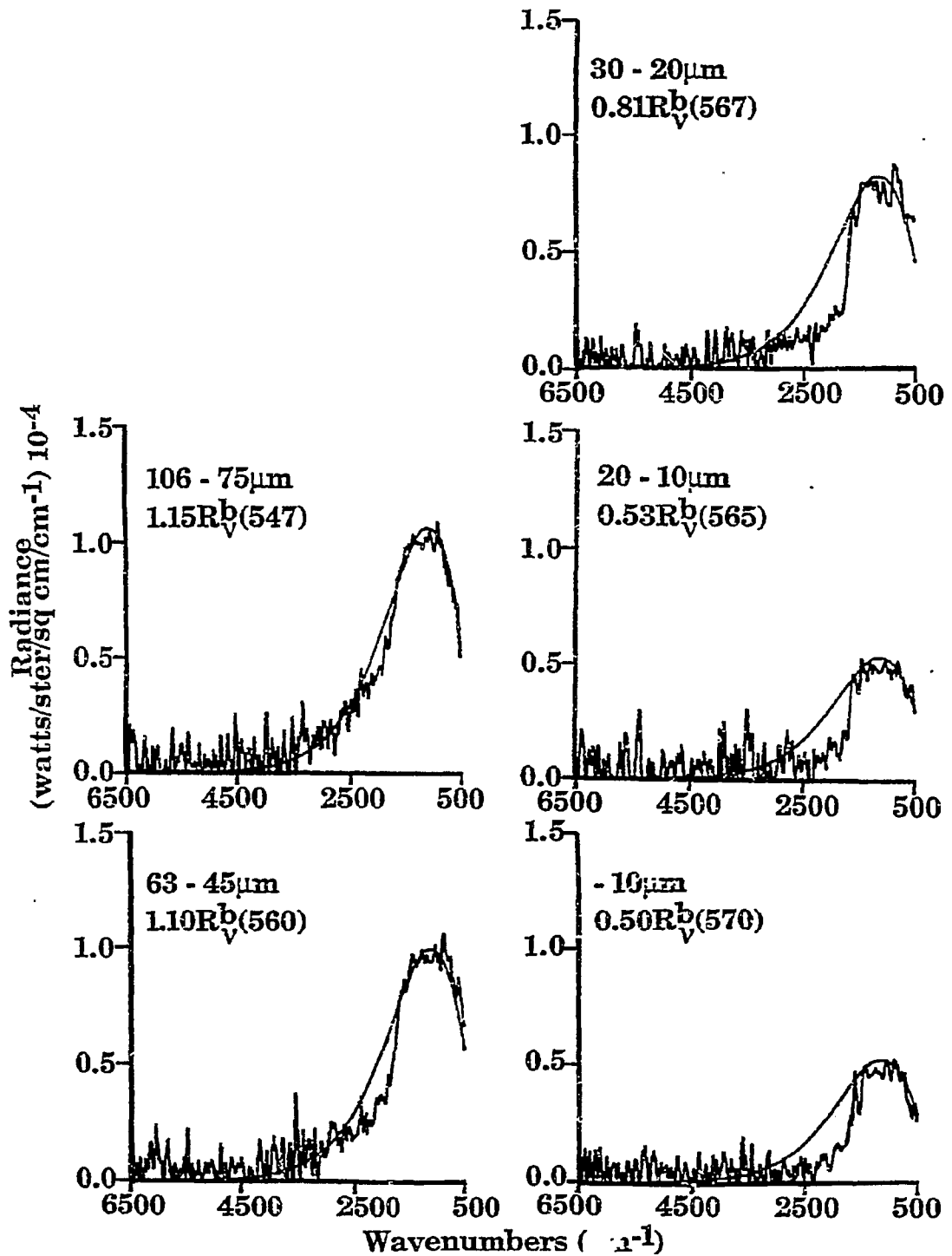


Figure IIA-38. Normalized Radiance Spectra for Different Particle Size Distributions of Lower Kittanning Bituminous Coal.

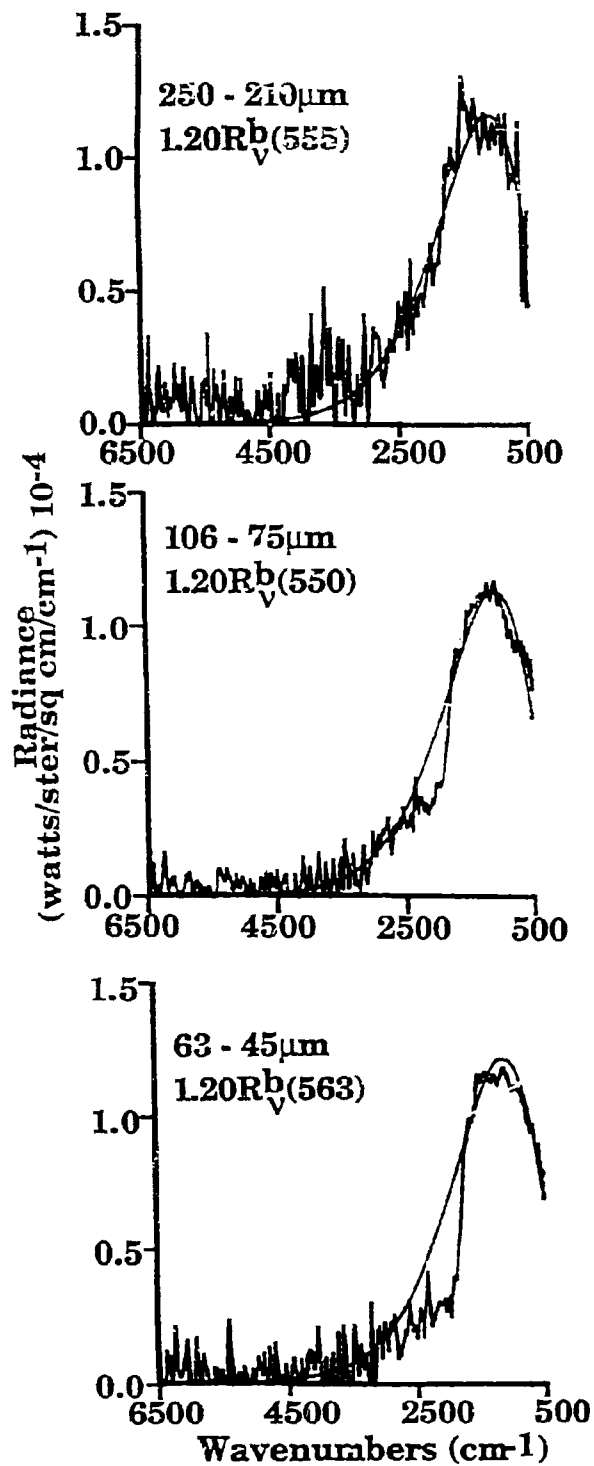


Figure IIA-39. Normalized Radiance Spectra for Different Particle Size Distributions of Beulah North Dakota Lignite.

The trend with particle size is consistent for all three coals. The largest particle size (250 - 210 μm) shows agreement close to the overlaid black-body over all of the spectrum. The smaller particle sizes continue this agreement for $\nu < 1700 \text{ cm}^{-1}$, but the emittance decreases for $\nu > 1700 \text{ cm}^{-1}$. The smaller the particle size, the larger is the decrease. The trend with rank is that the lower rank Beulah lignite and Smith Roland subbituminous coals show a slightly larger decrease above 1700 cm^{-1} than does the higher rank Lower Kittanning bituminous coal.

Figure II.A-40 compares six bituminous coals from the bulk AFR/BYU samples obtained for this program. For these similar size fractions (75-45 μm), again there is agreement with the overlaid black-body curve below 1700 cm^{-1} . The decrease above 1700 cm^{-1} does appear to become slightly more drastic with decreasing carbon content of the coals.

The spectral emissivity (ϵ_ν) for coal particles larger than 10 μm at wavelengths which coincide with strong infrared absorption bands should be approximately equal to 1. Therefore, F_{8500}^t is changing with particle size and rank as indicated by the different multiplier values used to fit $R_{\nu}^b(T)$ to the observed normalized radiance spectra. An attempt was made to determine the surface area of the particle stream by using a light source with an incident radiation that is well out of the diffraction and absorption regime for coal particles ($F_{\nu}^t = 1$). A He-Ne laser, 0.633 μm radiation, ($\sim 16,000 \text{ cm}^{-1}$) was directed through the coal stream to a photo-sensitive resistor. The output of this visible light detector was checked for linearity by partially blocking the laser beam with several different area sized light choppers. The source was also modulated (chopped) when directed through the coal to avoid room light interferences. The coal should be opaque to the laser radiation.

A plot of percent FT-IR beam attenuation at 6500 cm^{-1} , vs percent He-Ne laser beam attenuation is presented in Fig. II.A-41 for the size fractions of Smith Roland subbituminous coal. For the three large size fractions, where $\epsilon_\nu / F_{8500}^t > 1$ in Fig. II.A-37, the laser indicates that a larger value of $(1-\tau)_{6500 \text{ cm}^{-1}}$ should be used (i.e., the FT-IR is indicating a low amount of beam attenuation due to scattering of incident radiation back into the collection angle of our instrument, $F_{8500}^t < 1$). For the three smaller size fractions, where $\epsilon_\nu / F_{8500}^t < 1$ in Fig. II.A-37, the laser indicates that a smaller value of $(1-\tau)_{6500 \text{ cm}^{-1}}$ should be used (i.e., the FT-IR is indicating a high amount of beam attenuation due to a high efficiency of scattering incident radiation out of the collection angle of our instrument, $F_{8500}^t > 1$).

Although the He-Ne laser measurements begin to converge the spectral emittance for $\nu < 1700 \text{ cm}^{-1}$ towards 1 for the different particle sizes, it was observed that the moving particles contributed their own modulated signal to the visible light detector. This contribution, along with laser power and detector drift, did not allow this laser beam attenuation technique to be as accurate as desired in determining the surface area of the particle stream. Work is in progress on an accurate optical geometry for this determination.

Trends in the spectral emittance (R_{ν}^n/R_{ν}^b) as a function of particle size and rank are plotted in Fig. II.A-42. The value at 2500 cm^{-1} was calculated since it is out of the functional group emission region ($\nu < 1700 \text{ cm}^{-1}$) but still within the broad band emission region for coal particles at 300°C. The trends with rank and particle size are clearly shown. Figure II.A-43 compares the spectral emittance for one particle size distribution for nine different coals. The emittance remains fairly constant (~ 0.55) until above 85% carbon (DAF), at which point an increase in emittance is observed.

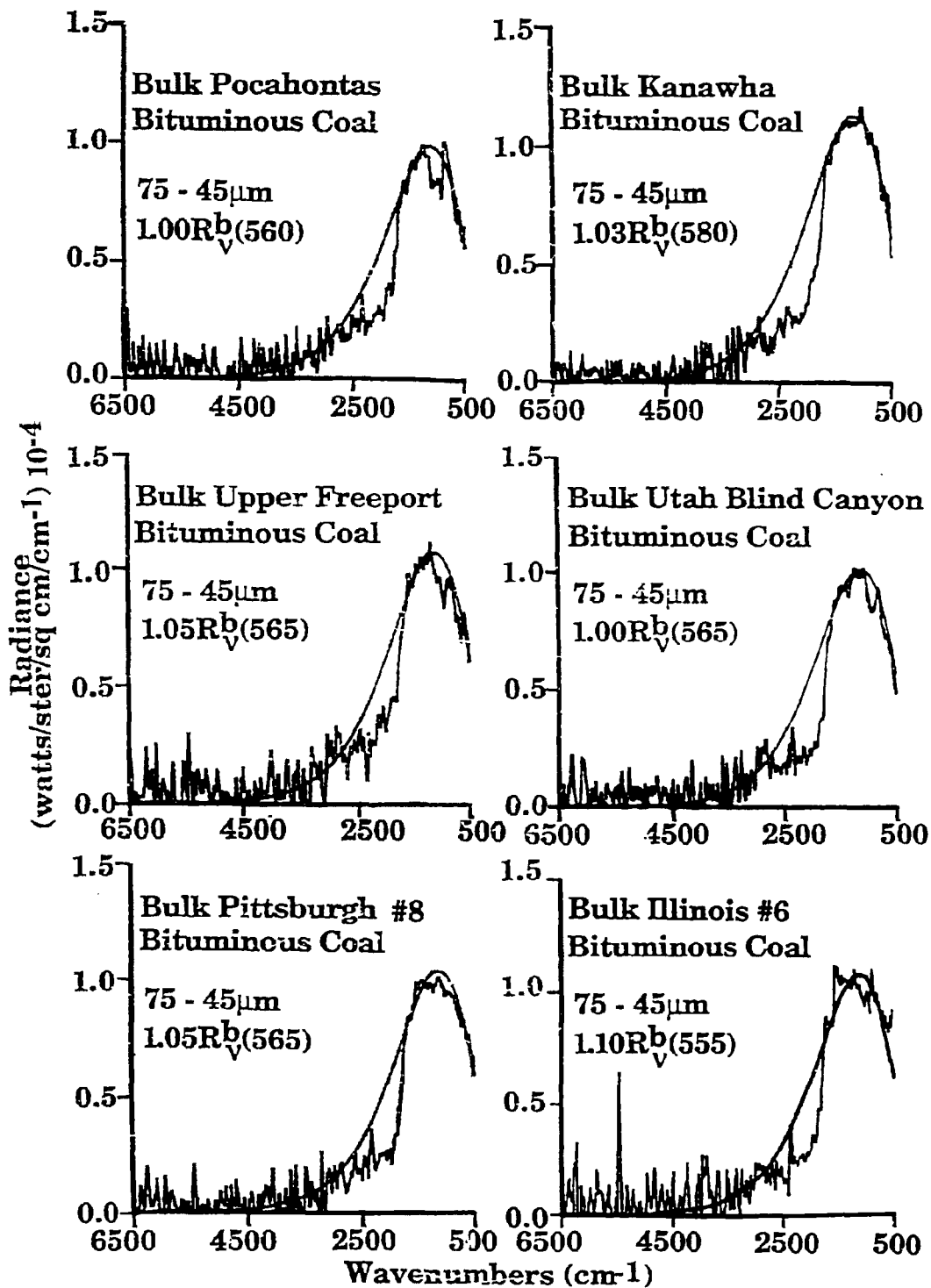


Figure IIA-40. Normalized Radiance Spectra for Bituminous Coals from the AFR/BYU Sample Bank (bulk samples). $R_V^b(T)$ is in Degrees Kelvin.

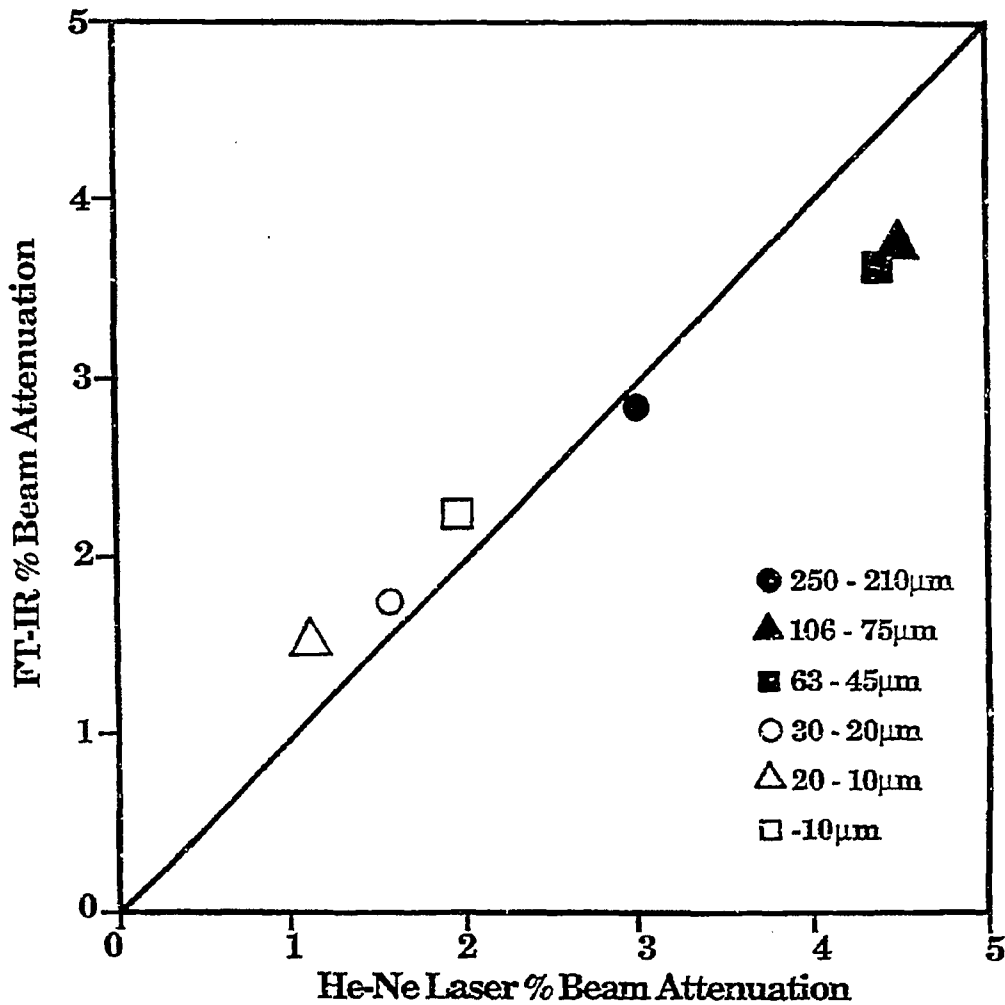


Figure IIA-41. FT-IR % Beam Attenuation at 6500 cm^{-1} vs. He-Ne Laser % Beam Attenuation for Different Particle Size Distributions of Smith Roland Subbituminous Coal.

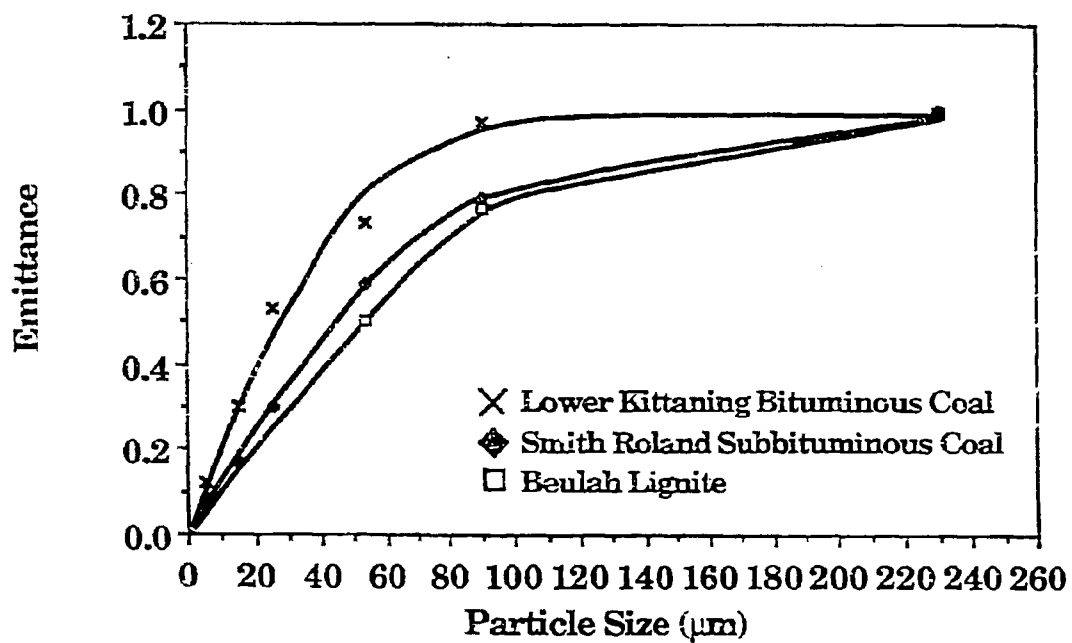


Figure IIA-42. Spectral Emittance (R_V^a/R_V^b) Calculated at 2500 cm^{-1} vs. Average Particle Size for Three Different Coal Samples.

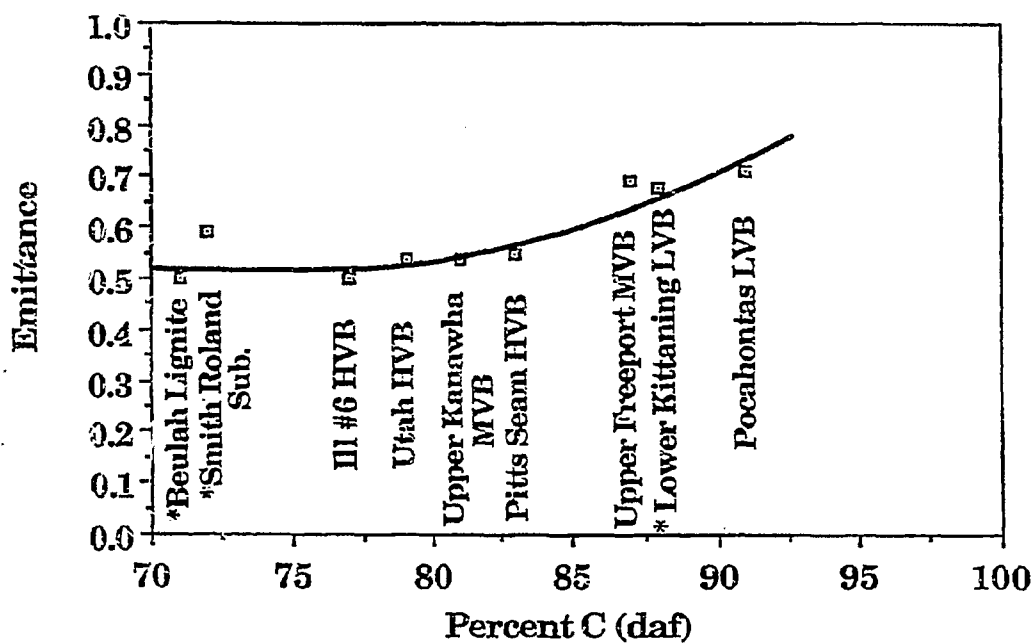


Figure II.A-43. Spectral Emittance (R_V^a/R_V^b) Calculated at 2500 cm^{-1} vs. Percent Carbon (daf) for Nine Coal Samples of Similar Particle Size Distribution (45-75 μm or *45-63 μm).

Conclusions

Although we can determine the trends in the spectral emissivity (ϵ_ν) for coal with varying particle size and rank, accurate values of F_ν^t (the total extinction efficiency for scattering out of the angular acceptance aperture of our instrument plus absorption) must be determined for the particles and experimental geometry used before accurate ϵ_ν can be determined. By choosing a light source (He-Ne laser) that should be well out of the diffraction and absorption regime for the samples used here, the ϵ_ν values in regions of strong infrared absorption bands for various particle sizes of the same material begin to converge. The laser attenuation values, however, are not as accurate as necessary for these determinations due to: 1) laser power drift, 2) detector response drift, and 3) signal contribution from extraneous modulation of the laser beam due to the traversing coal particles.

Plans

The improvements of the FG-DVC model will continue. During the next year, the model will be modified to include: a) rank dependent kinetics; b) polymethylenes; c) improved internal and external transport models. Work will continue on the viscosity/swelling model. Work will begin on an optical properties model and a char reactivity/annealing model. Additional literature and experiment studies will be done where necessary in order to provide data for model validation.

For the optical property measurements the plans are to a) design a better laser system to determine accurate particle blockage areas; b) develop a better understanding of the angular acceptance aperture of our instrument and how discrete changes will effect F_ν^t ; and c) use a theoretical Mie theory analysis to better understand F_ν^t .

II.B. SUBTASK 2.B. - FUNDAMENTAL HIGH-PRESSURE REACTION RATE DATA

Senior Investigators - Geoffrey J. Germane and Angus U. Blackham
Brigham Young University
Provo, Utah 84602
(801) 378-2355 and 6536

Student Research Assistants - Charles Monson, Russell Daines,
and Gary Pehrson

Objectives

The overall objectives of this subtask are 1) to measure and correlate reaction rate coefficients for pulverized-coal char particles as a function of char burnout in oxygen at high temperature and pressure and 2) to provide kinetic rate measurements of sulfur species with sorbents for a range of stoichiometries under laminar, high-pressure conditions.

The specific objectives for the second year reporting period include:

1. Design and construct the HPCP reactor and support systems.
2. Develop the HPCP reactor characterization test plan and elements of the char oxidation test plan.

Accomplishments

Four components of this subtask have been identified to accomplish the objectives outlined above: 1) char preparation at high temperature and high pressure, 2) determination of the kinetics of char-oxygen reactions at high pressure, 3) design and construction of a laminar-flow, high-pressure, controlled-profile (HPCP) reactor, and 4) measurements of fundamental sulfur capture rates by sorbents.

Component 1 - Char Preparation at High Temperature and High Pressure

The main objective of the char preparation aspect of the study is to prepare char with three different reactors: 1) a simple hot-tube reactor at atmospheric and elevated pressure, 2) the BYU high-pressure, entrained-flow gasifier, and 3) the high-pressure, controlled-profile (HPCP) reactor being fabricated for this subtask. After fabrication and testing of the HPCP reactor are completed, char samples will be prepared in this reactor to serve as reference chars to which other char samples from the simple hot-tube reactor and the gasifier will be compared. The purpose of this comparison will be to determine how closely the properties of the chars prepared with the simple reactor and the gasifier parallel the properties of the chars prepared by the HPCP reactor. If the properties are sufficiently close for the same temperatures, pressures, heating rates, and residence times, then confidence will be established in the measured values for the chars prepared with the simple reactor. Chars could then be prepared for the kinetic studies in the HPCP reactor at a significant savings in time and money. Otherwise, both the char preparation and the oxidation rate measurements will be performed in the HPCP reactor.

Chars will be prepared from five different coals from the Argonne premium coal sample bank: 1) Utah bituminous, 2) North Dakota lignite, 3) Wyoming subbituminous, 4) Illinois #6 bituminous, and 5) Pittsburgh #8 bituminous. A Utah bituminous coal which is similar to but not the same as the Utah coal in the Argonne bank, and which is in large supply at the BYU Combustion Laboratory, is currently being used to develop char preparation and analytical experience. Small samples of char from the Utah coal in the Argonne bank will be characterized and compared with the char samples from the BYU Utah coal.

Literature Survey - Wells and Smoot (1987) reviewed the preparation methods for chars and determined that to obtain satisfactory char samples for reactivity testing, the parent coals must be pyrolyzed in a reproducible manner. They also listed six criteria thought to be important to the selection of a pyrolysis method for char preparation. These included heating rate, maximum temperature, residence time, particle size, pressure and gas composition. Goetz et al. (1982) prepared char in nitrogen at 1728 K using a drop-tube furnace. They concluded that drop-tube furnaces and flat-flame burners achieve satisfactory heating rates on the order of 10,000 K/s, or higher. They also state that the residence time for pyrolysis should be long enough for complete pyrolysis, but not so long that the coal goes through condensation and polymerization. Residence times in the range of 10-70 ms at the temperature of interest are usually adequate.

A recent study of coal char gasification at elevated pressure was conducted by Guo and Zhang (1986). The chars were prepared by devolatilizing coal in nitrogen at 1070 K for 2 hours. The gasification runs were at 29 atm pressure (30 kg/sq. cm.) at temperatures of 1120-1220 K. The kinetics were determined by having the carrier gas pass through a sample of char placed in a tubular reactor (22 mm i.d.) and measuring the extent of burnout as a function of time. Under these conditions, the char reactivity followed first-order kinetics. Our approach for kinetics measurements will be under entrained conditions rather than the fixed-bed approach used in the study by Guo and Zhang. Another concern is that char should be prepared at temperatures higher than the temperatures at which the reaction rates are measured to avoid further devolatilization of the char.

Consideration has been given to the closeness of the particle temperature to the temperature of the walls of the ceramic tube in the simple hot-tube reactor. It has been assumed that the temperature of the particles passing through the reactor is the same as the temperature of the wall measured by a thermocouple. Solomon et al. (1986) concluded that "the heat transfer between the solids and the gases was so fast that in most cases the thermocouple temperature was predicted to be within 20°C of the coal particle temperatures" and "the thermocouple measurement provided a reasonably accurate determination of the particle's temperature history." The inside diameter of the tube in their reactor for very rapid coal pyrolysis was 5 mm.

Char Preparation Methods Used To Date - Char samples have been collected from a simple hot-tube reactor. The values for gas flows and temperatures at atmospheric pressure required to give satisfactory char samples have been determined. A schematic of this reactor is shown in Figure II.B-1. For pressures above 1 atm, this scheme has been modified by using stainless steel bulbs as the feeder and receiver, as shown in Figure II.B-2. These simple hot-

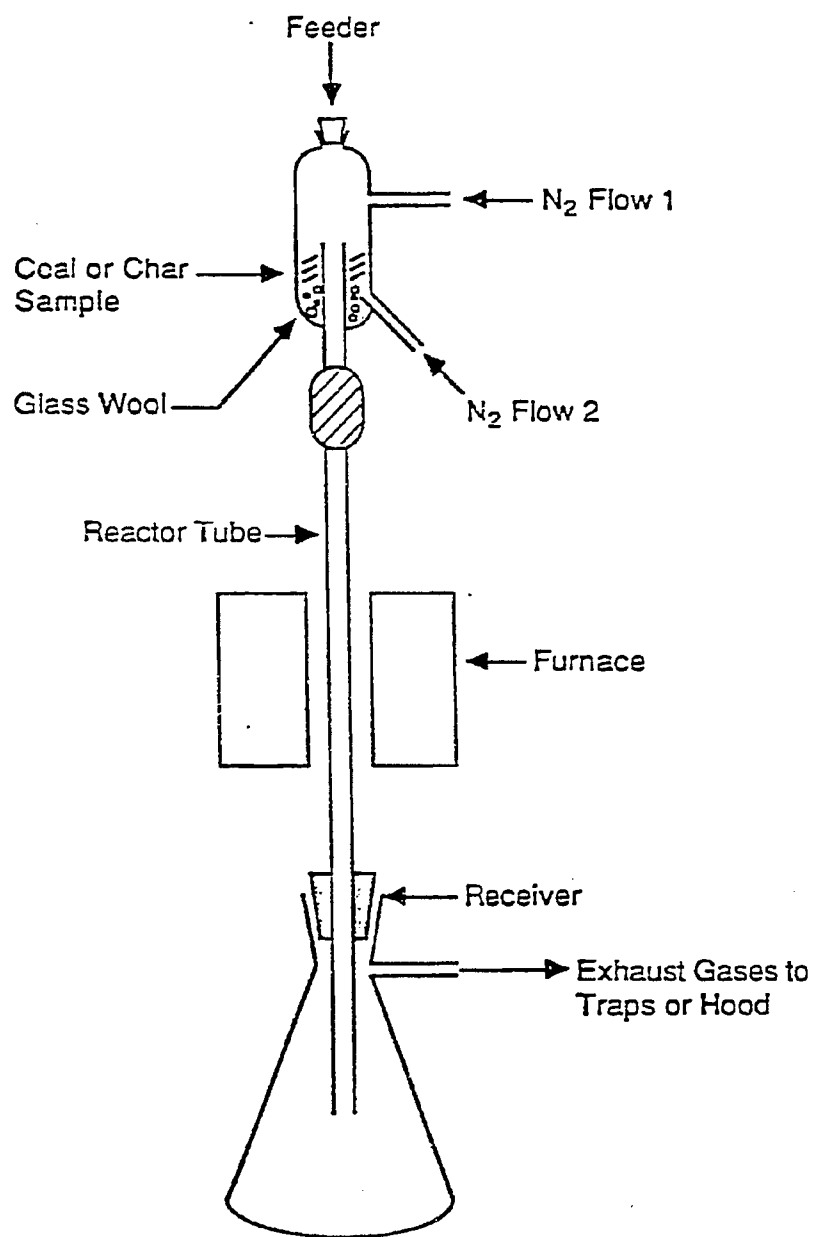


Figure II.B-1. A simple hot tube reactor for preparation of small samples of char.

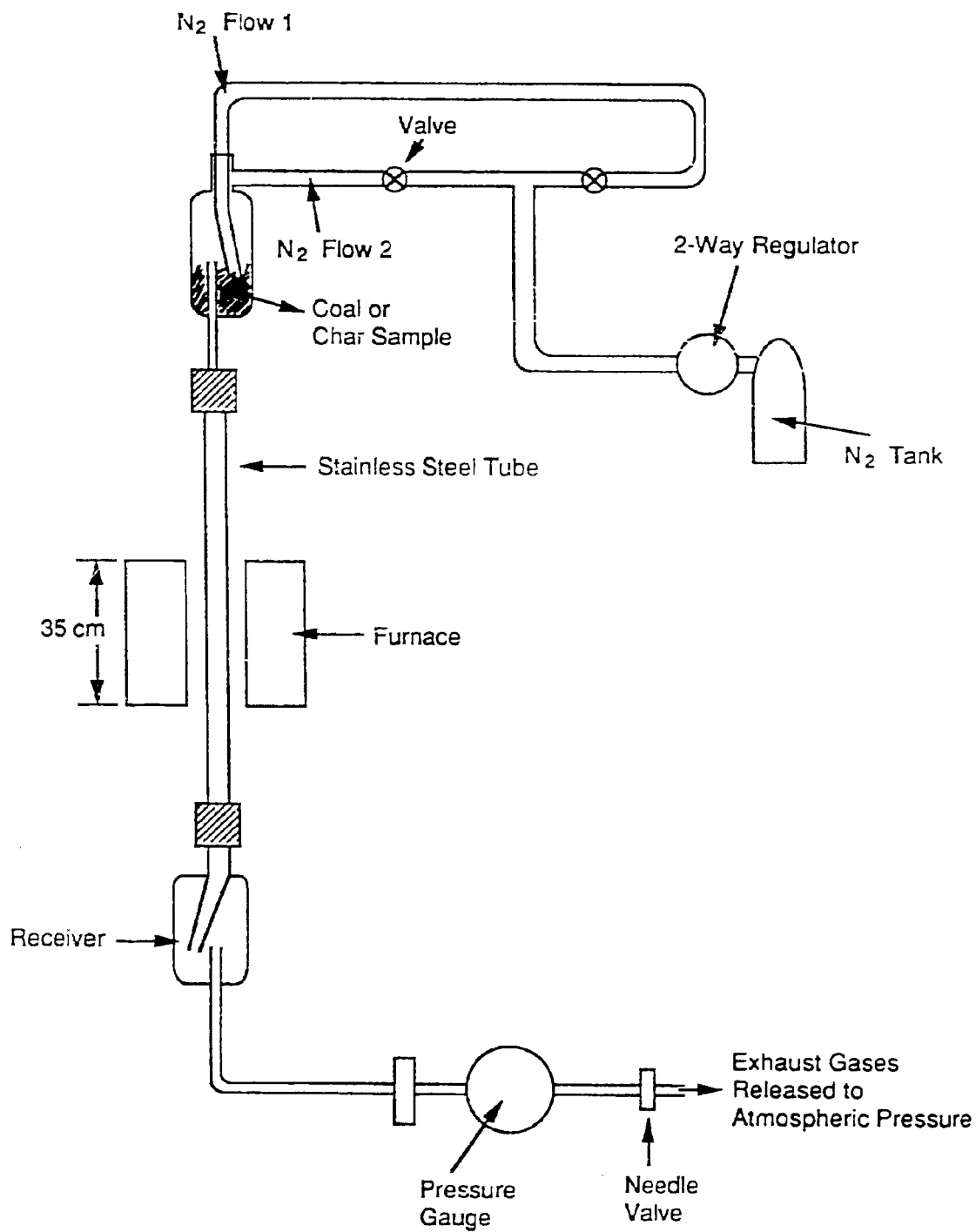


Figure II.B-2. High-pressure, hot-tube char preparation furnace

tube reactors have provided small amounts of char which have been analyzed. The hot-tube method allows for easy changes in the values for heating rate, residence time, temperature, and pressure. This flexibility will aid in determining the conditions which will be selected for the HPCP reactor. The samples were prepared by flowing nitrogen gas down the tube along with the coal. The bottom stream of gas in the feeder fluidizes the coal while the top stream entrains the particles and carries them into the tube. The char samples have been prepared at temperatures from 1173 to 1500 K. The samples used for the oxidation kinetics studies will be prepared at temperatures higher than those used for the kinetics measurements, to avoid further devolatilization of the char in the reactor.

Two runs were made at elevated pressure in a stainless steel reactor tube with an inside diameter of 2 mm. Only very small amounts of char were obtained due to plugging of the reactor tube. This tube has been replaced with an 8mm i.d. stainless steel tube to overcome this problem. A 7 mm i.d. ceramic tube was used to prepare char samples at atmospheric pressure.

Rationale - The rationale for char preparation in the simple hot-tube reactor may be developed in the following manner. The design of the HPCP reactor provides for accurate temperature measurement of the char particle after a period of time at a carefully controlled reaction temperature. This precise control of reaction variables is particularly needed in the measurement of the kinetics of oxidation of char samples. Therefore, the prime concern for the HPCP reactor is the measurement of reactivity even though char will also be prepared in the HPCP reactor. However, if char samples can be prepared in a reactor that has less control of the temperature profile and have essentially the same properties as samples prepared in the HPCP reactor, then it is more efficient to use the simpler reactor for the char preparation and the HPCP reactor only for the kinetics measurements.

As indicated above, in small-bore reaction tubes, the temperatures of the particles are essentially the same as the wall and gas temperatures because of the rapid collision of the particles with the wall under turbulent flow conditions. Even though the temperature profile of the simple reactor is not precisely controlled, it can be measured. From the measured temperature profile of the reaction tube and the assumption that the temperature of the particle is the same as the temperature of the wall at that point, heating rates and residence times of the particles undergoing devolatilization can be calculated. This has been done for most of the experimental runs as shown in the next section.

The BYU high-pressure, entrained-flow gasifier enables production and collection of large quantities of char. Data from these chars will be compared with the char samples prepared by the other two methods.

The HPCP reactor will also be used to prepare chars at pressures up to 20 atmospheres with careful control of heating rate, residence time and temperature. These chars will be designated as reference char samples to which the other char samples prepared via the other methods will be compared.

Analysis and Measurements - Several char samples have been collected from the simple hot-tube reactor at atmospheric and elevated pressures (up to 5.4 atm). A char sample from the BYU gasifier was also collected. All of these

samples have been analyzed using a CH Analyzer and a few with the Scanning Electron Microscope (SEM). Table II.B-1 lists the char preparation conditions (maximum temperature, residence time and heating rate) with the results of the CH analyses and any SEM micrographs that have been made.

The maximum temperatures, residence times, and heating rates of the char samples have been calculated based on the assumptions previously indicated about wall temperature and particle temperature. A temperature profile of the reaction tube was measured with a thermocouple for various settings of the reactor. This profile described the maximum temperature and length of the reaction zone used for the calculation of the volume in which the coal converted to char. The reaction zone was defined by the plateau of the temperature profile. The residence time is calculated by:

$$t_r = V_{\text{tube}} / w_{N_2} \quad (\text{II.B-1})$$

where V_{tube} is the volume of the reaction zone and w_{N_2} is the volumetric flow rate of the nitrogen gas through the tube. The flowrate was adjusted as the density of the nitrogen changed with temperature. The residence time was then calculated from Eq. II.B-1. Heating rate calculations were made based on the temperature profile. The temperature profile comprises the wall temperature of the reaction tube taken every 5 cm along the tube. An average volumetric flow rate was calculated for each 5 cm increment until the maximum temperature was reached. The heating rate for each increment was calculated from the change in temperature divided by the product of volume of the tube in the 5 cm increment and the reciprocal of the average flowrate. The heating rates for each increment, up to the maximum temperature, were averaged to obtain the average heating rate for the char sample.

CH analyses have been performed on all of the char samples prepared. As noted previously, it was expected that the hydrogen content of the char sample would decrease as the residence time increased. This trend is followed by most of the samples; however, some of the samples vary from this pattern. These discrepancies might be due to the fact that they are larger samples which required a longer time to collect and more coal to flow down the reactor tube. These two effects caused a build up of char/tar on the inside walls of the reactor tube effectively decreasing the inside diameter. A reduction of the inside diameter of the tube would cause a decrease in the residence time of the particle resulting in a change of conditions and characteristics for the particles flowing through the narrower tube.

Scanning electron micrographs were taken of five samples from the simple hot-tube reactor and the sample from the BYU high-pressure, entrained-flow gasifier. The micrographs revealed that the char samples from the simple reactor with longer residence times were more porous than those with shorter residence times. This trend is an indication that residence time calculations are reasonably accurate. The porous structure of these chars indicate that the coal particles were heated rapidly. The micrographs show particles with a wide range of diameters, which is probably due to the fact that the coal wasn't fractionated according to particle size prior to preparing the char. Micrographs of char samples prepared from fractionated coal (38-74 microns) show a more uniform particle distribution; however, there are still some particles

Table II.B-1

CHAR PREPARATION CONDITIONS AND ANALYSIS

Sample	Pressure (atm)	Maximum Temp(C)	Residence Time(ms)	Heating Rate(K/s)	CH Analysis		SEM Made
					%C	%H	
Utah Bit. Coal		----	----	----	74.7	5.7	X
Gasifer-1	Unknown	----	----	----	76.2	0.8	X
36	1	1235	28	12,700	74.7	1.9	
35	1	1235	30	11,800	72.7	2.8	
32	1	1235	42	8,450	78.3	0.4	
33	1	1235	42	8,450	78.4	0.3	
6	1	1210	29	12,200	75.1	2.8	X
16	1	1210	29	12,200	81.6	1.5	
24	1	1210	62	5,690	76.4	0.8	
23	1	1210	72	4,870	78.0	0.4	
13	1	1200	26	13,580	76.6	2.2	X
15	1	1200	29	11,980	77.4	1.3	X
12	1	1200	36	9,580	74.7	0.7	
7	1	1200	41	8,340	74.4	0.7	X
11	1	1200	54	6,391	77.7	0.8	X
64	4.8	900	66	4,400	61.8	4.4	
67	5.4	900	76	3,450	68.2	4.7	X
69	5.4	900	96	2,790	68.0	4.7	X

which are not within the above size fraction. The original micrographs showed particles of many sizes and particles which broke or chipped during the char preparation run.

The char from the BYU gasifier had a much different appearance than those from the simple reactor at low pressure. It was non-porous which might indicate that at elevated pressure, the volatile matter in the coal is not allowed to escape and open up pores. The chars prepared at elevated pressure in the simple reactor indicate a similar non-porous structure to those from the gasifier. Surface area measurements of the chars will be another criterion for characterizing the char samples, which will be determined using nitrogen and carbon dioxide adsorptions. It may be important to know the surface properties of char, i.e. total surface area, active surface area and pore volume, in order to understand the kinetics which govern the oxidation of the char particle.

Char Reactivity Plan - Five coals will be used to prepare chars by pyrolysis. Each char sample will be fractionated by sieving, and two of the fractions will be used for the determination of the kinetics of oxidation. For each size fraction of a particular char, kinetic runs will be made at three pressures and three temperatures. The rates of oxidation will be followed by analysis of the ash and, if possible, titanium content of the samples as a function of burnout. The calculations for the combustion rate parameters (rate constants, activation energies and reaction orders) were outlined by Solomon et al. (1987).

Component 2 - Kinetics of Char-Oxygen Reactions at High Pressure

This subtask component is aimed at determining the kinetic rate parameters for high-pressure oxidation of the chars prepared in Component 1. It will be initiated after completing the design and construction of the HPCP reactor.

Component 3 - High-Pressure Reactor Design and Fabrication

The HPCP reactor design has been completed, and assembly of the reactor components is in progress. The reactor collection system has been designed under independent funding to separate and collect coal char/tar/gas sets under known conditions. This added feature of the reactor will enable detailed study of the products of char production, as well as the oxidation rate for chars where the tar and gas fractions are also known.

Literature Review - Two papers of interest were presented at the Western States Section of The Combustion Institute in March, 1988. Mitchell (1988) used a laminar flow furnace to determine the reactivities of pulverized coal at atmospheric pressure. He employed an optical system of two-color pyrometry and particle imaging to simultaneously determine particle temperature, diameter, and velocity. Waters et al. (1988) also performed work using the same facility to determine how dimensional irregularity in char would affect the measurement of kinetic rates. Using non-spherical particles, they found that the measured kinetic parameters were relatively insensitive to the assumption that the particles were spherical. Saran char, which is highly irregular in shape, was used in a laminar flow furnace to study the effects of non-sphericity on the measurements. The variation in measured particle temperature increased significantly for the irregular particle, and diameter uncertainty increased by 15%. The Saran char is a worst-case situation for particle shape; no coal char

which will be used in the present study will likely be as irregular as the Saran char.

Flaxman and Hallett (1986) showed that particle heating rate increases with increasing secondary gas temperature and increasing particle diameter (up to 100 microns) because of wall radiation. The primary gas flowrate had little effect on the heating rate, and lower particle feed rates led to smaller variations in the temperature histories of different-sized particles. Essenhigh (1987) proposed a char combustion rate equation, "the extended resistance equation," that provides more accurate modelling of char combustion. A literature review of coal char/tar production and collection methods was conducted under independent funding (Smoot et al., 1988).

Final Reactor Design - The final design of the HPCP reactor was completed, and final construction and assembly is in progress.

Pressure Vessel - A flow diagram for the system and a cross-section of the reactor are shown in Figures II.B-3 and II.B-4, respectively. Particles are fed with primary gas through the injector, which is moveable to allow varying particle residence times. The ceramic honeycomb flow straightener, fastened to the end of the injector, keeps the injector at the centerline of the reaction tube and ensures laminar flow of the secondary gas. The secondary gas is preheated before flowing into the reactor. The primary and secondary flows mix in the reaction tube, initiating the particle reaction. A series of wall heaters maintain the desired temperature profile. Four holes, spaced every 90° in the reaction tube wall at the diagnostic level near the bottom of the reactor, and quartz windows on the outer shell, provide optical access. The collection probe collects the entire mass flow and quenches the particles just below the diagnostic volume. A virtual impactor separates the particles from most of the gas and tar. Particles are captured in a cyclone, tar is collected in filters, and the gas is either saved for analysis or vented from the system.

An overall view of the pressure vessel, which consists of the preheater, head, and body is shown in Figure II.B-5. The outer wall of each part of the vessel is 1.3 cm thick carbon steel tube, 32 cm in diameter. The three sections are joined together with flanges. At the most severe operating conditions, the shell will maintain 27 atm pressure while at a wall temperature of 535 K.

Each section is provided with a service access for the heating elements and instrumentation. The access port runs the entire length of the reactor body. This port encompasses the ends of the heaters which protrude from the reactor shell. A removable access port cover plate provides structural support to the outer shell when the reactor is pressurized and allows the removal and insertion of heaters and thermocouples for servicing. Two braces maintain reactor rigidity when the cover is removed. Power leads and thermocouple wires are fed into the port through sealing glands. The head has a similar but shorter access for its heating elements. The preheater has two access ports: one at the top for heating elements and another on the outer wall above the elbow for thermocouples. The cover plates bolt to the outer wall and are sealed with gaskets.

Figure II.B-4 shows the insulation detail for the reactor. A high-temperature layer of mullite insulation will surround the wall heaters. The space between this insulation and the shell will be filled with a castable

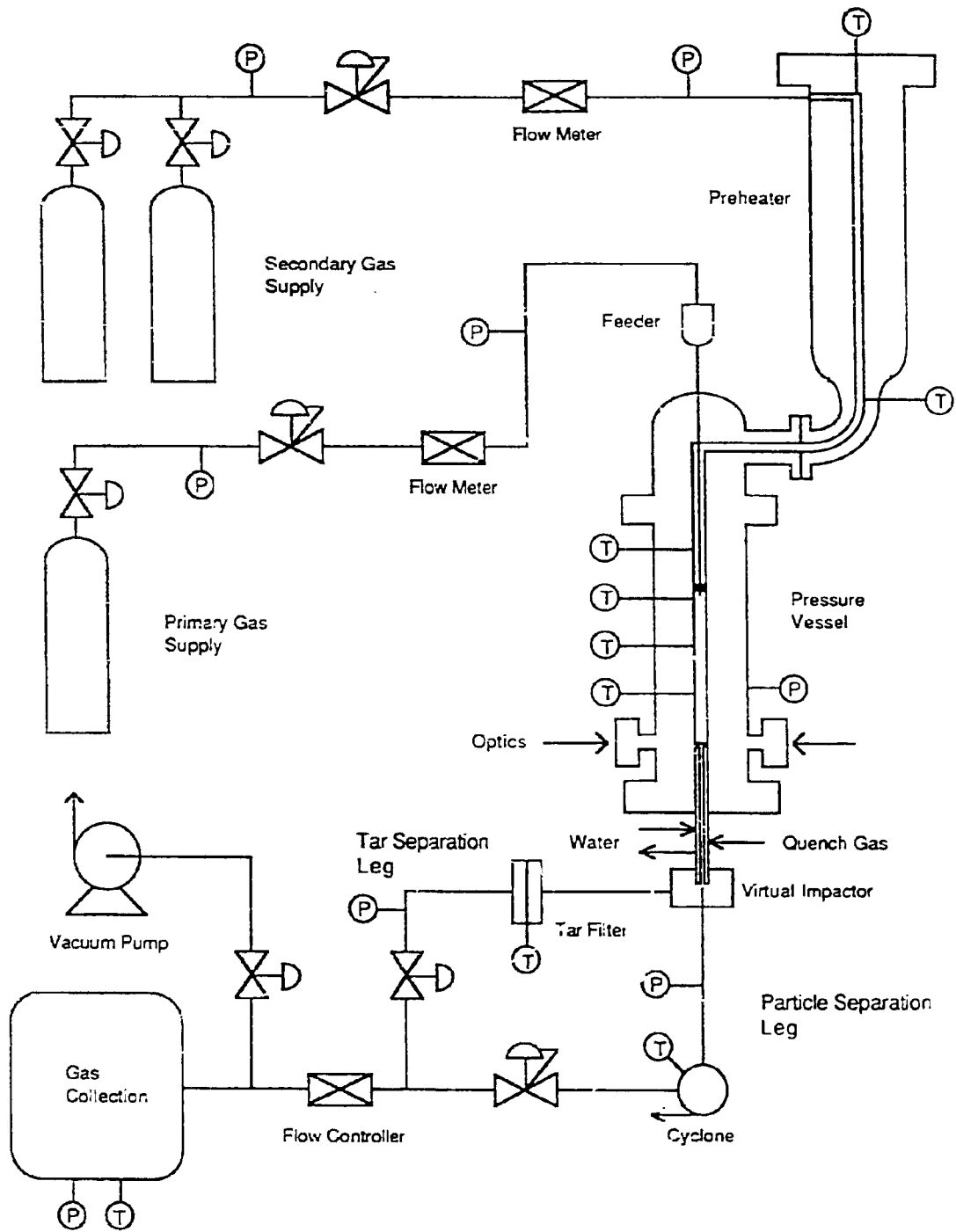


Figure II.B-3. HPCP flow diagram.

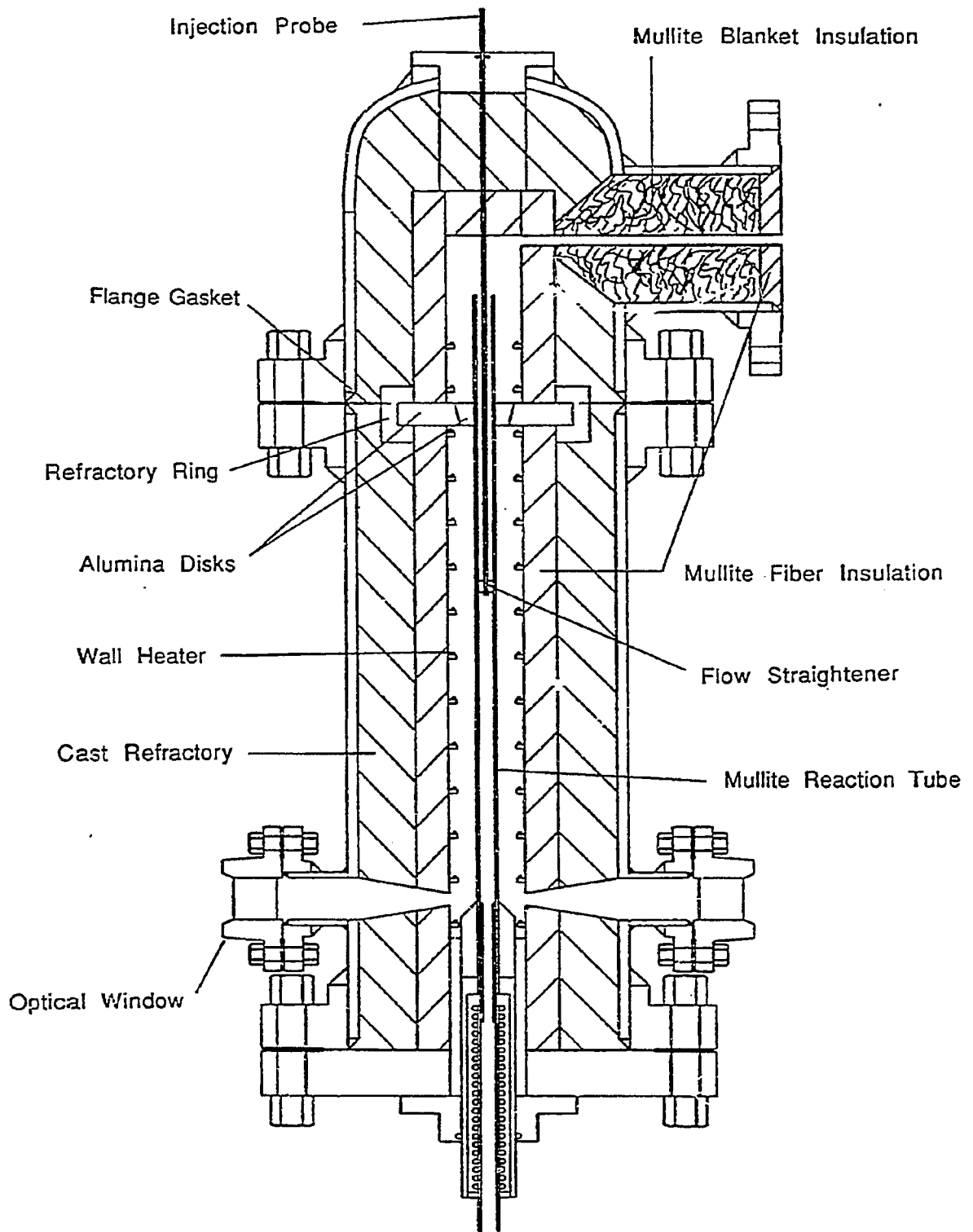


Figure II.B-4. Vertical cross sectional view of reactor.

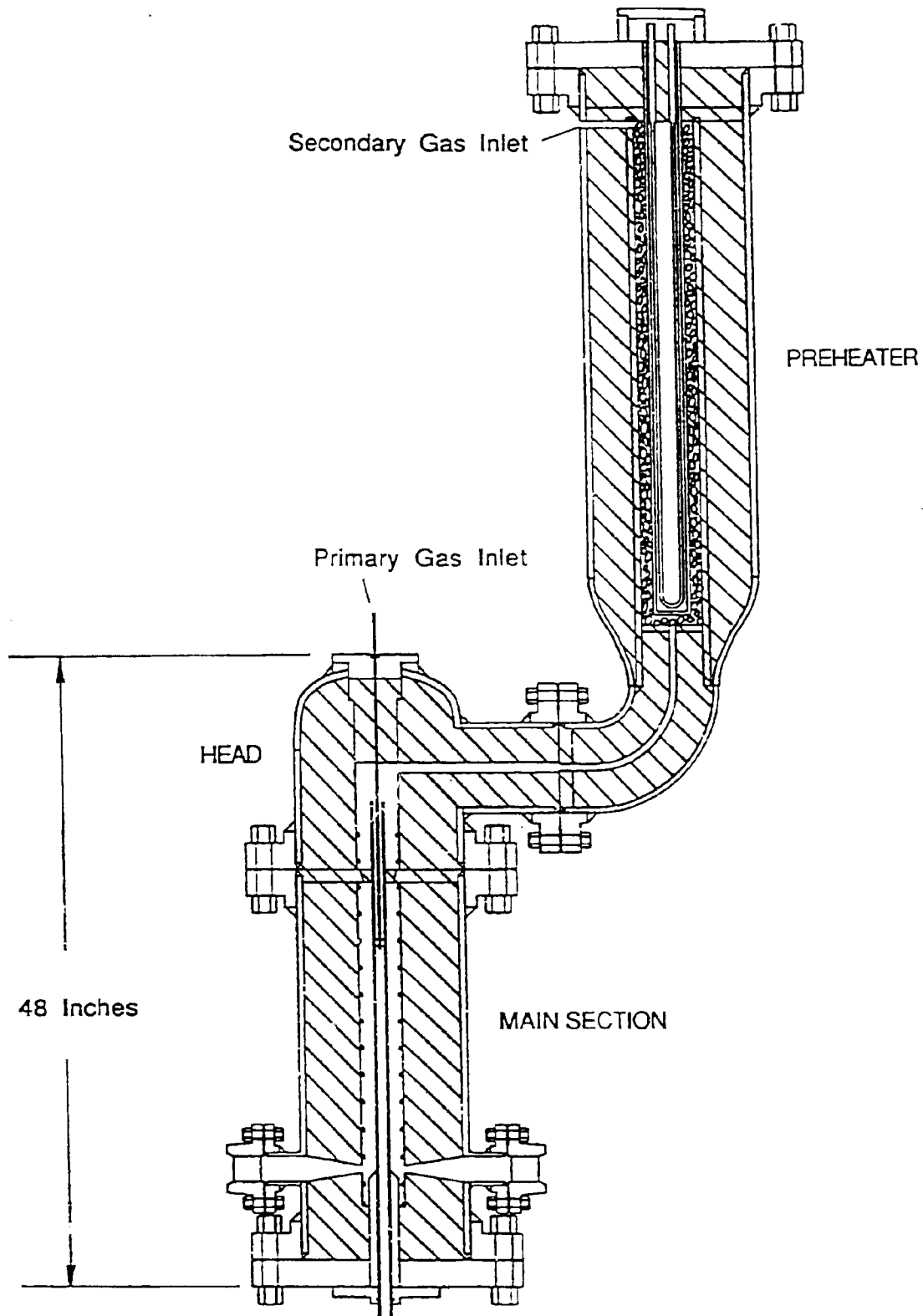


Figure II.B-5. HPCP reactor.

refractory. A mullite fiber blanket will insulate the preheated gas passageway into the reactor head. The seal between the reactor head and main section will be created by matching alumina disks. The inner disk will be cemented to the reaction tube while the outer disk will be held in place by the mullite insulation and a cast, high-temperature refractory ring. The flange gasket will extend into the inner portion of the reactor, being cast into the refractory ring at its inner diameter. This will ensure a good seal and prevent the secondary gas from flowing down along the wall heaters and into the reaction tube through the optical holes.

The design allows the use of reaction tube diameters from 1 to 5 cm. This is necessary to achieve the wide range of residence times at the conditions called for in the experimental plan. A reaction tube can be removed and exchanged for a different size without disassembling any of the main sections; only the injector and collector must be removed to gain access to the reaction tube. The reaction tubes are standard cast mullite with good thermal conductivity and thermal shock characteristics. At the bottom end of each reaction tube, four optical access holes have been drilled around the tube circumference. The four access holes line up with the four quartz windows in the reactor shell.

Heating System - The reactor heating system consists of 14 horseshoe-shaped molybdenum disilicide elements. These elements encircle the reactor centerline and are arranged axially along the reactor. Each heater lies on a ceramic tray that slides into the reactor to hold the element in its proper position. The tray is made of two parts, as shown in Figure II.B-6: a mullite fiber insulation block that positions the heater in the reactor, and a high density alumina ring that supports the fragile hot end of the element. Each tray also has a port for a thermocouple probe.

In order to provide an isothermal temperature distribution along the reaction tube, the wall heaters will be divided into three heat zones. Each of these zones as well as the preheater will be controlled by a phase-angle-fired, silicon-controlled rectifier (SCR) that will receive a control signal from a microcomputer. The computer will monitor thermocouples in each of the heat zones and adjust the SCR's to obtain the desired operating temperature profile. The number of heaters included in each heat zone will be varied to correspond to the position of the injection tube.

Preheater - The preheater consists of two molybdenum disilicide heating elements which will fit inside two cast alumina rectangular tubes. These will be placed in a packed bed of alumina ceramic pieces, all of which will be enclosed in fibrous ceramic insulation and a steel shell. The preheater, shown in Figure II.B-7, is offset and vertical above the main reactor section. The gas flow will enter at the top and flow downward through a 1-meter hot zone into the reactor head. Thermocouples will monitor both heater and gas temperatures. The maximum gas preheat temperature is 1700 K.

Feed System - A particle feeder has been built that will give a constant feed rate at very low flowrates and at elevated pressure. It consists of three separate, 9.5 mm acrylic reservoir tubes inside a 76 mm pressure tube. The tube is vibrated to agitate and somewhat fluidize the coal. The air inlet is at the top. A 3 mm i.d. feed tube is located at the center of each reservoir tube. The coal is fed from the top of each reservoir tube by drawing the center tubes

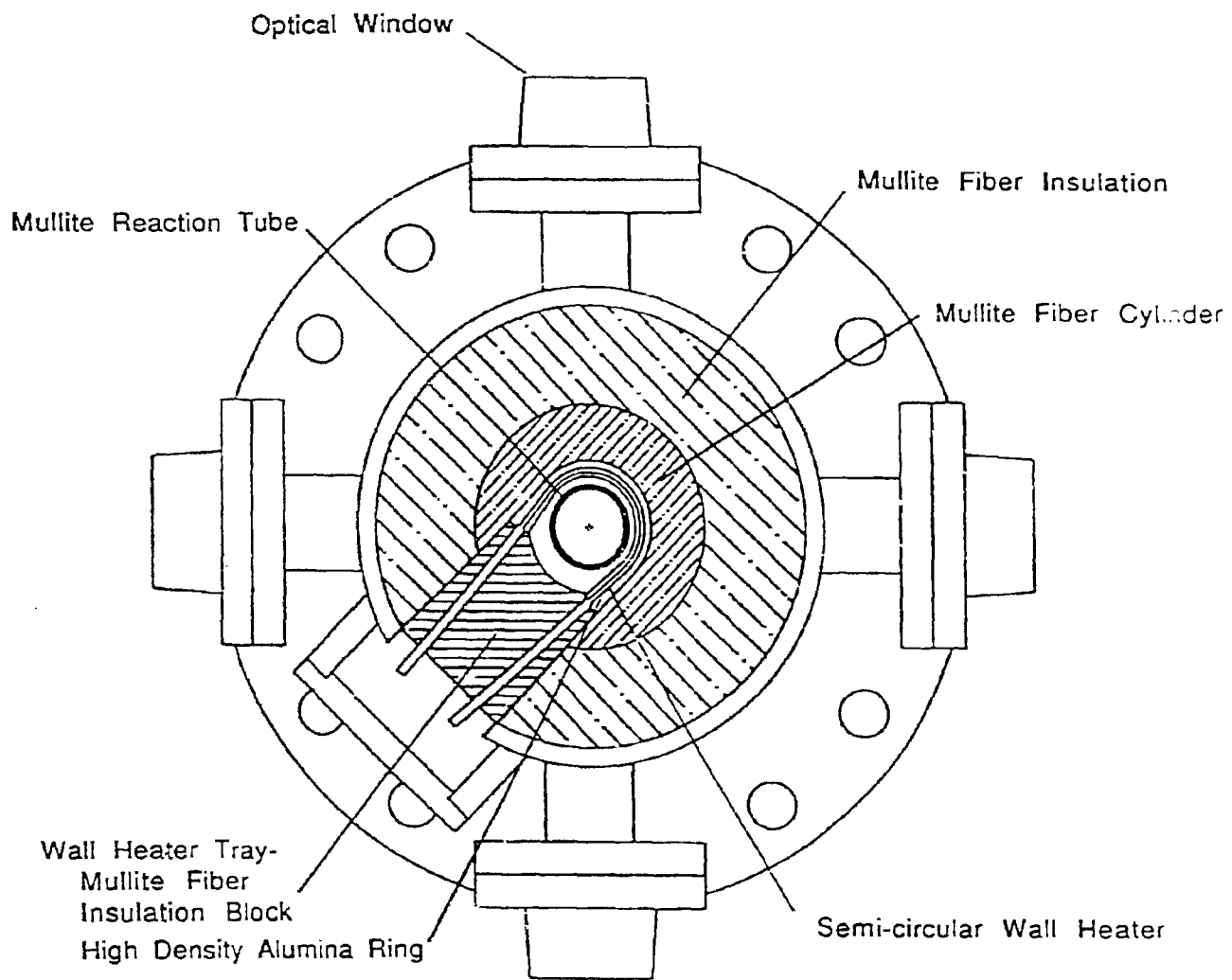


Figure II.B-6. Horizontal cross sectional view of reactor.

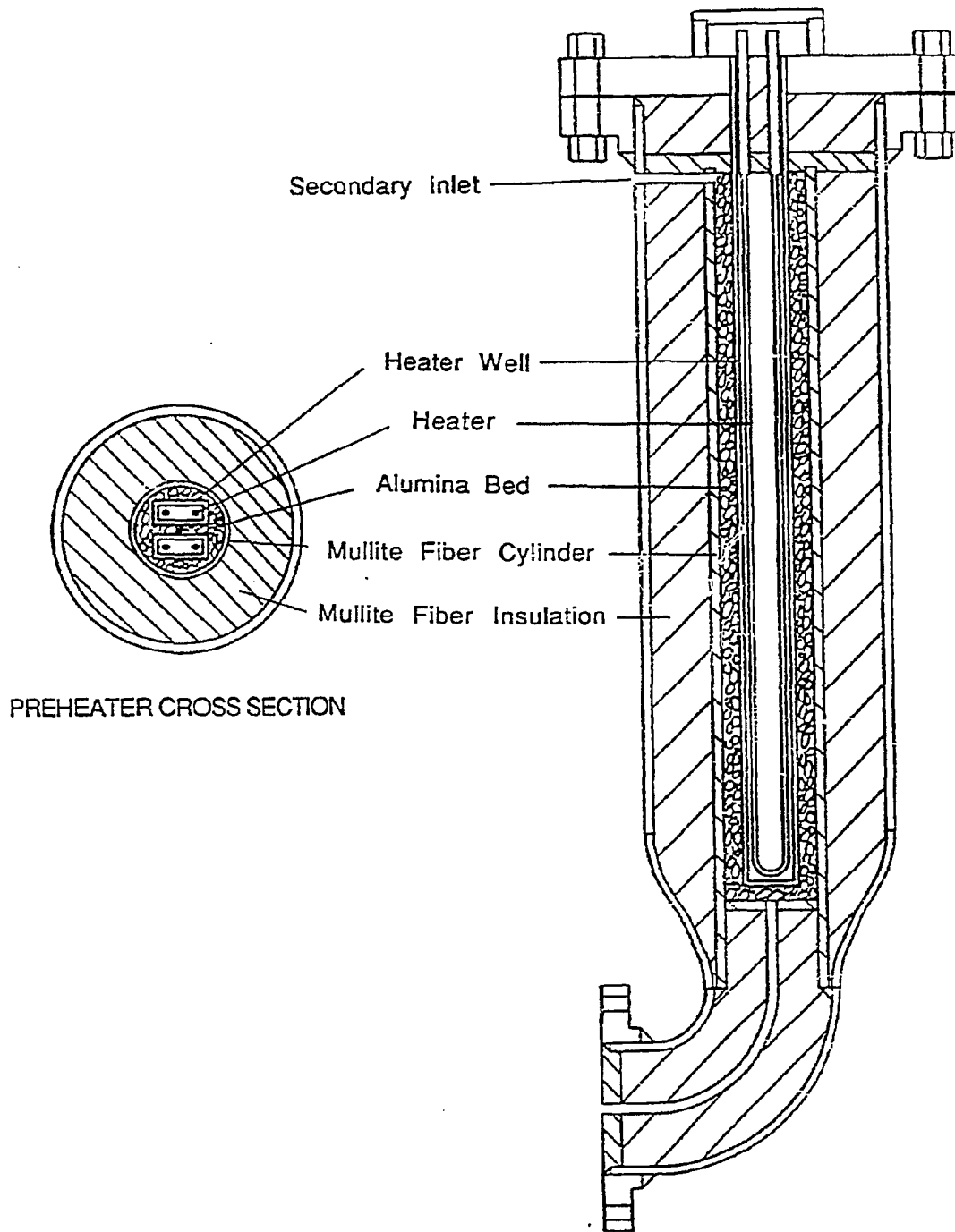


Figure II.B-7. Cross sectional views of preheater.

down very slowly with a stepper motor. The coal or char particles are picked up by the flowing air and entrained in the flow. The feed rate is varied by changing the speed of the center tube. The feeder is located above the injection tube so that particles will not collect in the lines.

Two injection probes will be used in the char tests: a water-cooled probe for coal pyrolysis and char oxidation and an uncooled ceramic probe for char oxidation. Both of these probes will be centered in the reaction tube by a flow straightener. A fluorocarbon seal in the reactor head cap will enable axial positioning of the probe.

The uncooled probe is an alumina tube, 1.5 mm i.d. by 3 mm o.d. It will be used in tests where the temperature is lower than those used to make the char. This probe will allow the char to attain the furnace temperature before it is introduced into the oxidizing atmosphere, which will simplify the analysis of particle temperature history.

The cooled probe is a stainless steel tube, 3.4 mm o.d. by 3 mm i.d. This tube is surrounded by another stainless steel tube 13 mm o.d., forming a water jacket. Cooling water is carried through three small tubes that run through the water jacket to the tip of the probe. The water then flows back up the probe via the water jacket. The probe is sheathed in ceramic fiber insulation to reduce heat transfer from the hot secondary gas and reaction tube.

Collection System - In an independently funded research project, the reactor collection system is being modified to collect and separate the products of coal pyrolysis: tar, char, and gas. The separation system will enhance the quality of the char samples for the char oxidation studies, since it is possible that tar may condense on the char, changing the properties of the char. The new separation system, shown in Figure II.B-8 will almost completely separate the char and tar before appreciable condensation occurs.

The collection probe is similar in design to the cooled injection probe. Cold water flows to the tip of the probe through tubes passing through the water jacket. Other small tubes pass through the water jacket to deliver quench gas to the probe tip. A permeable inner liner inside the main probe tube allows quench gas to be injected radially along the length of the probe to reduce particle and tar sticking inside the probe.

A virtual impactor will follow in-line with the collection probe to aerodynamically separate the tar-laden gases from the heavier particles. The momentum of the char will cause it to be carried into the char collection probe, along with a small amount of carrier gas and tar, while most of the tar aerosol will follow the main gas flow to a filter system maintained at room temperature to collect the tar. The flow containing the char will go to a cyclone which will be sized to remove the char, then to a secondary filter to remove any tar in the flow. The two flows will then rejoin to be collected in plastic bags for gas analysis or exhausted. Each flow leg will have control valves and flow meters to keep the flow rates constant and to ensure good sampling. A vacuum pump will be used during atmospheric pressure runs. Various collection system components, such as the virtual impactor, cyclone and vacuum pump, will be used for the char oxidation tests.

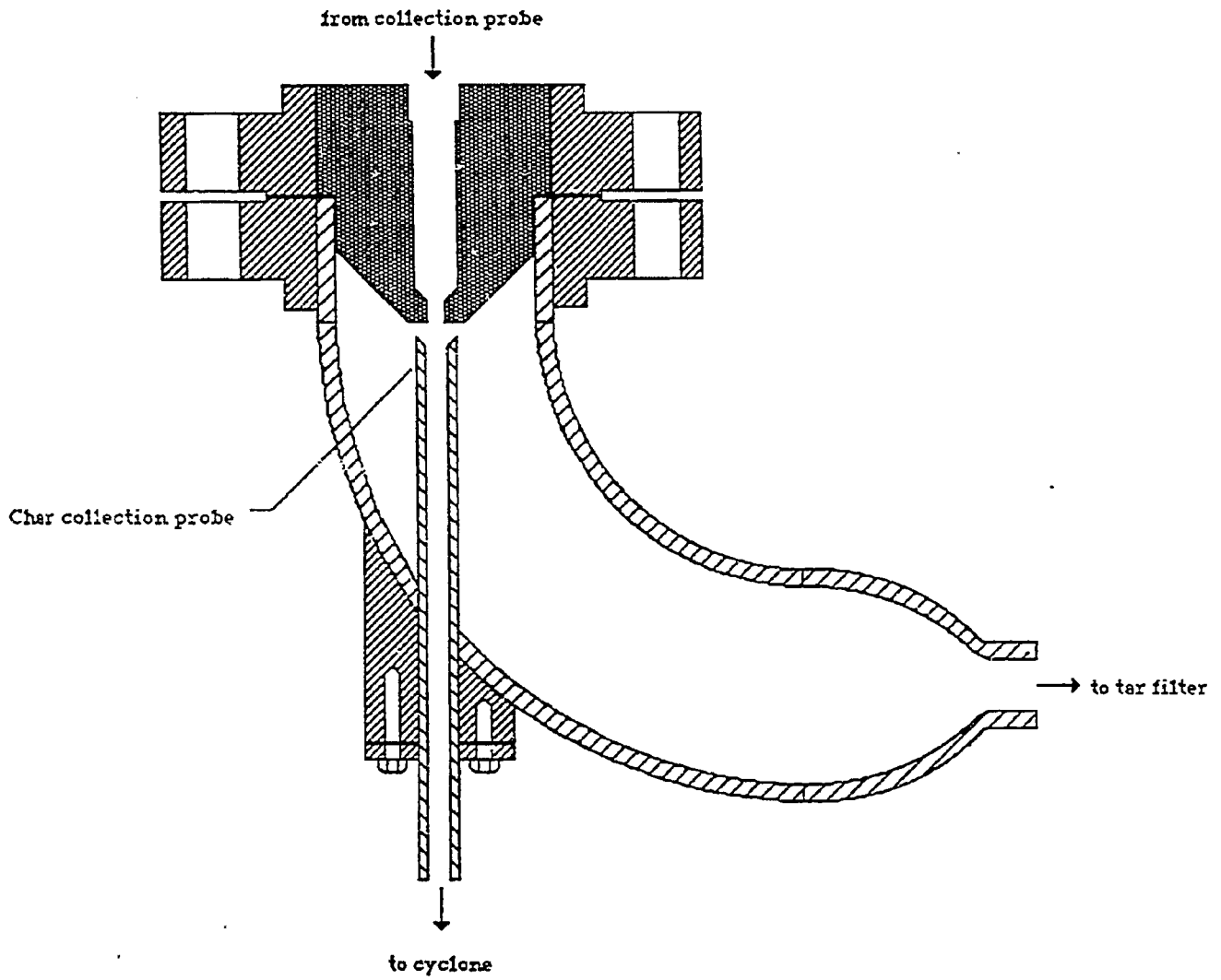


Figure IIB-8 Virtual impactor for char-tar separation

Instrumentation - Optical breadboards for the pyrometry and particle imaging system, as well as a table to support them, have been fabricated. No commercial optical tables are available which can support the weight of the reactor while providing enough flat table space for the optics. A related study at the BYU Combustion Laboratory will share many components of the optical instrument with this project in an effort to reduce cost. It is planned to share two photomultiplier tubes with their amplifiers and filters, a laser detector, and a digital oscilloscope. The trigger laser, lenses, apertures, beam splitter, and calibration components will be separately maintained, since their placement relative to each other and the reactor is critical, and because these parts must be aligned and solidly mounted. Type S thermocouples will measure the gas and heater temperatures along the reaction tube and at the preheater exit. These temperatures will be collected by a microcomputer and its acquisition system.

Reactor Performance Tests - The following tests will be conducted to ensure acceptable reactor performance in advance of detailed char preparation and oxidation tests.

1. **Structural Integrity** - The vessel will be pressure tested to 1.5 times its maximum pressure at maximum shell temperature. All joints will be checked for proper sealing.
2. **Injection Probe** - An uncooled injection probe will be used in some experiments where the char oxidation tests will be conducted at temperatures lower than those used to prepare the char. Tests will be conducted to assess the effect of heatup in the injector. Char will be injected into a nitrogen atmosphere where it is expected that with no oxidizer present, char properties should not change. The char subjected to this condition will be collected and analyzed to compare with its properties before the run.
3. **Collection Probe** - During the char oxidation experiments, char reactions will be quenched in the collection probe by both cooling and dilution with nitrogen. The quenching process will be tested by feeding char and nitrogen for the primary flow and nitrogen for the secondary flow, with air as the quench gas. It is expected that when proper quenching is achieved, there will be no change in char characteristics due to oxidation.
4. **Optical Instrumentation** - The optics will be tested using nonfriable carbon spheres (spherocarb), as well as with the calibration system that will be built into the instrumentation.

Reactor Characterization Tests - In order to characterize reactor operation, the following adjustments will be made for each of the experimental conditions (at a specific temperature, pressure, and residence time) required for the char tests.

1. **Temperature Profile** - For many experiments, an isothermal temperature profile will be necessary. It is also desired to maintain a constant particle heating rate at various injection probe positions. The heater zone configurations and temperatures, preheater temperature, injection probe cooling water flow, and the collection probe cooling

water and quench gas flows will be adjusted to accomplish this. The temperature profile will be measured using a platinum thermocouple sheathed in ceramic that will be inserted through the injection probe and moved axially through the reaction tube for a number of injection probe positions.

2. **Particle Flow** - In order to ensure that all particles undergo similar heatup rates and have the same residence time, all particles must flow down the centerline of the reaction tube. This will occur when the flow through the reaction tube is completely laminar. The primary and secondary gas flows will be adjusted to accomplish this. The laser and detector from the optical instrumentation will be used to indicate when this occurs. When particles fall through the optical volume, light from the laser is scattered and a signal is generated by the detector. Signals generated when the optical volume is adjusted to positions off of the reaction tube centerline will indicate that particles are not flowing properly.
3. **Particle Feed** - The char particles must be fed into the reactor at a constant rate to ensure proper operation of the optical instrumentation. Some adjustments can be made with the feeder tube size and vibrator frequency. Optical measurements, similar to those just described, will indicate the steadiness of the feed.

Component 4 - Fundamental Sulfur Capture Experiments

The work in this area was not emphasized during most of the reporting period. However, a literature review was continued from the first year of the study which is summarized here. Gullett and Bruce (1987) conducted a series of tests at 800°C. They showed that calcined CaCO_3 has a cylindrical pore structure, while Ca(OH)_2 has a slit-like pore structure, which is important when modeling the sulfur capture reaction. Increased conversion of Ca(OH)_2 from calcium oxide to calcium sulfate, evident only at times longer than 40 seconds in their experiments, is due to greater particle expansion of the hydrate. Sintering the sorbent at the test temperature decreased the surface area but had little effect on the porosity or the sorbent conversion.

Simons et al. (1987) used a pore tree representation to model the sulfur capture reaction at various pressures. They showed that the rate constant has a first order dependence on SO_2 partial pressure. Their study is only the second to use elevated total pressures, using 2 and 9.5 atmospheres for the sulfur capture experiments. The sorbents used were 42-78 micron diameter dolomite particles and 1-15 micron diameter limestone particles. The sulfation reaction rate decays faster with calcium utilization at low pressure than at high pressure. This suggests that greater calcium utilization is possible at higher pressures. However, higher pressure during calcination yields a lower initial surface area, which decreases the initial rate of reaction. Simons also quoted a study by Beittel et al. (1984) that showed that sintering was insignificant when sorbent was injected for 1.3 seconds in a temperature field that ranged from 1478 K to 1225 K.

Other Activities

One of the senior investigators met with Dr. Michael Slaughter of General Electric Corporate Research to discuss the interest of GE in the planned studies of sulfur capture with sorbents and char oxidation at high pressure.

The research team made a semi-annual technical review presentation to the AFR management team at Brigham Young University during the reporting period. A member of the research team was invited to present the details of the HPCP reactor design to a regional American Society of Mechanical Engineers' student paper contest in Phoenix, Arizona.

The research team organized a char preparation and analysis coordination meeting with other research groups at Brigham Young University who are doing related work under separate funding. Technical presentations were made at the meeting to exchange information concerning char preparation and measurement of char properties, and to initiate an arrangement to share analytical equipment and expertise.

Members of the research team met with Dr. Ian Smith and Dr. Brian White of CSIRO in Sydney, Australia, who were visitors to the BYU Combustion Laboratory, to discuss char preparation and oxidation. A technical review meeting was also held at BYU with Dr. Michael Serio of AFR during which char oxidation and advanced measurement techniques were discussed.

Plans

When the construction and testing of the HPCP reactor are completed, chars from the five standard coals will be prepared in the HPCP reactor. To establish a reference operating condition, data from atmospheric pressure runs in the HPCP reactor will be compared with those obtained by other researchers using similar conditions. Potential sources are Wells (1985), Solomon (1982), Nsakala (1979), and Kobayashi (1976). If a specific char compares favorably with the char from the same coal but prepared in the simple hot-tube reactor, then both reactors will be used for char preparation. This will permit more time for kinetic runs in the HPCP reactor. The elevated-pressure, simple hot-tube reactor will be used to provide additional char samples. These will be prepared in the 8 mm i.d. stainless steel tube. This reactor tube will also be fitted with ceramic tubes of varying diameter so that a ceramic tube surface can be used at elevated pressure but still be contained by the stainless steel boundary. The kinetic runs will be completed during the next year.

During the next quarter, the instrumented reactor, with the exception of the optical pyrometry and particle imaging system, will be completed. The laser and detector will be set up for use in characterizing the reactor performance, while the remainder of the optical system will be completed in the following quarter. Testing of the reactor systems and reactor performance characterization will be initiated in the next quarter and completed in the following quarter.